THE TRANSCRIPTION FACTOR PEBBLED/RREB1 REGULATES INJURY-INDUCED AXON DEGENERATION

A Dissertation Presented

By

JONATHAN EDWARD FARLEY

Submitted to the Faculty of the
University of Massachusetts Graduate School of Biomedical Sciences, Worcester
in partial fulfillment of the requirements for the degree of

DOCTOR OF PHILOSOPHY

DECEMBER 11, 2017

PROGRAM IN NEUROSCIENCE

THE TRANSCRIPTION FACTOR PEBBLED/RREB1 REGULATES INJURY-INDUCED AXON DEGENERATION

A Dissertation Presented
By

JONATHAN EDWARD FARLEY

This work was undertaken in the Graduate School of Biomedical Sciences
Program in Neuroscience

Under the mentorship of

Marc Freeman, Ph.D., Thesis Advisor

Eric Baehrecke, PhD., Member of Committee

Yang Xiang, PhD., Member of Committee

Alexandra Byrne, PhD., Member of Committee

Justin Thackeray, PhD., External Member of Committee

Patrick Emery, Ph.D., Chair of Committee

Anthony Carruthers, Ph.D.,
Dean of the Graduate School of Biomedical Sciences

December 11, 2017

Dedication

This work is dedicated to my grandfather, Edward Nuzenski, who told me that no matter what happens in life, I'll always have my education.

You were right, I do have a good thing going.

Acknowledgements

First and foremost, I would like to thank my mentor, Marc Freeman, for giving me the opportunity to work in his lab. His support and enthusiasm for science has allowed me to grow and develop as a scientist, while teaching me to never underestimate the power of a good Manhattan.

Thank you to the members of my thesis research committee members for all their scientific input, discussions, and guidance throughout this entire process.

To all past and present members of the Freeman lab, I cannot express how lucky I am having had the opportunity to work alongside each of you. You truly became a second family to me.

Thank you to all my friends and family members for the constant stream of overwhelming love and support. Remington, your endless entertainment provided a much-needed escape from the everyday stress of graduate school. Mom and Dad, I would not be where I am today without all you've done and sacrificed for me, and I cannot thank you enough.

Finally, to Nathan – you are always there for me and have supported me in every sense of the word. I would not have been able to do this alone, and for that, I am forever grateful. I love you.

Abstract

Neurons establish complex networks within the nervous system allowing for rapid cell-cell communication via their long, thin axonal processes. These wire-thin projections are susceptible to a number of insults or injuries, and axonal damage can lead to disruption in signal propagation and an overall dysfunction of the neural network. Recent research focused on investigating the underlying mechanisms of injury-induced axon degeneration led to the discovery of a number of endogenous, pro-degenerative molecules such as dSarm/Sarm1, Highwire/Phr1, and Axundead. These signaling molecules are thought to execute axon degeneration in response to injury locally within the distal severed axon, but the exact mechanism of action is unclear.

To further identify novel participants of the axon death signaling cascade, we performed an unbiased forward genetic mutagenesis screen using the sensory neurons within the adult wing of *Drosophila melanogaster.* We identified a novel role for the C_2H_2 zinc finger transcription factor, Pebbled (Peb)/Ras-responsive element binding protein 1 (RREB1) in partially suppressing injury-induced axon degeneration. Loss of function *peb* mutant glutamatergic neurons present two distinct axon degeneration defects: either complete protection from axotomy, or they exhibit a novel phenotype in which axons fragment into long, continuous pieces instead of undergoing complete degeneration. Additionally, we show an enhancement of the *peb* protective phenotype when *dSarm* levels

are decreased, but not with reduced levels of *axundead.* These data provide the first evidence of a transcription factor involved in regulating injury-induced axon degeneration signaling *in vivo*.

Table of Contents

Title……...i
Reviewer Page…… ii
Dedication……..……iii
Acknowledgements……..iv
Abstract ……v
Table of Contents ……vii
List of Figures ……...ix
List of Tables…….……xi
List of Abbreviations ……..xii
List of Third Party Copyrighted Materials ……xv
Preface……xvi

CHAPTER I: Introduction……..1
Neurons and Their Networks…….. 2
Wallerian Degeneration……... 3
Axon Death Can Be Blocked ……..5
Nmnat2: The Essential Survival Factor Hypothesis, Revisited ……9
Drosophila as a Model Organism……10
Modeling Wallerian Degeneration in *Drosophila* ……...12
dSarm/Sarm1 Regulates Wallerian Degeneration ……14
Highwire/Phr1 Controls Axonal Nmnat2 Levels……17
Axundead Signals Downstream of dSarm in Axon Death……19
Pebbled, a C_2H_2 Zinc Finger Transcription Factor ……20
Thesis Overview ……24
Figures ……25

CHAPTER II: Screening for Endogenous Regulators of Wallerian Degeneration *In Vivo*……..29
Abstract ……30
Results & Discussion ……31
Materials & Methods ……..34
Figures & Tables……36

CHAPTER III: The Transcription Factor Pebbled/RREB1 Regulates Injury-Induced Axon Degeneration……...40
Introduction……..41
Results ……44
Discussion……56
Materials & Methods ……..61
Figures & Tables……69

CHAPTER IV: Discussion.....89
Summary of Findings.....90
How is *peb* Regulating Axon Degeneration.....95
The Partially Fragmenting Axon Phenotype.....100
Cell Type Specific Protection in *peb* Mutants.....102
How Do Transected Axons Survive?.....104
Identifying Remaining Axon Death Signaling Molecules.....106
Axon Death Molecules and Neurodegeneration Therapeutics.....108
Conclusion.....110
Figures.....112

Appendices.....113
Appendix I: RNA-seq of *peb* Knockout in GM2 Cells.....114
Appendix II: Gain of Function dSarmΔARM Suppressor Screen.....119
Appendix III: *Pebbled* Mutant Neurons Within the Wing Display Abnormal Dendrite Morphology.....125

References.....130

List of Figures

Figure 1.1	Transected Axons Undergo Stereotyped Degeneration
Figure 1.2	Current Model of Injury-Induced Axon Degeneration Signaling
Figure 1.3	Protein Structure of the Zinc Finger Transcription Factor, Pebbled
Figure 2.1	Modeling Wallerian Degeneration in the Adult Wing
Figure 2.2	Schematic of F1 and F2 Genetic Screens Using the *Drosophila* Wing
Figure 3.1	Mutation 345x Causes Defective Wallerian Degeneration *In Vivo*
Figure 3.2	345x Encodes the Transcription Factor Pebbled
Figure 3.3	Uninjured Control and peb^{345x} Clones
Figure 3.4	Pebbled is Expressed in Neurons Within the Developing Wing
Figure 3.5	Pebbled is Not Detectable in the CNS
Figure 3.6	Human RREB1 Functionally Rescues Axon Death Defect in *peb* Mutants
Figure 3.7	Pebbled Axon-Protective Phenotype Observed Only in Glutamatergic Neurons
Figure 3.8	Quantifications of Injured Control Clones 7dpa
Figure 3.9	Pebbled Protective Phenotype is Enhanced When Removing One Copy of *dSarm*
Figure 4.1	Expanded Model of Wallerian Degeneration Signaling
Figure A1.1	CRISPR Knockout of *peb* in GM2 Cells
Figure A2.1	Pebbled Protective Phenotype is Enhanced When Removing One Copy of *dSarm*
Figure A2.2	Primary Hits Identified from Suppressor Screen

Figure A3.1 Pebbled Mutant Neurons Show Abnormal Dendrite Morphology

Figure A3.2 Abnormal Dendrite Morphology is Rescued by Genomic *peb*^{BAC}

Figure A3.3 The C-Terminal Zinc Fingers and hRREB1 Can Rescue the Dendrite Phenotype

List of Tables

Table 2.1	Total Chromosome Arms Screened
Table 2.2	List of Genotypes Used in Wing Screen
Table 3.1	X-chromosome Coverage of Deficiency Lines Tested for Axon Death Defects
Table 3.2	Top Candidate Genes from ChIP-seq
Table 3.3	List of Animal Genotypes Used in Figures
Table A.2	Total Number of Chromosome Arms Screened in Gain of Function dSarmΔARM Suppressor Screen

List of Abbreviations

AAA+	ATPases Associated with diverse cellular Activities
AAD	acute axon degeneration
ADP	adenosine diphosphate
AKAP	a kinase anchoring protein
AM	anterior midgut
ARM	Armadillo/HEAT domain
AS	amnioserosa
ase	asense
ATP	adenosine triphosphate
axed	axundead
BAC	bacterial artificial chromosome
BACK	BTB and C-terminal Kelch
bsk	basket
BTB	broad-complex, tramtrack, bric-a-brac
C_2H_2	Cys_2-His_2
Ca^{2+}	calcium ion
cAMP	cyclic adenosine monophosphate
Cas	CRISPR associated
cb	cell body
ChAT	choline acetyltransferase
ChIP-seq	chromatin immunoprecipitation sequencing
CHX	cyclohexamide
CNS	central nervous system
CRISPR	clustered random interspaced palindromic repeats
dlk	dual leucine kinase
dpa	days post axotomy
dpe	days post eclosion
DRG	dorsal root ganglia
dsarm	*Drosophila* sterile-α and Armadillo motif
E-cycle	endoreplication cycle
EGTA	ethylene glycol tetraacetic acid
EMS	ethyl methane sulfonate
FBD1	FSN-1 binding domain 1
FLP	flippase
FRT	flippase recognition target
GEF	guanine exchange factor
GFP	green fluorescent protein
GM2	Genetics, Milano 2
Hh	hedgehog
hep	hemipterous

hiw	highwire
hnt	hindsight
hpa	hours post axotomy
IHC	immunohistochemistry
IRF	interferon-regulatory factor
jbug	jitterbug
JNK	c-Jun N-terminal kinase
M-cycle	mitotic cycle
MAPK	mitogen associated protein kinase
MKK	MAP kinase kinase
MKKK	MAP kinase kinase kinase
MARCM	mosaic analysis using a repressible cell marker
N70	N-terminal 70 amino acids
NAD+	nicotinamide adenine dinucleotide
NMJ	neuromuscular junction
Nmnat	nicotinamide mononucleotide adenylyltransferase
nvy	nervy
nSyb	synaptobrevin
ORN	olfactory receptor neurons
peb	pebbled
PFA	partially fragmented axons
Phr1	Pam/highwire/rpm1
PKA	protein kinase
PlexA	Plexin A
PM	posterior midgut
PNS	peripheral nervous system
puc	puckered
RBD	RAE-1 binding domain
RING	really interesting new gene ubiquitin ligase domain
RLD	RCC1-like GEF domain
RNA-seq	ribonucleic acid sequencing
RREB1	Ras-responsive element binding protein 1
S2	Schneider 2
SAM	sterile-α motif
SCF	Skp/Cullin/F-box
SCG	superior cervical ganglia
Sema-1a	Semaphorin 1a
shRNA	short hairpin RNA
siRNA	small interfering RNA
SOP	sensory organ precursor
TBI	traumatic brain injury
TIR	toll/interleukin receptor
TS	temperature sensitive
UAS	upstream activating sequence

UPS	ubiquitin proteasome system
UTR	untranslated region
VCP	vasolin-containing protein
VNC	ventral nerve cord
WD	Wallerian degeneration
WldS	Wallerian degeneration Slow
wnd	wallenda
ΔARM	dSarmΔARM

List of Third Party Copyrighted Materials

Figure Number	Publisher	License Number
Figure 1.3	Differentiation	4214860135127
Figure 2.1	Cell Press	no permission required
Figure 2.2	PNAS	no permission required

Preface

All of the work presented in this thesis was performed by myself in collaboration with a previous graduate student, Thomas Burdett, in the laboratory of Marc Freeman, PhD at the University of Massachusetts Medical School. Specific attribution for experiments are given in the preface of each chapter.

CHAPTER I: Introduction

Neurons and Their Networks

The nervous system is a series of intricate, interconnected neural networks working cooperatively to send and receive messages throughout an organism. Sensory networks of the peripheral nervous system (PNS) relay a multitude of external environmental inputs to the central nervous system (CNS) for interpretation, further processing, and execution of a certain organism response. Overall, the nervous system of an organism can be divided into two broad classes of cells: neurons and glia. Neurons are remarkable cells involved in fast, long-distance information communication and processing, while surrounding glial cells not only provide structural and metabolic support, but homeostatic functions as well (Freeman and Doherty, 2006).

Neurons are composed of four parts, each with distinct roles necessary for successful signal propagation. Dendrites receive a number of inputs which are integrated in the cell body. The signal is then transmitted down a long, relatively thin axon and relayed to a downstream effector cell through the axon terminal. Maintaining the health of each of these components is essential for proper neural circuit function within an organism. Focusing specifically on the axon, their extreme length makes them particularly vulnerable to a number of insults and injuries. Whether these insults may be intrinsic, such as defects in axon transport or energy depletion (Chevalier-Larsen and Holzbaur, 2006; Gilley and Coleman, 2010), or due to external physical lesions seen in axotomy and

traumatic brain injury (TBI) (Waller, 1850; Johnson et al., 2013; Henninger et al., 2016), they can all lead to axon loss and network dysfunction.

Wallerian Degeneration

Physical transection of the distal axon from the cell body leads to stereotypical degenerative process, known as Wallerian degeneration (WD). This phenomenon was first discovered in 1850 by Augustus Waller when he severed the hypoglossal nerve in the tongue of a frog and recorded the morphological changes of the distal nerve over the course of the following two weeks. Waller's initial observations described the three distinct phases the distal axon underwent during the degenerative process. Initially, the anatomy of the severed nerve remained unchanged, however, over time, Waller noted it began to appear "more varicose that usual". At the end of two weeks, all traces of the distal nerve were gone, appearing to have been "removed by absorption" (Waller, 1850).

Since Waller's initial characterization, degeneration of the distal axon has been studied in depth and is well-characterized (Figure 1.1). Immediately following injury, the membrane on both proximal and distal axons quickly reseal in a calcium-dependent manner (Eddleman et al., 1998) and form dystrophic end-bulbs due to the accumulation of retrograde and anterograde transport of proteins and organelles (Zelená et al., 1968; Wang et al., 2012). The sudden influx of calcium ions (Ca^{2+}) local to the injury site activates calpain proteases, required for breaking down the cytoskeletal proteins and effectively degenerating

hundreds of micrometers of the newly resealed axon membrane (George et al., 1995; Kerschensteiner et al., 2005). This process, known as “acute axon degeneration” (AAD), precedes a latent phase in which the distal axon remains quiescent and there are no gross morphological changes observed to the integrity of the axonal membrane. A second slow influx of extracellular Ca^{2+} occurs throughout the entirety of the distal axoplasm, initiating the final destructive phase of WD. Similar to AAD, cytoskeletal proteins spectrin, microtubules and neurofilaments are broken down by calpain proteases (Johnson et al., 1991; Ma et al., 2013), resulting in mitochondrial swelling, energy depletion, and ultimately complete and explosive fragmentation of the detached axon fragment (Wang et al., 2012; Park et al., 2013). Over time, the lingering axonal debris is cleared from the environment by engulfment from surrounding phagocytes (MacDonald et al., 2006; Doherty et al., 2009).

Calcium has been proven to play a critical role in the execution of WD. Pharmacological calpain inhibitors or overexpression of the endogenous calpain inhibitor, calpastatin, modestly delay axon degeneration after axotomy (Yang et al., 2013; Zhang et al., 2016). Similar effects are seen *in vitro* when extracellular calcium concentrations are decreased by use of chelating agents such as ethylene glycol tetraacetic acid (EGTA), or inhibiting axonal calcium influx by chemical antagonists to L-type calcium channels, as they are sufficient to block the final stage of fragmentation of the axon (Schlaepfer, 1974; George et al., 1995; Ma et al., 2013; Vargas et al., 2015). Conversely, facilitating the influx of

intracellular Ca^{2+} by addition of different calcium ionophores (ionomycin and A23187) *in vitro* is sufficient to quickly drive axon degeneration in the absence of injury (Schlaepfer and Hasler, 1979; George et al., 1995; Knoferle et al., 2010). Together these data indicate calcium is necessary and sufficient to drive degeneration and that the execution of the final phase of WD is dependent on the influx of Ca^{2+} ions after injury.

Axon Death Can Be Blocked

After Waller's groundbreaking discovery in 1850, it was widely accepted that transected axons undergo passive degeneration – that is to say, they simply waste away. Many postulated that, due to the separation of the distal axon from the nutrient providing cell soma, established reservoirs of essential "survival factors" fell below a critical threshold inducing a self-destructive process (Lubińska, 1977). This idea of passive axonal atrophy held true for nearly 150 years, until the serendipitous discovery of the novel mutant mouse strain, C57BL/Ola, changed how the field viewed injury-induced axon degeneration. When sciatic nerves of these mice were severed, distal axons within the nerve bundle remained morphologically intact for weeks, compared to wild-type mice whose axons began to degenerate within hours of injury. Not only were the axons of the C57BL/Ola mice physically unchanged, but they proved to have the capacity to conduct action potentials up to 14 days after injury. Conduction of action potentials within severed wild-type nerves failed after only 2 days (Lunn et

al., 1989). The opportune discovery of this spontaneous mutation provided the first evidence that WD could be blocked.

The C57BL/Ola mouse strain, aptly renamed *Wallerian degeneration Slow* (*Wld*^{S}), harbored a mutation that mapped to chromosome 4 (Lyon et al., 1993). The nature of the mutation was found to be an 85-kb tandem triplication of the genome (Coleman et al., 1998) whose rearrangement resulted in the fusion of two genes, which when expressed, generated a novel chimeric protein. The neomorphic Wld^S protein is comprised of 3 distinct domains. The N-terminal 70 amino acids (N70) stem from the truncated N-terminus of the E4-type ubiquitin ligase, Ube4b, followed by a novel 18 amino acid peptide sequence generated from the 5' untranslated region (UTR) of the nicotinamide adenine dinucleotide (NAD) biosynthetic enzyme, *nicotinamide mononucleotide adenylyltransferase 1 (nmnat1).* The C-terminal 285 amino acids compose the functional, full-length Nmnat1 protein (Mack et al., 2001). The Wld^S protective phenotype is dosage-dependent, as transgenic animals expressing higher levels of Wld^S display stronger levels of axon protection compared to lower expressing animals (Mack et al., 2001). Wld^S is functionally conserved across species; not only does over-expression of the Wld^S protein provide robust axon protection from injury in other vertebrate models such as rats (Adalbert et al., 2005), zebrafish (Martin et al., 2010), and human neurons (Kitay et al., 2013), Wld^S also inhibits degeneration in *Drosophila* models of WD (MacDonald et al., 2006; Xiong et al., 2012; Neukomm et al., 2014).

To understand how Wld^S preserves axons after injury, we must first look at each of its domains independently. In yeast, Ube4b is essential for the multi-ubiquitination of proteins and is a key component of the ubiquitin proteasome system (UPS) (Koegl et al., 1999; Hoppe, 2005). Blocking the UPS with a pharmacological inhibitor, MG132, is sufficient to delay, but not inhibit WD completely, both *in vitro* and *in vivo* (Zhai et al., 2003). While N70 of Wld^S does not retain the ability to ubiquitinate, it can bind known Ube4e substrates. Specifically, N70 interacts directly with the AAA+ (ATPases Associated with diverse cellular Activities) ATPase family member vasolin-containing protein (VCP), and this association regulates the subcellular distribution of Wld^S, re-localizing it from the nucleus to the axoplasm (Laser et al., 2006; Wilbrey et al., 2008; Avery et al., 2009). Specific overexpression of the N70 domain can mildly delay axon degeneration *in vitro* (Zhai et al., 2003). N70's inability to ubiquitinate its substrates is thought to have a dominant negative effect on the UPS, resulting in defective axon degeneration after injury.

The C-terminal domain of Wld^S encodes the full-length *Nmnat1* gene (Mack et al., 2001). Initial characterizations of the *Wld^S* mouse indicate a marked increase of Nmant1 enzymatic activity without showing any alterations to the overall steady-state of NAD+ levels (Mack et al., 2001). Multiple studies confirm these findings and give evidence that the enzymatic activity of Nmnat1 is required for the protective nature of the *Wld^S* mutation, as mutations in the catalytic domain of Nmnat1 within Wld^S render the protein inactive in the context

of axon protection. (Araki, 2004; Wang et al., 2005; Avery et al., 2009; Sasaki and Milbrandt, 2010). Interestingly, overexpression of Nmnat1 is significantly weaker at protecting axons from degenerating *in vitro* and *in vivo,* as compared to Wld^S mutant and transgenic mice (Conforti et al., 2007). Furthermore, decreasing expression levels of Nmnat1 in *Nmnat* heterozygous mice shows no effect on the rate of WD (Conforti et al., 2011). Together, these data suggest Nmnat1 activity is necessary but not sufficient to phenocopy the robust protective phenotype of Wld^S.

In mammals, there are three paralogs of Nmnat: Nmnat1, Nmnat2, and Nmnat3. Nmnat1 is expressed in the nucleus, whereas Nmnat2 and Nmnat3 localize to the Golgi and mitochondria, respectively (Zhang et al., 2003; Berger, 2005; Mayer et al., 2010). As previously mentioned, overexpression of Nmnat1 alone could not offer axonal protection, however when the nuclear localization signal is disrupted, Nmnat1 translocates to the cytoplasm where it phenocopies the protective nature of *Wld*^{S} (Beirowski et al., 2009). This is not surprising since the direct interaction with VCP relocates Wld^S outside of the nucleus (Wilbrey et al., 2008). These findings suggest the protective mechanism of action of Wld^S occurs in the cytoplasm and requires both the enzymatically active Nmnat1, and the N70 Ube4b substrate binding domain to prevent degeneration.

Nmnat2: The Essential Survival Factor Hypothesis, Revisited

The finding that cellular redistribution of Nmnat1 from the nucleus to the cytoplasm robustly protects axons after injury reinvigorated the previously dismissed essential survival factor hypothesis; that is, separation of the distal axon from the cell body inhibits the anterograde transport of trophic factors required for axon survival. Since Nmnat1 expression is restricted to the nucleus, researchers turned their attention towards the other Nmnat homologs, Nmnat2 and Nmnat3, assaying their role in axon degeneration. Overexpression of any of the three proteins were sufficient to protect axons from degeneration only if they are translocated to the cytoplasm (Beirowski et al., 2009; Yahata et al., 2009; Avery, 2010; Gilley and Coleman, 2010). Conversely, only depletion of endogenous Nmnat2 by short interfering RNA (siRNA) knockdown in mouse superior cervical ganglia (SCG) and dorsal root ganglia (DRG), was sufficient to trigger axon degeneration in the absence of injury. Both knockdown of Nmnat1 and Nmnat3 had little effect on the health and morphology of the axons (Gilley and Coleman, 2010). Similarly, overexpression of Nmnat1 or Nmnat3 was not sufficient to compensate for the loss of Nmnat2 by siRNA knockdown, as cultured neurons still degenerated. Taken together, these data provide substantial evidence that Nmnat2 is required for promoting and maintaining the survival of the axon.

To confirm Nmnat2 is provided by the cell body and not synthesized locally within the distal axon, nascent protein synthesis was blocked *in vitro* by

local application of a pharmacological translational inhibitor, cyclohexamide (CHX), using compartmentalized Campenot cell culture chambers (Campenot, 1977). CHX application only to cell bodies but not neurites of SCG cultures induced axon degeneration. Therefore, maintenance and survival of the axon depends on the anterograde transport of Nmnat2 translated within the cell body (Gilley and Coleman, 2010).

Nmnat2 is the most labile of the three Nmnat isoforms, with an observed half-life of approximately 4 hours *in vitro* (Gilley and Coleman, 2010). Coincidentally, this correlates precisely with the onset of axon degeneration *in vitro*. Blocking the transport of Nmnat2 to distal axons either by physical transection or by pharmacologically inhibiting nascent translation of Nmnat2, identifies Nmnat2 as an essential protein in axon maintenance and supports its role in the essential survival factor hypothesis of WD.

Drosophila as a Model Organism

The initial identification of the *Wld*^{S} gene turned the axon degeneration field on its head. No longer was WD thought to be a simple, passive cellular process, but in fact it could be blocked by overexpressing the Wld^{S} protein. The notion that axons can persist for weeks in the absence of support from their cell bodies implied there may be an intrinsic pathway signaling an axon to degenerate upon injury, but the key players regulating this process remained unknown. Identifying these endogenous regulators required a model organism that was suitable for

large scale *in vivo* genetic screens, one that was simple to work with, and most importantly, one in which the process of WD was conserved. Satisfying these criteria made *Drosophila melanogaster* an excellent model organism to investigate the genes that execute WD *in vivo*.

A wide array of sophisticated tools available allow for simple, yet elegant genetic manipulations in *Drosophila*. The GAL4-UAS (upstream activating sequence) binary system, originally identified in the yeast *Saccharomyces cerevisiae,* allows for tissue specific labeling (Duffy, 2002). Protein expression of the GAL4 transcriptional activator is regulated by surrounding enhancer elements within the *Drosophila* genome. GAL4 will bind UAS and drive expression of a downstream gene of interest in a tissue specific manner. Using this technique, we can label specific subsets of cells with fluorescent markers or even ectopically express proteins for analysis in small or large subsets of cells.

A second advantage of using *Drosophila* as a model organism is the ease with which unbiased, forward genetic screens can be performed *in vivo*. The common chemical mutagen ethyl methane sulfonate (EMS) randomly induces mutations within the genome, primarily with a bias towards guanine/cytosine to adenine/thymine transitions (St Johnston, 2002; Bökel, 2008). These lesions can result in frameshift mutations, missense mutations, truncated peptides due to the introduction of premature stop codons, or even small genomic deletions. To avoid lethality when mutating essential genes, screens can be performed employing mosaic analysis with a repressible cell marker (MARCM) (Lee and

Luo, 2001). MARCM uses the Gal4/UAS binary system along with the Gal4 repressor (GAL80), in combination with homologous recombination via the flippase recombinase (FLP) and FLP recognition target (FRT) system (Golic and Lindquist, 1989). After induction of post-mitotic FRT recombination by tissue specific FLP expression, a population of GAL4 expressing cells will be homozygous mutant in the otherwise heterozygous background of the animal. Combined, these genetic tools and techniques set the stage to investigate mechanisms of WD in *Drosophila*.

Modeling Wallerian Degeneration in *Drosophila*

The first experiments modeling WD in *Drosophila* fluorescently labeled a subset of olfactory receptor neurons (ORNs) in the adult using the *OR22a-GAL4* driver (Dobritsa et al., 2003; MacDonald et al., 2006). The cell bodies of these peripheral neurons reside in the distal most antennal segments, project their axons into the head capsule and synapse within specific glomeruli of the neuropil, called the antennal lobe. To model WD, antennae were mechanically ablated, severing the distal axons from their respective cell bodies. The distal axons within the head undergo the stereotyped degenerative process in which they fragment 24 hours post axotomy and are cleared by the surrounding glia within 3 days (MacDonald et al., 2006). As mentioned in previous sections, this WD is completely blocked by the ectopic expression of Wld^S (Avery et al., 2009; MacDonald et al., 2013). The development of this ORN system and the ability to

perform large-scale, forward genetic screens in *Drosophila* that led Osterloh *et al.* to discover *dsarm* (*Drosophila* sterile-α and Armadillo motif), the first gene shown to be essential for the execution of WD (Osterloh et al., 2012).

A second model of WD, the larval nerve crush, takes advantage of an earlier stage of development in *Drosophila*. Segmental nerves bridge the connection between the body wall and the ventral nerve cord (VNC) of the animal and contain both efferent motor neurons and afferent sensory neurons (Xiong et al., 2010; Rooney and Freeman, 2014). In this model, fluorescently labeled segmental nerves are easily visualized *in vivo* along the ventral side of the animal through the thin, transparent cuticle. To simulate injury, the nerves are firmly compressed using forceps, typically resulting in the paralysis of the animal posterior to the crush site (Xiong et al., 2010). By taking a combinatorial approach, first using larval crush and then the ORN assay, Xiong *et al.* discovered that a mutation in *highwire (hiw),* a gene encoding an E3 ubiquitin ligase, protected axons from WD (Xiong et al., 2012). This crush model is ideal for not only studying WD in the distal axon segment, but also cellular responses in the proximal axon or cell body, degeneration of synapses at the neuromuscular junction (NMJ), and peripheral neuron regeneration. While the larval nerve crush facilitates the study of these aspects of degeneration, however, one limiting factor of the system is its short time-frame (2-3 days) to make observations before the animal undergoes metamorphosis (Hales et al., 2015).

The time-consuming nature of ORN ablation and the restrictive developmental window associated with the larval nerve crush inspired the development of a new model to study WD in *Drosophila* – the adult wing. Mechanosensory neuron specific GAL4 drivers can label different subpopulations of the 250 neurons within the adult wing (Fang et al., 2012; Neukomm et al., 2014). The cell bodies of these mechanosensory neurons position themselves throughout the L1 vein along the anterior margin of the wing, projecting their axons into the thoracic ganglia. Similar to the larval nerve crush, the transparency of the wing cuticle allows for visualization of the fluorescently labeled neurons without labor intensive dissections or time consuming antibody staining required for the ORN assay. The wing is simply cut in half, injuring most of the labeled neurons and inducing degeneration, while those neurons that remain uninjured serve as internal controls. As such, WD can be studied along-term neuron maintenance within the same wing.

dSarm/Sarm1 Regulates Wallerian Degeneration

In 2012, a large-scale forward genetic screen using the *Drosophila* ORN system identified *dsarm* as the first endogenous regulator of WD *in vivo.* (Osterloh et al., 2012). Injury-induced degeneration is strongly inhibited in *dsarm* mutant axons and morphologically preserved axons are present for the life of the animal (~50 days) (Osterloh et al., 2012). Importantly, the axon protective phenotype is

conserved in mammals and can be observed *in vitro and in vivo*. DRG explants from *Sarm1*$^{-/-}$ mice are protected from degeneration for 72 hours after injury *in vitro*, while distal nerve bundles from lesioned sciatic nerves display morphologically intact axons up to 2 weeks post-injury *in vivo* (Osterloh et al., 2012; Gerdts et al., 2013). *dsarm/Sarm1* appears to function specifically in the axonal injury response, as loss of function mutations do not influence normal developmental pruning, induced apoptosis, or trophic factor withdrawal (Osterloh et al., 2012; Gerdts et al., 2013).

dSarm/Sarm1 is a member of the toll/interleukin-1 receptor (TIR) domain adaptor protein family (O'Neill and Bowie, 2007) and was initially discovered to be a negative regulator of NF-κB and interferon-regulatory factor (IRF) activation during immune response signaling (Carty et al., 2006). Involved not only in immune signaling, the *Caenorhabditis elegans* homolog, *tir-1,* gives evidence that Sarm proteins signal to downstream mitogen-activated protein kinase (MAPK) cascades to regulate a number of cellular processes (Mink et al., 2001; Chuang and Bargmann, 2005). dSarm/Sarm1 protein consist of multiple domains, each with distinct predicted functions. Structure-function studies indicate the N-terminal Armadillo/HEAT domain (ARM) acts as an auto-inhibitory domain, blocking active Sarm signaling until released by an unknown factor (Chuang and Bargmann, 2005; Gerdts et al., 2011; Neukomm et al., 2017). Two tandem sterile-α motif domains (SAM) establish protein-protein interactions and are necessary for the multimerization of Sarm molecules (Kim and Bowie, 2003;

Chuang and Bargmann, 2005; Gerdts et al., 2013). Finally, the C-terminal toll/interleukin-1 receptor homology domain (TIR) domain executes the communications to the downstream effector proteins in the signaling cascade (Chuang and Bargmann, 2005; O'Neill and Bowie, 2007; Gerdts et al., 2013).

As axonal NAD+ levels and Nmnat2 activity have previously been implicated as important factors involved in axon degeneration. Recent research has attempted to identify potential correlations with between dSarm/Sarm1 and these molecules, but the results are conflicting. Elegant *in vitro* experiments show rapid depletion of NAD+ levels within minutes of the activation of Sarm1-induced degeneration, later proven to be due to an intrinsic NADase activity within the SAM-TIR domains of the Sarm1 protein (Gerdts et al., 2015; Essuman et al., 2017). Resupplying NAD+ by increased cytoplasmic Nmnat2 enzyme activity can sufficiently block Sarm1-induced axon degeneration, suggesting Sarm1 acts upstream of Nmnat2 (Gerdts et al., 2015). In *Drosophila*, spontaneous degeneration caused by *dnmnat* loss of function is suppressed in *axed,* but not *dsarm,* mutant neurons. This places *dSarm* genetically upstream of *nmnat.* In contrast to these data, *in vivo* studies of *Nmnat2*$^{-/-}$ show perinatal lethality is completely rescued in *Nmnat*$^{-/-}$*, Sarm1*$^{-/-}$ double mutant mice. These double knockout mice develop normally, are viable, and exhibit no overt axon morphology or behavioral phenotypes, suggesting *Sarm1* is epistatic to *Nmnat2* (Gilley et al., 2015; 2017). Therefore, further investigation is required to fully

understand where Nmnat2 functions in the current axon death pathway (Figure 1.2).

Highwire/Phr1 Controls Axonal Nmnat2 Levels

Highwire is an E3 ubiquitin ligase and was the second endogenous regulator of injury-induced axon degeneration to be discovered. Loss of *hiw* confers significant protection from nerve crush in segmental nerves within the *Drosophila* larva, as well as in ablated ORN in the adult antennae (Xiong et al., 2012). *Hiw* mutant nerves are both morphologically and functionally preserved, as they still produced spontaneous excitatory junction potentials 24 hours after crush (Xiong et al., 2012). Similar to *dsarm/Sarm1*, the loss of *Phr1* (Proteins associated with Myc, Hiw, RPM-1), the mammalian homolog of *hiw*, modestly protects axons from WD both *in vivo* and *in vitro* (Babetto et al., 2013).

Structurally, Hiw is a large protein (larger than 400kDa) and is comprised of the following domains: RCC1-like GEF domain (RLD), two PHR family specific domains, an RAE-1 binding domain (RBD), an FSN-1 binding domain 1 (FBD1) and a really interesting new gene (RING) ubiquitin ligase domain (Grill et al., 2016). Together, these domains are required to modulate a number of cellular processes regulating synaptic growth and development, cytoskeletal stabilization, axon guidance, as well as degeneration and regeneration (Wan et al., 2000; McCabe et al., 2004; Massaro et al., 2009; Shin and DiAntonio, 2011; Fang and Bonini, 2012; Grill et al., 2016).

In the context of degeneration, Phr1 limits levels of axonal Nmnat2 through association with members of an atypical Skp/Cullin/F-box (SCF) type E3 ubiquitin ligase complex (Yamagishi and Tessier-Lavigne, 2016). Nmnat2 levels were found to be increased in neurites of both *Phr1*$^{-/-}$ and Skp1a knockdown DRG explants (Babetto et al., 2013; Yamagishi and Tessier-Lavigne, 2016). Decreasing Nmnat2 levels by short hairpin RNA (shRNA) in *Phr1*$^{-/-}$ DRG explants reversed the protective phenotype and induced spontaneous degeneration (Babetto et al., 2013). Phr1 drives axon degeneration through regulation of the axoplasmic concentration of Nmnat2, while mutations in *hiw/Phr1* result in the stabilization and accumulation of Nmant2, promoting to axon survival.

Similarly, through ubiquitination, Hiw/Phr1 also regulates the levels of *dual leucine kinase/wallenda (dlk/wnd)*, a MAP kinase kinase kinase (MKKK) shown to promote axon degeneration after injury (Miller et al., 2009; Xiong et al., 2010). Loss of function mutations in *dlk/wnd* show mild protection from axotomy, a weak phenotype most likely due to compensation from other redundant members in the MAPK/JNK signaling pathway. *In vitro* data from mammalian DRG axotomy experiments shows modest protection of axons after injury only when there is knockdown of both MKK4/MKK7 (MAP kinase kinase 4/ MAP kinase kinase 7) or all three JNK signaling molecules (JNK1/JNK2/JNK3) simultaneously (Yang et al., 2015).

Axundead Signals Downstream of dSarm in Axon Death

Most recently, Neukomm and Burdett *et al.* identified *axundead (axed)* as the third novel gene proven to endogenously regulate injury-induced axon degeneration (Neukomm et al., 2017). In *Drosophila, axed* encodes a protein with two primary domains. The broad-complex, tramtrack, bric-a-brac (BTB) domain is canonically involved in protein-protein interactions as well as multimerization (Bardwell and Treisman, 1994; Chaharbakhshi and Jemc, 2016). As for the BTB and C-Terminal Kelch (BACK) domain, it has been shown to bind various substrates, however not much else is known (Stogios and Privé, 2004; Chaharbakhshi and Jemc, 2016). BTB-Kelch proteins aid the Cullin3-based-ubiquitin ligase complex recognize substrate proteins targeted for proteasome degradation (Pintard et al., 2004), further corroborating the involvement of the UPS in WD.

Axed mutant neurons demonstrate complete inhibition of WD for the life of the animal, a level of protection that rivals *dsarm* mutants. Similar to *dsarm*, there is no apparent bias towards specific neuronal subtypes, as axon degeneration was blocked in all neurons assayed. Loss of function *axed* mutants are capable of blocking gain of function dSarmΔARM induced degeneration, indicating that dSarm signals through Axed to execute axon death. Epistatic analysis between *axed* and the *Drosophila Nmnat2* homolog *dnmnat* (*Drosophila* only have one Nmnat isoform, where mammals have three) places *axed* downstream of Nmnat as *axed* mutants completely suppress Nmnat depletion

induced degeneration (Neukomm et al., 2017). These data together indicate the known WD and axon degeneration signaling cascades converge on Axed to execute axon degeneration (Figure 1.2).

Pebbled, a C_2H_2 Zinc Finger Transcription Factor

Pebbled (peb), also annotated as *hindsight (hnt)* in previous literature*,* encodes an evolutionarily conserved zinc finger transcription factor required for various cellular processes during *Drosophila* development, including, but not limited to: large scale epithelial cell movement, cell polarity and recently identified, axon guidance (Yip et al., 1997; Pickup et al., 2002; Oliva et al., 2015). Peb expression is restricted to the nucleus and can be found within specific tissues of the developing embryo, such as the amnioserosa (AS), anterior midgut, and posterior midgut. As the animal enters later stages of development. The Peb expression pattern changes and is present in the trachea, peripheral nervous system, and neuronal precursors within the imaginal discs (Yip et al., 1997; Pickup et al., 2002), however Peb remains undetectable in the CNS throughout development (Oliva and Sierralta, 2010). *peb* is an essential gene, as loss of function *peb* mutants fail to develop correctly, resulting in lethality (Strecker and Yip, 1991; Yip et al., 1997; Reed et al., 2001).

Structurally, Peb is 1893 amino acids long, contains two predicted α-helical coiled-coil domains and fourteen zinc finger motifs clustered along the length of the protein (Yip et al., 1997). The two α-helical coiled-coil domains are

predicted to be involved in protein-protein interactions, while the zinc finger domains are predicted to bind target DNA (Figure 1.3). Peb is a member of the Cys_2-His_2 (C_2H_2) zinc finger protein family. The C_2H_2 domain is the founding member of the zinc finger domain containing proteins and is the most common motif across all zinc finger proteins (Razin et al., 2012). Within each motif, a zinc ion forms four bonds between the two N-terminal cysteine residues and the C-terminal histidine residues, and the domain assumes a finger-like protrusion. This "finger" associates with and grasps the major groove of its target DNA sequence (Wolfe et al., 2000; Klug, 2010). The α-helical domain within each finger is capable of recognizing and binding to three nucleotide base pairs within the groove, and it is amino acids -1, 3, and 6 within the α-helix that determine the DNA sequence specificity (Razin et al., 2012).

Peb was initially identified in AS maintenance and is required for germ band retraction, a developmental process involving large-scale changes in cell shape, morphology, and ultimately tissue rearrangement within the embryo (Frank and Rushlow, 1996; Yip et al., 1997; Lynch et al., 2013). During normal development, the germ band elongates as cells reposition themselves along the anterior-posterior axis, displacing the AS cells in a process known as germ band extension. The tightly associated AS cells, compressed along the dorsal-ventral axis and now sandwiched between the fully extended germ band, return to their original position facilitating the shortening and retraction of the germ band (Frank and Rushlow, 1996; Schöck and Perrimon, 2002). Embryos with loss of *peb*

expression in the AS cells fail to undergo proper germ band retraction, resulting in an over extended, U-shaped germ band phenotype, ultimately leading to premature loss of AS cells (Frank and Rushlow, 1996; Lamka and Lipshitz, 1999).

Following germ band retraction, a second developmental process requiring *peb* is dorsal closure, or the elongation and migration of dorsal epithelial cells over the exposed AS of the embryo. Proper dorsal closure requires both focal adhesion complex formation as well as c-Jun N-terminal Kinase (JNK) signaling within the leading edge of the dorsal epithelial cells (Reed et al., 2001; 2004). Prior to the commencement of dorsal closure, a sudden spike in JNK signaling levels occurs in AS cells then drastically decrease in a *peb* dependent manner. Peb is found to positively regulate expression of *puckered (puc)*, the JNK phosphatase, thus reducing levels of active JNK signaling specifically within AS. It is this establishment of a low-high boundary of JNK signaling between the AS and the leading edge of the migrating dorsal epithelium that permits focal adhesion formation required for efficient cellular migration (Llense and Martín-Blanco, 2008). AS cells of *peb* mutants retain high JNK signaling and inhibit the establishment of focal adhesions, resulting in dorsal closure failure (Reed et al., 2001).

Peb has been shown to regulate cellular proliferation and differentiation through Notch and Hedgehog (Hh) signaling. Follicular epithelial cells covering the germline stereotypically undergo a series of mitotic cellular divisions (M

cycle) then switch to an endo-replication cycle (E cycle) prior to differentiation. This M/E cell cycle conversion requires Notch-Delta signaling, and disruptions in this signaling cascade results in over-proliferation or premature differentiation of the follicle cells (W M Deng, 2001). *Peb* mutant follicle cells fail to downregulate expression of known Notch signaling molecules required for the M/E cycle switch, *cut* and *string,* and cannot successfully transition between the M/E cycle. Conversely, cells ectopically expressing Peb prematurely differentiate by inhibiting cell proliferation through indirect suppression of Hh (Lum and Beachy, 2004; Sun and Deng, 2007).

More recent work has identified Peb's role in regulating axon guidance. Firstly, overexpression and mosaic knockdown of Peb in larval and adult visual systems results in the mistargeting of photoreceptor axons to their correct destinations (Oliva and Sierralta, 2010). This overshooting of axon terminals is a result of the altered expression levels of *jitterbug/Filamin (jbug)*, the actin binding protein, and other axon guidance and cytoskeletal regulating proteins (Oliva et al., 2015). Secondly, biochemical assays and chromatin immunoprecipitation (ChIP) data demonstrate Peb directly binds to and acts as a negative regulator to *nervy* (*nvy*) in the larval salivary gland (Ming et al., 2013). *nvy*, the *Drosophila* homolog of the mammalian proto-oncogene myeloid translocation gene 8 (MTG8), has a predominantly nuclear expression pattern, but is implicated in a non-canonical cytoplasmic role regulating axon guidance (Terman and Kolodkin, 2004). In the cytoplasm, Nvy acts as a kinase anchoring protein (AKAP),

coupling the cyclic adenosine monophosphate (cAMP) dependent protein kinase (PKA) to the Semaphorin 1a (Sema-1a) receptor Plexin A (PlexA) (Terman and Kolodkin, 2004).

Thesis Overview

The overall goal of this thesis was to identify previously unidentified genes required to drive WD *in vivo.* To do so, I participated in a large-scale, unbiased, forward genetic screen using the *Drosophila* adult wing to model and identify regulators of WD. In CHAPTER II, I describe the setup and execution of the wing screen in which we identified *peb* and alleles of other genes as regulators of WD. CHAPTER III focuses on a detailed characterization of *peb* mutants and their role in WD, the identification of a novel degenerative phenotype, and cell type specificity of axon protection after injury. CHAPTER IV is a discussion of how Peb adds to the current model of axon degeneration and novel questions that arise with this discovery. Finally, in the appendices, I present the data generated from two other projects: the gain of function dSarmΔARM suppressor screen, and observations of abnormal dendrite morphology in loss of function *peb* wing sensory neurons.

Figures & Tables

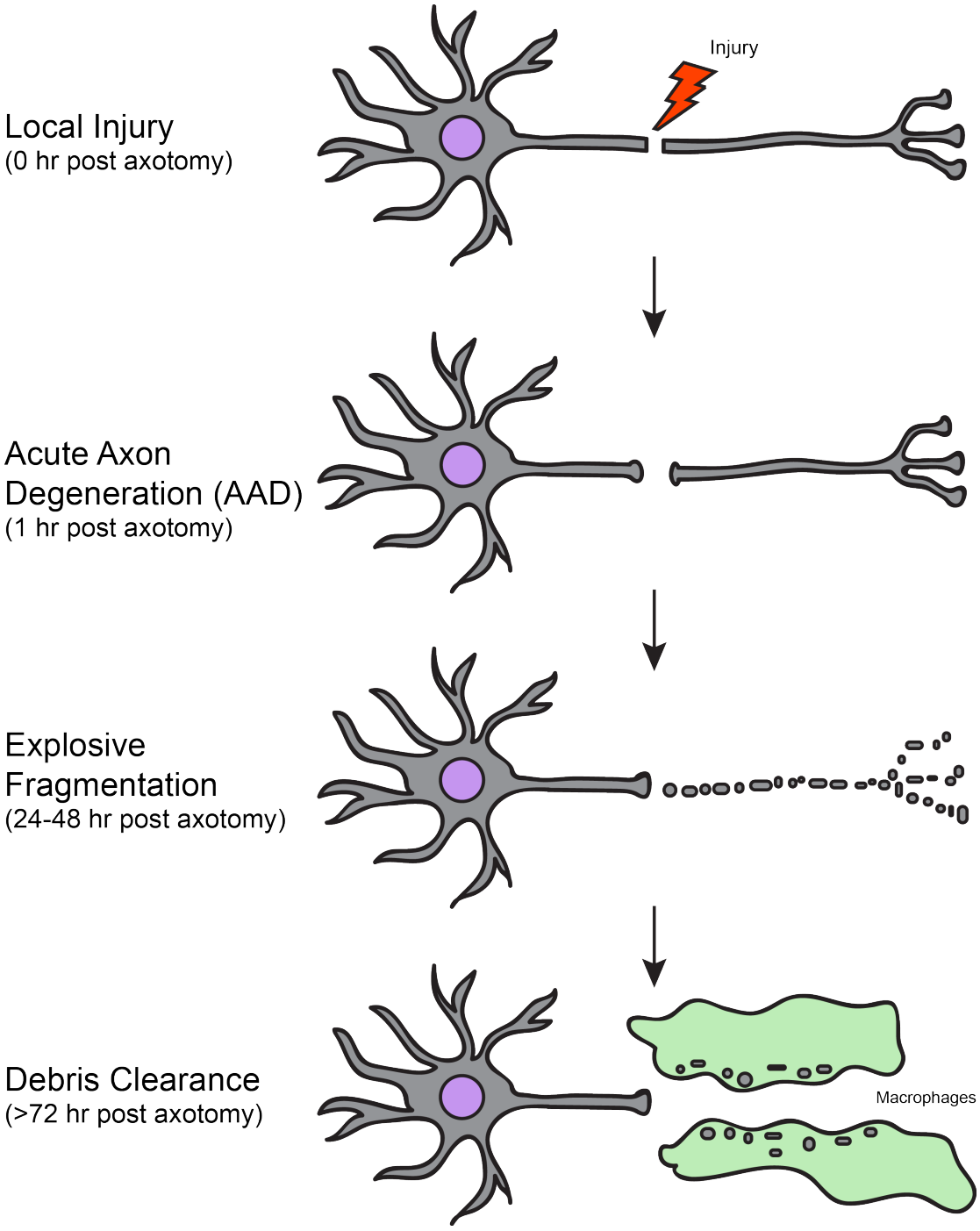

Figure 1.1. Transected Axons Undergo Stereotyped Degeneration.

Figure 1.1. Transected Axons Undergo Stereotyped Degeneration.
Schematic representing the different stages of Wallerian degeneration *in vivo*. The distal axon is separated from the proximal cell body by local injury. Within 1 hour post axotomy, both proximal and distal axon stumps form dystrophic endbulbs and degenerate a few hundred micrometers in a process called acute axon degeneration (AAD). Following a latent phase lasting 24-48 hours in which there are no gross morphological changes, the distal axon segment loses structural integrity and undergoes an explosive fragmentation event. Surrounding macrophages (green cells) actively engulf the axonal debris over the course of the next few days, with full clearance approximately 5 days post axotomy.

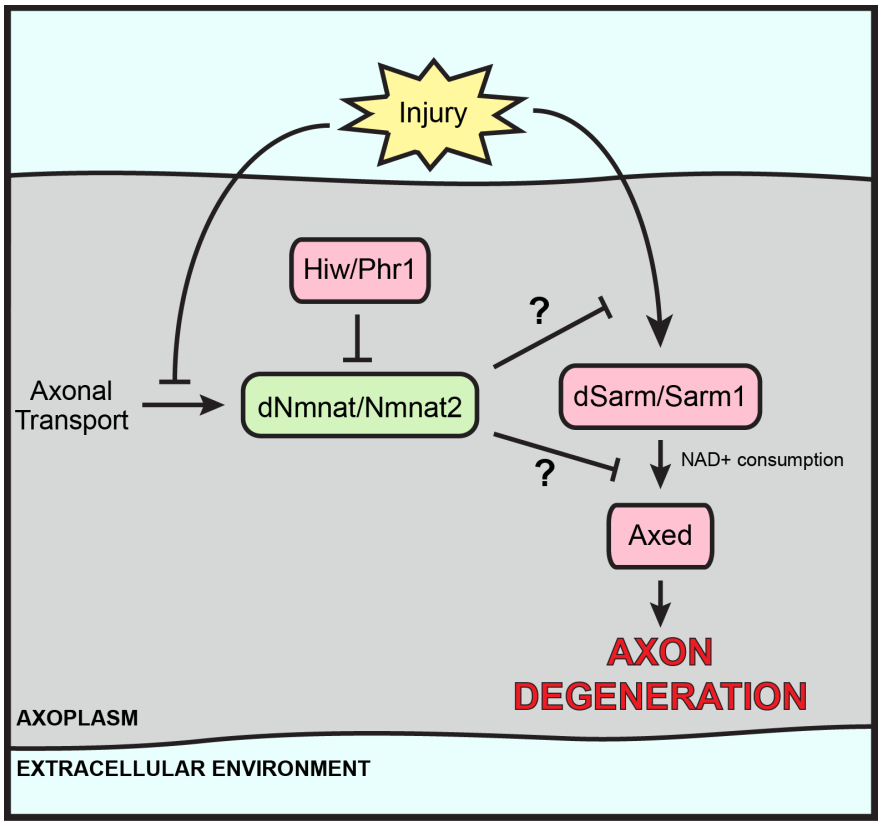

Figure 1.2. Current Model of Injury-Induced Axon Degeneration Signaling. Schematic describing the current model of intra-axonal signaling after injury with both pro-degenerative molecules (red) and protective molecules (green). External injury activates a local, pro-degenerative dSarm/Sarm1-Axed signaling cascade within the distal axon, while simultaneously inhibiting transport of nascent dNmnat/Nmnat2 molecules from the cell soma. Hiw/Phr1 regulates axonal dNmnat/Nmnat2 levels by targeting it to the proteasome for degradation. The exact placement of dNmnat/Nmnat2 in this pathway remains controversial, as there are conflicting data placing it both upstream and downstream of dSarm/Sarm1.

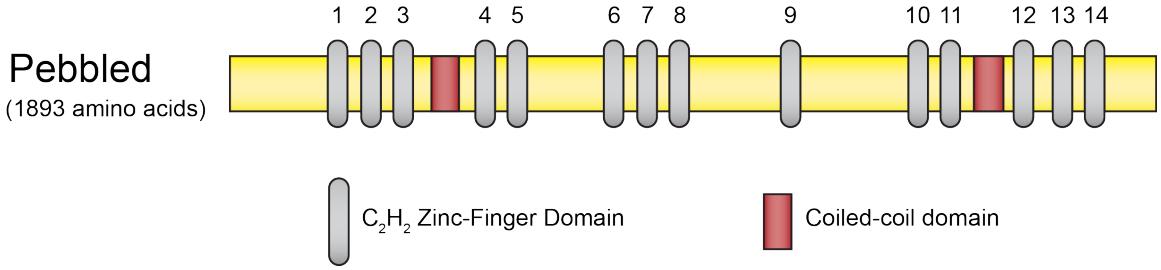

Figure 1.3. Protein Structure of Pebbled.
pebbled encodes the zinc finger transcription factor Pebbled. It is a 1,893 amino acid long protein and contains fourteen Cys2-His2 (C_2H_2) zinc finger binding motifs (gray ovals) as well as two predicted coiled-coil domains (red squares). (Diagram adapted from Ming *et al.,* 2013, with permission from *Differentiation*)

CHAPTER II: Screening for Endogenous Regulators of Wallerian Degeneration

This work in this chapter was conducted in the laboratory of Marc Freeman at the University of Massachusetts Medical School. I performed a forward genetic screen, alongside Lukas Neukomm, Thomas Burdett, and Elizabeth Allen. Lukas Neukomm established the wing system and built all necessary *Drosophila* lines required for the screening of chromosomes 1, 2, and 3. While I was unsuccessful in isolating a mutant allele from this screen, Thomas Burdett identified the peb^{345x} allele, which I characterized and is the focus of work described in CHAPTER III. The other mutant alleles identified from this screen are described in the following publications: 11 *hiw* alleles – Neukomm *et al., PNAS* 2014; 1 $dsarm^{4314}$, $axed^{0011}$, and $axed^{2094}$ – Neukomm and Burdett *et al., Neuron* 2017.

Abstract

The ability to perform powerful forward genetic screens in *Drosophila* makes it possible to identify genes involved in the regulation of certain biological processes. One such example is the recent discovery of *dsarm* as the first endogenous regulator of Wallerian degeneration (WD) *in vivo*. With this new evidence of an intrinsic axon death mechanism, we sought to identify other genes involved in the injury-induced dSarm signaling cascade, however the established model of antennal ablation to cause WD is time consuming, low-throughput, and labor intensive. Using a newly established adult wing model of WD, we screened through over 40,000 chromosome arms and isolated a number of mutant alleles, including two novel genes, shown to regulate axon death after injury. In the work in this chapter will describe the initial set-up, execution, and preliminary identification of alleles generated from the mutagenesis screen.

Results & Discussion

Unbiased Mutagenesis Screening in the *Drosophila* Adult Wing

Using the wing model of WD previously established in the Freeman Lab described in Neukomm *et al.,* 2014, we sought to identify and characterize novel genes involved in the regulation of axon degeneration after injury. In this model, we fluorescently label a subset of peripheral mechanosensory neurons within the adult wing by expressing membrane-tethered green fluorescent protein (GFP) under the expression of the glutamatergic specific driver, *OK371-GAL4*. *OK371-GAL4* labels approximately 40 neurons within the L1 vein of the wing, however, the high number of GPF^{+} axons make injury quantifications difficult. To avoid this problem, we use MARCM to generate a low number of glutamatergic clones, allowing for single cell resolution. Briefly, we induce post-mitotic homologous recombination between FRT sites on independent chromosomes through the expression of FLP under the promoter of the neural precursor, *asense* (*ase-FLP)*. A series of *ase-FLP* were generated by random insertion throughout the *Drosophila* genome by mobilization, with each new insertion having a different level of expression. Ase-FLP expression was tested for optimal clone induction for each chromosome arm (*FRT19A, FRT40A, FRTG13, FRT2A,* and *FRT82B)*.

The fast and simple readout of the wing model of axotomy makes it an ideal system to look for suppressors of axon death. Taking advantage of the transparent nature of the wing, we can image the axons of GFP^{+} neurons directly

through the cuticle in uninjured wings (Figure 2.1A). To simulate WD, wings of live, anesthetized animals are surgically cut in half and aged for 7 days, allowing for axon degeneration and debris clearance to occur (Figure 2.1B). The aged, injured wings are removed from the animal and processed for imaging. Axons present in the proximal wing are quantified as well as the cell bodies of neurons that were not injured. Under normal WD conditions, the ratio of axons:cell bodies will be 1:1. Animals from the screen that have mutations in genes required for WD will have a greater number of axons as compared to the number of cell bodies present.

Two types of forward genetic screens, F_2-based and F_1-based, are required for coverage of the X chromosome and both autosomes, respectively (Figure 2.2). For assaying WD suppressors on the X chromosome, we were required to perform an F_2-based EMS screen, as this method requires the two X chromosomes from females for successful MARCM. *FRT19A* P_0 males were fed EMS to randomly induce mutations throughout the germline and subsequently crossed to X-balanced virgin females. Independent mutant stocks were generated when single F_1 virgin females harboring EMS mutations were crossed to X-balanced hemizygous males. Virgins from the resulting individual mutant F_2 stocks were crossed to “tester” males containing all required genetic elements to induce MARCM clones within the wing. F_3 MARCM females were then assayed for suppression of WD.

To screen autosomes, we performed a faster, F_1-based EMS mutagenesis screen. In this screen P_0 males containing FRT sites corresponding to the chromosome arm of interest were fed EMS and then crossed to "tester" virgin females. Rather than generating independent mutant stocks, wings from F_1 MARCM males were immediately assayed for WD defects. Mutant F_1 males displaying the correct phenotype were then crossed back to autosomal balanced virgin females for mutation recovery and validation. F1 males showing normal WD were discarded.

At the end of this screen, we analyzed over 40,000 mutant chromosome arms, while isolating and recovering 15 alleles of genes causing defective WD phenotypes (Table 2.1). Three mutations recovered from the F_1-based screen were mapped to the left arm of chromosome 3 – one was an allele of *dsarm (dsarm^{4314}*), the other two were alleles for the previously uncharacterized gene *axed (axed^{0011}, axed^{2094})* (Neukomm et al., 2017). Eleven of the twelve axon death defective alleles isolated in the F_2-based X chromosome screen were characterized to be alleles of the E3 ubiquitin ligase, *hiw* (Neukomm et al., 2014). The last mutant on the X chromosome, initially described as *345x* and later identified as *pebbled*, showed a novel degenerative phenotype as well as a partial suppression and delay of WD. These data show a dual approach pairing forward genetic screening with modeling WD in the *Drosophila* wing results in a fast and effective method to identify novel regulators of injury-induced axon degeneration.

Materials & Methods

Fly Strains

Flies (*D. melanogaster*) were kept on standard cornmeal agar supplemented with dry yeast at 25°C unless stated otherwise. The following lines were obtained from Bloomington Drosophila Stock Center unless otherwise stated:

X Chromosome: *y, w^{1118}, Nrg/FM7c, ElaV-Gal4, hs-FLP, UAS-mCD8::GFP, tub-GAL80,* and *FRT19A.*

2nd Chromosome: *OK371-Gal4, UAS-mCD8::GFP, FRT40A, FRTG13, tub-GAL80. ase-FLP^{2a} and ase-FLP^{2e}* ((Neukomm et al., 2014))

3rd Chromosome: *UAS-mCD8::GFP, FRT2A, FRT42B, tub-GAL80. ase-FLP^{3a} and ase-FLP^{3b}* ((Neukomm et al., 2014))

Mutagenesis screen and wing injury

Mutagenesis was performed as described previously (Neukomm et al., 2017). In brief, males were starved for 12 hours before consuming mutagen (25 mM ethyl methane sulphonate (EMS, Sigma) in 1% sucrose). Males were transferred in fresh vials for 12 hours prior to breeding to clean off residual EMS. Wing injury was performed as described previously (Neukomm et al., 2014). Wings were cut with MicroPoint Scissors (EMS, VANNAS Scissors; #72933–04) and mounted on a microscope slide in Halocarbon Oil 27 (Sigma, H8773) and covered with a

coverslip. Mounted samples were immediately used for imaging on a Zeiss spinning disc confocal microscope (Intelligent Imaging Innovations, Denver, CO).

Figures & Tables

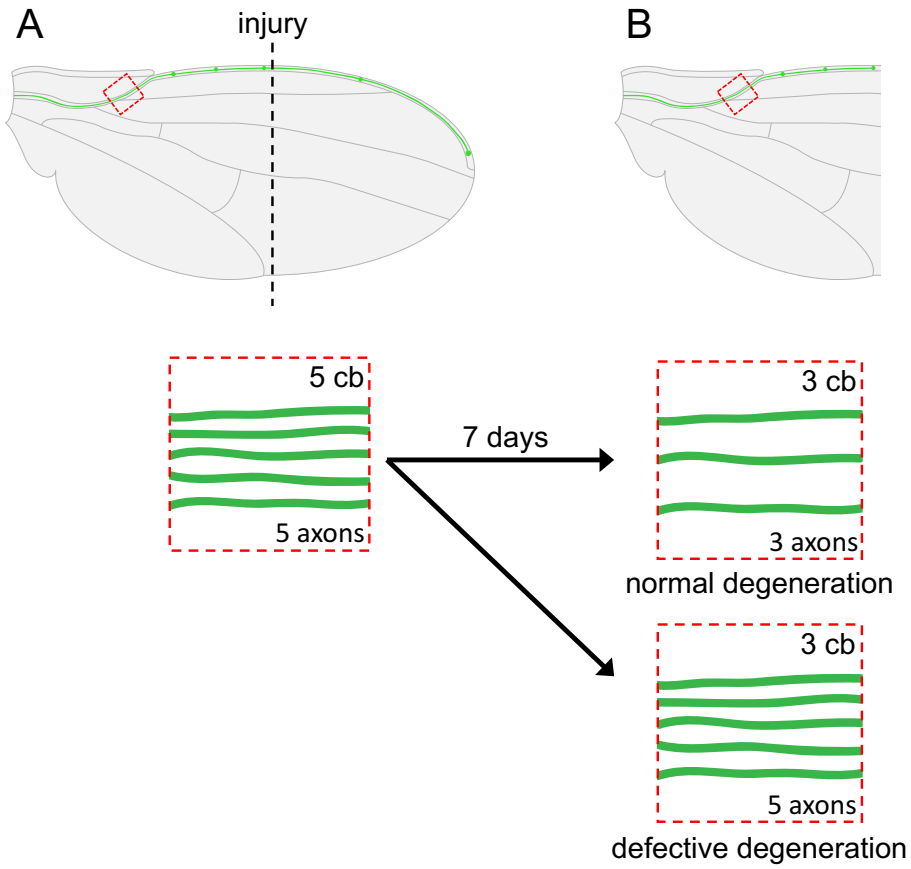

Figure 2.1 Modeling Wallerian Degeneration in the Adult Wing.
(A) Diagram of uninjured adult wing containing GFP^+ neurons within the L1 vein. Black dashed line represents injury site. Red dashed box indicates axon bundle imaging field of view, enlarged below. 5 representative GFP^+ axons are pictured with their corresponding cell bodies (cb) indicated in upper right corner. (B) Injured wing 7 days post axotomy. Enlarged insets represent two degenerative phenotypes: normal degeneration having equal number of axons and cb (3:3), or defective degeneration showing a surplus of axons as compared to uninjured cb (5:3).

Figure adapted from Neukomm and Burdett *et al.,* 2017, *Neuron,* no permission required.

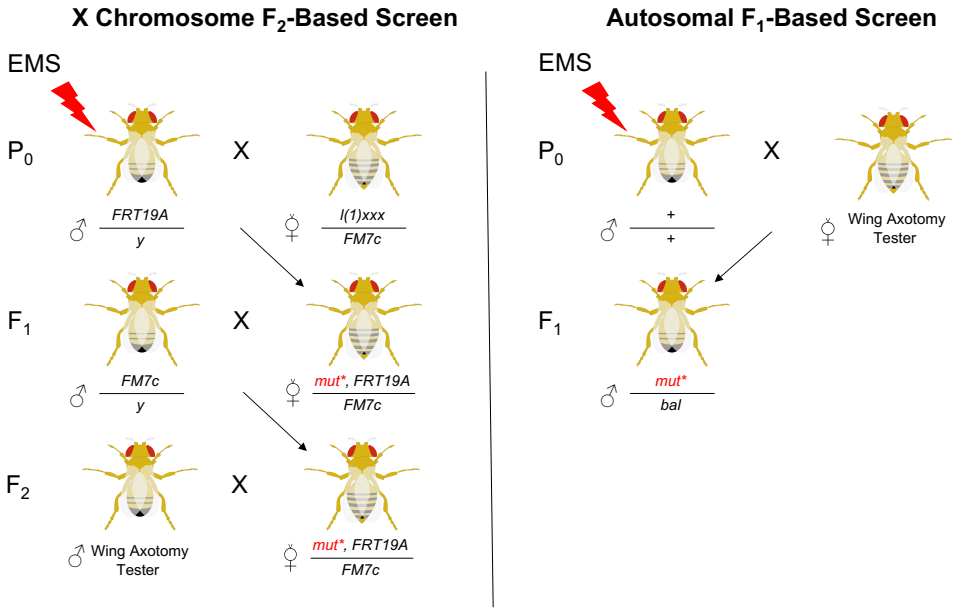

Figure 2.2. Schematic of F1 and F2 genetic screens using the *Drosophila* wing.
X chromosome F_2-based screen: individual mutagenized *FRT19A* males (P_0) are first crossed to X chromosome balanced (*lethal gene xxx/FM7c)* virgins. The next generation heterozygous F_1 mutant (*mut**) virgins are crossed to hemizygous balancer (*FM7c/y)* males to establish individual mutant stocks. F_2 virgins from individual mutant stocks are crossed to wing axotomy tester males. F_3 female progeny will contain homozygous mutant MARCM clones in wing sensory neurons and will be assayed for axon death defective phenotypes. Autosomal F_1-based screen: mutagenized P_0 males are crossed into wing axotomy tester virgins. F_1 mutant males will contain homozygous mutant MARCM clones in wing sensory neurons and will be assayed for axon death defective phenotypes.

Figure and images adapted from Neukomm *et al., PNAS,* 2014, no permission required.

Table 2.1. Total Chromosome Arms Screened

Chromosome Arm	X	2L	2R	3L	3R	Total
Number Screened	2,045	15,959	7,286	7,647	7,383	40,320
Recovered Alleles	12	0	0	3	0	15

Table 2.2. List of Genotypes Used in Wing Screen

X Chromosome
FRT19A
Nrg/FM7c
tub-GAL80, hs-FLP, FRT19A ; ok371-GAL4,UAS-mCD8::GFP,aseFLP^{2a}/ CyO ; UAS-mCD8::GFP,aseFLP^{3b}/TM3, Sb, e
Chromosome 2L
w^{1118} ; FRT40A, FRTG13/CyO
ElaV-GAL4, UAS-mCD8::GFP ; tub-GAL80, FRT40A ; UAS-mCD8::GFP, aseFLP^{3a}
Chromosome 2R
w^{1118} ; FRT40A, FRTG13/CyO
ElaV-GAL4, UAS-mCD8::GFP ; FRTG13, tub-GAL80; UAS-mCD8::GFP, aseFLP^{3b}
Chromosome 3L
w^{1118} ; ; FRT2A, FRT82B
w^{1118} ; ok371-GAL4,UAS-mCD8::GFP,aseFLP^{2e}/ CyO ; tub-GAL80, FRT2A
Chromosome 3R
w^{1118} ; ; FRT2A, FRT82B
w^{1118} ; ok371-GAL4,UAS-mCD8::GFP,aseFLP^{2e}/ CyO ; FRT82B, tub-GAL80

CHAPTER III: The Transcription Factor Pebbled/RREB1 Regulates Injury-Induced Axon Degeneration

The following chapter is a preliminary author's manuscript submitted to the scientific journal, *Proceedings of the National Academy of Sciences*, and was under revision at the time this dissertation was written. All supplemental figures have been incorporated into this thesis, therefore, figures have been renumbered and reformatted. This text in this chapter may change per required edits and will appear under following title:

The transcription factor Pebbled/RREB1 regulates injury-induced axon degeneration.

Farley JE*, Burdett TC*, Barria R, Neukomm LJ, Kenna KP, Landers JE, Freeman MR

* these authors contributed equally to this work

This work was conducted in the laboratory of Marc Freeman at the University of Massachusetts Medical School. I performed the forward genetic screen, alongside Lukas Neukomm, Thomas Burdett, and Elizabeth Allen. Thomas Burdett screened deficiency lines on the X chromosome, initially isolated, identified, and performed preliminary characterization on the gene *pebbled*. I performed all subsequent experiments. Technical assistance with imaging was provided by Romina Barria and Jaeda Coutinho-Budd. Next generation sequencing analysis for ChIP-seq and RNA-seq datasets was done by Kevin Kenna in the laboratory of John Landers at the University of Massachusetts Medical School.

Introduction

Neurons are connected over long distances by their axons, which can extend over more than a meter in humans. Maintenance of axon integrity is essential for sustained neural circuit function since axon breakage can block nervous system signal propagation. Axon loss is a hallmark of nervous system injuries such as traumatic brain injury and spinal cord injury (Hagg and Oudega, 2006; Kelley et al., 2006; Henninger et al., 2016), is a unifying feature of neurodegenerative diseases (Adalbert and Coleman, 2013), and is strongly correlated with functional loss in patients (Coleman and Perry, 2002). However, molecular pathways that drive axon loss in any context remain poorly defined.

Wallerian degeneration (axotomy) serves as a useful model to study basic aspects of axon biology, and to identify axon death signaling molecules. Severed axons, after a defined latent phase, undergo explosive fragmentation and are ultimately cleared by surrounding phagocytes (Waller, 1850; Saxena and Caroni, 2007; Conforti et al., 2014). The discovery of the slow Wallerian degeneration (*Wld*^{S}) mutant mouse, where severed distal axons survived for weeks after axotomy, radically changed our view of axonal biology after injury from a passive wasting away to an active destruction process (Lunn et al., 1989). The observed long-term survival of axon fibers in *Wld*^{S} animals demonstrated that axon degeneration is a controlled process, and that under some conditions, axons could survive for weeks without a cell body (Glass et al., 1993; Mack et al.,

2001; MacDonald et al., 2006; Martin et al., 2010). How this happens remains a mystery, but the observation suggested that axons don't simply waste away due to a lack of nutrients. Indeed, a growing number of studies in a diversity of species support the notion that the competence to undergo degeneration is likely a genetically programmed event: in the rock lobster, distal severed axons have been found to survive for a year after transection *in vivo,* and remain capable of evoked release at NMJs (Atwood et al., 1989; Parnas et al., 1991); fragments of *Aplysia* axons can survive *in vitro* for extended periods of time without degeneration (Benbassat and Spira, 1994); and in *C. elegans,* most distal severed axons never degenerate (Neumann et al., 2011). Despite these surprising observations, to our knowledge, nothing is known about transcriptional mechanisms that regulate the competence of axons to degenerate.

In axons that do undergo Wallerian degeneration, the execution of degeneration is driven by axon death signaling molecules. *Drosophila* dSarm (sterile α, ARM, and TIR domain protein) was the first endogenous molecule shown to actively promote axon death (Osterloh et al., 2012). Sarm1 functions in a conserved role in mammals (Osterloh et al., 2012; Gerdts et al., 2013), where it has been proposed to act as an NAD^+ hydrolase that drives axonal degeneration through promoting metabolic catastrophe (Gerdts et al., 2015; Essuman et al., 2017). *Drosophila* dSarm is similarly capable of NAD^+ hydrolysis (Essuman et al., 2017), but requires signaling downstream through the BTB/BACK domain molecule Axundead to execute axon death *in vivo* (Neukomm et al., 2017). The

E3 ubiquitin ligase Highwire/Phr1 also modulates axon death signaling (Xiong et al., 2012; Babetto et al., 2013) through a mechanism that appears to involve regulating levels of the NAD^+ biosynthetic molecule dNmnat/Nmnat2 (Gilley and Coleman, 2010; Xiong et al., 2012). In both *Drosophila* and mammals, all neurons tested thus far have been strongly protected by loss of function mutations in dSarm/Sarm1 (Osterloh et al., 2012; Gerdts et al., 2013; Gilley et al., 2015), which suggests that axon death signaling molecules are engaged to drive destruction in a wide array of, or perhaps all, neuronal subtypes.

In this study, we present the identification and characterization of a novel role for Pebbled (peb), a transcription factor, in axon degeneration. *Peb* mutations were identified in a forward genetic screen for mutants that suppressed Wallerian degeneration. *peb* mutants show two predominant axon death defective phenotypes: 1) severed distal axons are fully preserved morphologically, or 2) the axon shaft breaks into large fragments (partially fragmented axons, PFAs) that fail to disintegrate further, lingering in the nervous system for weeks. The PFA phenotype in *peb* mutants is not observed in control or axon death mutants (*dsarm, axed,* or *hiw*), and therefore define a new genetically accessible step in axon death signaling. Surprisingly, while PFAs form in all tested neurons, the ability of *peb* mutations to completely suppress axon degeneration was only observed in glutamatergic neurons, and not in cholinergic neurons, arguing that Peb functions to differentially modulate competence to undergo axon degeneration in distinct subsets of neurons.

Results

Isolation of a new mutant that suppresses Wallerian degeneration

To identify novel endogenous regulators of Wallerian degeneration (WD), we performed an X chromosome-based F_2 forward genetic screen in glutamatergic sensory neurons in the adult *Drosophila* wing using mosaic analysis using a repressible cell marker (MARCM) (Neukomm et al., 2014). Flies were bred to generate neuronal MARCM clones using the *OK371-GAL4* driver, and axons were severed by surgical removal of the distal half of the wing with microdissection scissors. Animals were aged for 7 days post axotomy (dpa), after which wings were dissected from the animal and axon death was quantified and imaged the proximal wing vein. Neurons with cell bodies that were proximal to the injury site remained healthy and uninjured, and served as internal controls, represented by 'cb' in the upper right corner of each figure panel.

In control wings, injured axons typically undergo fragmentation by 12 hours post axotomy (hpa), degenerate fully by 24 hpa, and are cleared by surrounding glia after 5 dpa (Neukomm et al., 2014). We screened ~2000 independent X-chromosome mutant stocks, and identified one, *345x,* that exhibited suppression of Wallerian degeneration (Figure 3.1A). While uninjured *345x* mutant axons were similar in morphology to control, 60% of injured axons in *345x* mutants remained partially or fully preserved at 7dpa compared to 0% in wild type control: 22% of severed *345x* mutant axons remained morphologically

intact, while 38% initiated fragmentation, but were maintained in a partially fragmented state (PFAs, partially fragmented axons) (Figure 3.1B). We defined PFAs as GFP^+ axon fragments that spanned the imaging field of view, and were aligned linearly such that they appeared to represent the remnants of a previously intact axon. We rarely observed PFAs in control animals, and only early in the phase of axon degeneration (Figure 3.1D), but never in *dsarm*, *axundead*, or *highwire* mutants (Osterloh et al., 2012; Xiong et al., 2012; Neukomm et al., 2017). Therefore, *345x* mutations result in a novel axon death phenotype, apparently specific to the execution phase of axonal destruction. *345x* mutants were homozygous lethal, suggesting the affected gene is an essential gene. MARCM clones in uninjured glutamatergic neurons exhibited no overt changes in axon morphology, axonal mitochondrial size, and they showed no signs of spontaneous axon degeneration for at least 2 weeks after eclosion.

To distinguish PFAs from normal cellular debris produced by degenerating axons, we measured the length of all GFP^+ axonal membrane debris from both control and *345x* clones at 7 dpa. The sparse debris in controls averaged 0.9 μm in length, while *345x* mutant axons fragments averaged 3.0 μm, ranging in size from 0.2-25.5 μm in length (Figure 3.1C). Preserved intact axons and PFAs persisted in *345x* mutants over time, as severed intact axons and PFAs were observed even 14 dpa (Figure 3.1D-E), although at reduced levels.

While one portion of a severed axon in *345x* mutants was fully protected, it was plausible that PFAs might be generated at other positions along the axon.

To explore this possibility, we scored axon morphological integrity with single axon resolution along the entire length of individual severed intact axons in the wing vein of *345x* mutants (Figure 3.1F-G). We found that when axons were preserved in the proximal wing, 100% of those axons remained morphologically intact along their entire length (Figure 3.1H). We conclude that severed axons in *345x* mutants fall into one of three phenotypic categories: (1) they are morphologically preserved along their entire length, (2) they generate PFAs along their entire length, or (3) they degenerate and are cleared normally.

Mitochondrial dysfunction is a hallmark in axon degeneration, and is observed after axotomy and in neurodegenerative diseases (Lin and Beal, 2006; Knott et al., 2008; Itoh et al., 2013). In Wld^S-expressing axons, mitochondria remain intact after axotomy long after mitochondria in control animals have been destroyed (Avery et al., 2012). We therefore examined mitochondrial morphology before and after axotomy in control and *345x* mutant clones. Using a GFP targeted to mitochondria, we found no significant difference in the average mitochondria length in uninjured neurons between control and *345x* mutants (Figure 3.1I). Just prior to the explosive fragmentation stage of the distal axon, at 8 hours after injury, wildtype mitochondria began to decrease in size, with an average length of 0.36 μm. At 8 hpa, mitochondria of *345x* mutants were significantly longer, with lengths averaging 0.9 μm (Figure 3.1I). However, when we look at injured axons 24 hours after injury, mitochondria in control axon debris and severed intact *345x* mutant axons were indistinguishable (Figure 3.1J).

These data show that *345x* mutant mitochondria exhibit a normal, albeit delayed, morphological response to axon injury within axon death defective axons. This loss of mitochondria even in 345x mutant axons that are morphologically intact, is strikingly different from *dsarm* null mutant (Figure 3.1I-J) or Wld^S-expressing severed axons (Avery et al., 2012). Surprisingly, *345x* mutations are capable of preserving axon integrity despite the loss of mitochondria.

The *345x* mutation maps to the C_2H_2 Zinc Finger transcription factor Pebbled/RREB1

In order to identify the gene affected by the *345x* mutation, we backcrossed the *345x* stock over 5 generations to remove background mutations. The early lethality associated with the *345x* mutation co-segregated with the axon death phenotype, supporting the notion that the *345x* mutation affects an essential gene. We used whole-genome sequencing to identify novel mutations in the *345x* mutant that remained after 5 generations of backcrossing, confirmed these with PCR and genome sequencing, and then compared these to the original *345x* stock before backcrossing. The only identified mutation that co-segregated with the axon death defective phenotype was a mutation in the *pebbled (peb)* gene that resulted in the loss of a splice donor site in exon 2 and generated a novel premature stop codon (Figure 3.2A). In a parallel set of experiments, we screened a collection of X chromosome deficiency lines that had been recombined onto an FRT chromosome with the MARCM approach. In total,

these deficiencies removed 38.7% of X chromosome genes, and two non-overlapping deficiency lines led to a suppression of axon death (Table 3.1). The first deficiency uncovered the E3 ubiquitin ligase Highwire, a known axon death signaling molecule (Xiong et al., 2012; Babetto et al., 2013). The second overlapped with the genetic region to which we mapped *345x*, and included the *peb* gene.

Peb (RREB1 in mammals) is a conserved transcription factor that contains 14 C_2H_2 zinc finger domains (Ming et al., 2013). In *Drosophila* embryos, Peb is expressed in amnioserosa (AS), anterior and posterior midgut (AM and PM, respectively), trachea, and in the peripheral nervous system and imaginal discs during later stages (Yip et al., 1997; Wilk et al., 2000; Pickup et al., 2002). Loss of Peb function leads to defects in embryonic germband retraction and dorsal closure of the embryonic epidermis, resulting in lethality. Peb also plays important roles in axon guidance in photoreceptor cells in the developing *Drosophila* visual system (Oliva and Sierralta, 2010; Oliva et al., 2015), but roles for Peb/RREB1 in axon death have not been previously reported. We performed immunohistochemistry (IHC) of early stage embryos with α-Peb antibodies and confirmed that Peb was localized to the AS, and both the AM and PM (Figure 3.2B) (Yip et al., 1997). Consistent with our prediction that the *345x* mutations would lead to a loss of Peb protein product, we found that embryos homozygous for *345x* lacked α-Peb immunoreactivity (Figure 3.2B).

To confirm that the mutation of *peb* was responsible for the axon death phenotype, we assayed axon death in adult wing glutamatergic neurons with a second *peb* allele, peb^{E8} (Strecker and Yip, 1991). We found that peb^{E8} mutant clones phenocopied the *345x* mutant phenotype, although the phenotype was slightly weaker: in peb^{E8} mutant MARCM clones 12% of severed axons remained morphologically intact, and 21% formed PFAs (Figure 3.2C-D). We next crossed a bacterial artificial chromosome (BAC) containing the genomic copy of *peb* into *345x* mutants, and found that reintroduction of a wild type copy of peb^{BAC} into *345x* mutants completely rescued the axon death phenotypes (i.e. both axon degeneration, the production of PFAs, and clearance of axonal debris) to control levels (Figure 3.2E-F) Addition of peb^{BAC} had no effect on uninjured axons (Figure 3.3). Furthermore, we found that the peb^{BAC} rescued the lethality of the *345x* mutation. We conclude that *345x* is a novel mutation in the *peb* gene, and henceforth refer to it as peb^{345x}.

Peb is expressed in wing sensory neurons in imaginal discs

To determine when Peb might act to regulate axon death, we assayed Peb expression using the α-Peb antibody. Wing sensory neurons are derived from sensory organ precursors (SOPs) that develop in the wing imaginal disc (Furman and Bukharina, 2008). Peb is known to be expressed in both the eye/antennal and wing imaginal discs in SOPs that give rise to neurons at the 3rd instar larval stage (Pickup et al., 2002). We confirmed this expression by performing IHC

with α-Peb on imaginal wing discs from animals driving *Peb-GAL4* expression of membrane-tagged GFP (Figure 3.4A-E). Peb expression was maintained in wing disc cells at 36 hours after puparium formation (apf), and colocalized with the neuronal marker ElaV (Figure 3.4A'-E'). Peb expression was maintained in adult sensory neurons as evidenced by: 1) strong neuronal expression GFP by *Peb-GAL4* in the wing, colocalized with pan-neuronal expression of Tomato by *nSyb-QF2 (*Figure 3.4A''-E'') and 2) detection of Peb protein in dissected wing veins on Western blots probed with α-Peb antibody (Figure 3.4F). Conversely, Peb expression was undetectable in the central nervous system by either α-Peb antibody immunostaining (Figure 3.5) or GFP expression by the *Peb-GAL4* driver (Sweeney et al., 2007; Oliva and Sierralta, 2010). Visualization of individual neurons at mid pupal stages indicated Peb is largely restricted to the nucleus and is not detectable in the axoplasm (Figure 3.4G), which is consistent with the notion that Peb acts as a transcription factor. Together these data argue Peb is expressed early in SOPs, prior to the expression of markers of post-mitotic neurons, and Peb expression is maintained in adult wing sensory neurons.

Human RREB1 can functionally substitute for Pebbled

To explore how Peb regulates axon death, we drove expression of cDNA constructs encoding full-length Peb, truncated Peb containing zinc fingers 1-8 or 10-14, and the human homolog, RREB1 (Peb, Peb^{1-8}, Peb^{10-14}, and hRREB1, respectively) in control and peb^{345x} clones, and quantified axon degeneration 7

dpa (Figure 3.6A, Figure 3.3). Over expression of full length Peb using the GAL4/UAS system (and driving expression with the *OK371-GAL4* driver) was sufficient to completely rescue the blockade of axon degeneration observed in peb^{345x} clones: 100% of mutant axons initiated axon fragmentation (Figure 3.6B-C). Expression of the C-terminal zinc finger domains 10-14 (in Peb^{10-14}) was sufficient to rescue the axon death defect in *peb* mutants. In contrast, expression of N-terminal Peb^{1-8} failed to rescue the axon protective phenotype. This defines the key domains essential for Peb function in pro-degenerative signaling, and provides additional support for a transcriptional role for Peb, consistent with previous work demonstrating that C-terminal domains are required for Peb to bind DNA *in vitro* (Ming et al., 2013). Expression of the human Peb ortholog, Ras-responsive element binding protein 1 (hRREB1), was also sufficient to fully rescue the blockade of axon degeneration (Figure 3.6B-C, Figure 3.3), arguing that Peb and hRREB1 exhibit similar properties with respect to target gene regulation. However, while the initiation of axon fragmentation was strongly rescued, 17% of the GFP^+ injured axons persisted as PFAs in peb^{345x} background rescued with Peb. This approximates the percentage of axons that form PFAs in peb^{345x} mutant clones expressing a *UAS-LacZ* control rescue construct, and we observed PFAs in peb^{345x} mutants rescued with hRREB1 expression. Additionally, expression of either Peb or hRREB1 in control animals led to the production of PFAs, which are only ever rarely observed in the earliest phase of normal axon degeneration (Figure 3.6B-C). These data suggest Peb

expression levels may need to be fine-tuned for proper rescue of execution of axon death and destruction of PFAs, with too much or too little Peb resulting in PFA formation.

Peb loss can fully preserve severed axons in glutamatergic, but not cholinergic neurons

There are ~250 sensory neurons in the *Drosophila* wing that send axonal projections to the thoracic ganglion in the CNS (Fang and Bonini, 2012). These cells fall into two subsets based on neurotransmitter profiles: cholinergic (~145 cells labeled by *ChAT-GAL4*) and glutamatergic neurons (~40 cell labeled by *vGlut-QF2* or *OK371-GAL4*) (Figure 3.7A-B) (Neukomm et al., 2014). Since the peb^{345x} mutation was identified and characterized in glutamatergic neurons, we wished to determine whether it also regulated axon death signaling in cholinergic neurons. Approximately 23% of severed peb^{345x} glutamatergic clones failed to undergo axon degeneration at 7 dpa, and ~40% of severed axons formed PFAs (Figure 3.7C-D). When we assayed cholinergic peb^{345x} clones, we found a complete lack of protection from axon degeneration: 100% of all neurons began fragmenting (Figure 3.7C-D). Of severed axons, 19% form PFAs, indicating that *peb* also regulates PFA formation at some level in cholinergic neurons as compared to control clones that underwent normal axon death (Figure 3.8). In axotomy assays with the pan-neuronal driver *nSyb-GAL4*, we observed only 4% of severed mutant clones remaining intact, and there was no change in PFAs as

compared to *peb*^{345x} glutamatergic clones. Control pan-neuronal clones had a normal degenerative response to injury. Given that glutamatergic neurons represent 20% of the *nSyb-GAL4*$^{+}$ cells, we suspected the only cells protected in this background by the *peb*^{345x} mutation were the glutamatergic neurons. Indeed, after screening many hundred clones of injured axons where we simultaneously labeled cholinergic neurons (with *ChAT-GAL4*) and glutamatergic neurons (with *vGlut-QF2*), we only found a single severed, intact axon that expressed *ChAT-GAL4*, and it was also positive for *vGlut-QF2* and therefore also glutamatergic (Figure 3.7E). The observation that only glutamatergic neurons can be fully protected by *peb*^{345x} mutations, while PFAs appear with equal frequency in both cholinergic and glutamatergic neurons, further supports the notion that the initiation (i.e. fragmentation) and execution (i.e. full degradation) of axons are genetically separable and differentially regulated by Peb levels. Moreover, ability of *peb* mutants to completely block axon death is limited in the wing to glutamatergic sensory neurons.

peb mutations do not block dSarm-induced axon death, although _dsarm_ mutations can enhance _peb_ mutant phenotypes in axon death

Activation of Sarm1 signaling potently drives axon death in mammalian and *Drosophila* neurons (Gerdts et al., 2015). To determine whether Peb acts downstream of dSarm, we crossed *peb*^{345x} mutants into a background expressing a gain-of-function version of dSarm (dSarm$^{\Delta ARM}$) (Neukomm et al., 2017) and

assayed for suppression of axon death. Loss of Peb function was not sufficient to block dSarm$^{\Delta ARM}$-induced axon death (Figure 3.9A-B), arguing that Peb does not act genetically downstream of dSarm, and demonstrating that constitutive activation of dSarm is sufficient to eliminate the appearance of PFAs. We next sought to determine whether *peb* mutants exhibited any dominant genetic interactions with components of the axon death signaling cascade including *dsarm* (Osterloh et al., 2012), *axundead* (Neukomm et al., 2017), or *highwire* (Xiong et al., 2012). We crossed loss of function mutations of *dsarm* or *axed* into the *peb*^{345x} background, and found that loss of a single copy of *dsarm* was sufficient to double the number of intact axons in *peb*^{345x} animals, while loss of a single copy of *axed* had no effect (Figure 3.9C-D, Figure 3.3). Removal of one copy of *dsarm* or *axed* in control clones had no effect on axon degeneration (Figure 3.8). In addition to the increase in fully protected axons, loss of one copy of *dsarm* also reduced the number of PFAs in *peb*^{345x} mutants (Figure 3.9C). Reciprocally, we found that overexpression of dSarm in a *peb*^{345x} background led to a partial suppression of the ability of *peb*^{345x} to fully protect axons, and an increase in the number of PFAs. Manipulation of Axed or Hiw had no effect (Figure 3.9E-F, Figure 3.3). Overexpression of dSarm, Axed, and Hiw in control clones had no effect on axon degeneration (Figure 3.8). Thus, the neuroprotective effects of *peb*^{345x} mutants are highly sensitive to dSarm levels, with a slight decrease or increase in dSarm levels enhancing or suppressing,

respectively, the efficacy of *peb* mutants to fully block the initiation of axon degeneration after axotomy.

Discussion

Distal axons separated from their cell bodies can survive in a functionally competent state for days to weeks after axotomy in multiple species (Parnas et al., 1991; Stengl, 1995; Neukomm et al., 2017). It therefore seems plausible that some axons are programmed to degenerate while others are not. In this study, we identify the transcription factor Pebbled (Peb)/RREB1 as a novel essential modulator of axon death in *Drosophila*. Through epistatic analysis, we can place *peb* upstream of *dSarm* or in a separate, parallel pathway which ultimately converges on axon death. The simplest interpretation of our data is that Peb regulates axon death signaling in glutamatergic axons at the transcriptional level. Human RREB1 can rescue axon death phenotypes associated with loss of *peb,* arguing for strong conservation of the binding properties of Peb and hRREB1, and implying that RREB1 may play similar roles in axon biology in mammals.

Pebbled appears to identify a novel step in the axon death signaling cascade. Loss of Pebbled function resulted in the appearance of three axon phenotypes after injury: (1) full morphological preservation with a slightly delayed loss of mitochondria; (2) the generation of partially fragmented axons (PFAs) that linger in the nervous system for weeks, but which also lose mitochondria after a short delay; or (3) apparently normal axon death signaling and clearance. The cell biology of axon preservation in *peb* mutants is unique, and implies that *peb* mutants identify a new genetically accessible step in axon death signaling. PFAs

have not been observed in other axon death mutants (i.e. *dsarm*, *hiw*, or *axed*), as these mutants all fully block axon degeneration after axotomy (Osterloh et al., 2012; Babetto et al., 2013; Neukomm et al., 2017). Understanding the nature of PFA production compared to normal axon degeneration is an important goal for future study. In the case of *dsarm* mutants, in addition to the axon shaft maintaining integrity, mitochondria also appear well-preserved. That was not the case in *peb* mutants where mitochondria degenerated after only a short delay, and preserved axons were severely depleted of mitochondria for the duration of their extended survival. Interestingly, the phenotype of individual *peb* mutant axons is consistent along the entirety of the axon shaft—we never observed an axon that generated PFAs in one portion, but was fully protected elsewhere. Unraveling the molecular basis of this all-or-none type of phenotypic expression is of great interest for the future. Finally, while some PFAs are observed in control animals immediately after the initiation of axon fragmentation, they quickly undergo explosive degeneration and are cleared. From these data, we conclude that Peb functions both at the initial phase of axon breakage into smaller fragments, and subsequently during the phase of explosive degeneration.

To date all known axon death signaling molecules—dSarm, Hiw, and Axed—have been proposed to function locally in the axon to drive destruction, and their neuroprotective effects extend to both glutamatergic and cholinergic neurons (Osterloh et al., 2012; Xiong et al., 2012; Neukomm et al., 2017). Based on its expression in the nuclei of wing sensory neuron precursors and mature

neurons, and the fact it is a C_2H_2 zinc finger transcription factor, we propose that Peb functions at the transcriptional level to help establish and/or maintain competence to undergo axon degeneration. While Peb appears to be expressed broadly in wing sensory neurons, surprisingly, the ability of *peb* mutants to fully block axon fragmentation is restricted to glutamatergic neurons. How Peb selectively protects glutamatergic axons is unclear, but could modify axonal phenotypes through the JNK signaling cascade. During embryogenesis, in amnioserosa *peb* mutants show increased levels of AP-1 transcriptional activity downstream of the JNK signaling cascade (Reed et al., 2001), which in turn inhibits cytoskeletal rearrangements that allow for cell migration (Yip et al., 1997; Reed et al., 2001; Scuderi and Letsou, 2005). We have found a lack of evidence to support a role for JNK signaling in axon death (Osterloh et al., 2012; Neukomm et al., 2017), but some data support a neuroprotective role for this pathway by controlling baseline levels of Nmnat (Walker et al., 2017). Peb has also been shown to negatively regulate *nervy*, the *Drosophila* homolog of mammalian MTG8 proto-oncogene (Wildonger and Mann, 2005; Ming et al., 2013); however, we observed no alterations in axon death when we overexpressed nervy in glutamatergic neurons.

The nuclear localization requirement of the carboxy terminal DNA binding zinc finger domains of Peb for rescue suggests that Peb is regulating injury-induced axon degeneration at the transcriptional level. We attempted to identify direct transcriptional targets of Peb by expressing a tagged version of Peb in the

Drosophila embryonic cell line, GM2 (Genetics, Milano 2) (Mosna and Dolfini, 1972), and performing chromatin immunoprecipitation with antibodies specific to tagged Peb and subsequent deep sequencing (ChIP-seq). This approach successfully identified the one known target for Peb, the transcriptional regulator Nervy, whose elimination did not block axon death, and several novel new potential Peb targets (Table 3.2). We did not find evidence for direct binding of Peb to regions containing known axon death signaling genes (i.e. *dsarm*, *axed*, or *hiw*). This could indicate that Peb does not directly modulate axon death genes *in vivo* to exert its effects, although it remains unclear how similar Peb transcriptional activity in GM2 cells might be compared to neurons.

Our analysis of *peb* mutant phenotypes reveals new features of the cell biology of axon death. Our discovery of PFAs in *peb* mutants implies that axon degeneration can be genetically dissected into activation and execution phases: we propose that PFAs represent an activation, but failure to execute axon death. We found that either increased or decreased Peb levels could lead to the production of PFAs, arguing that fine-tuning of Peb levels is essential for appropriate execution of axon death. Furthermore, Peb modulation of PFA production is not limited to glutamatergic neurons, since we found PFAs in cholinergic neurons under both loss- and gain-of-function Peb conditions. Interestingly, Peb allows us to genetically separate mitochondrial loss from axon degeneration. We observed mitochondrial degeneration even in fully protected

peb mutant axons, indicating that mitochondrial destruction must occur through a Peb-independent signaling pathway.

Materials & Methods

Fly strains

Flies (*D. melanogaster*) were kept on standard cornmeal agar supplemented with dry yeast at 25°C unless stated otherwise. The following lines were obtained from Bloomington Drosophila Stock Center: y, w^{1118}, $FM7c^{Kr\text{-}GAL4,\ GFP}$, *FRT 19A, hs-FLP,tub-GAL80,FRT19A,* hnt^{E8}, *ChAT-GAL4, vGlut-QF2, UAS-IVS-myr::tdTomato, QUAS-mtdTomato-3xHA, UAS-mito-HA-GFP, nSyb-GAL4, FRT2A, FRT82B, 5xUAS-mCD8::GFP. OK371-GAL4* (Mahr and Aberle, 2006), *ase-*FLP^{2a} *and ase-*FLP^{3e} (Neukomm et al., 2014), *UAS-hRREB1, UAS-*$Peb^{1\text{-}8}$, *and UAS-*$Peb^{10\text{-}14}$ (gift from H. Lipshitz, U of Toronto, Toronto, Canada), *Pebbled-GAL4* (Sweeney et al., 2007), *UAS-nls-LacZ,* $dSarm^{896}$ (Osterloh et al., 2012), *FRT2A, FRT82B,* $axed^{0011}$, *UAS-dSarm, and UAS-axed* (Neukomm et al., 2017), *UAS-Hiw* (Wu, 2005), peb^{BAC} was generated by injection of the bacterial artificial chromosome CH321-46J02 (BAC PAC Resources, Children's Hospital Oakland Research Institute) with Phi31-mediated integration into the genomic locus *attP2* (BestGene).

Transgenic constructs

UAS-Peb was generated by amplifying *peb* from cDNA clone GH10905 (Drosophila Gene Collection, Berkeley Drosophila Genome Project) for cloning with Gibson Assembly (New England Biolabs) into the pJFRC5-5XUAS-IVS-

mCD8::GFP vector (Pfeiffer et al., 2010). *UAS-Peb::Myc* was generated cloning amplified *peb* cDNA with Gibson Assembly (New England Biolabs) into 5XUAS::5XMyc, modified from pJFRC5-5XUAS-IVS-mCD8::GFP. *UAS-Nvy* was generated by subcloning the *nvy* ORF from cDNA clone LD17501 into the pJFRC5-5XUAS-IVS-mCD8::GFP vector. Plasmids were sequenced and injected with Phi31-mediated integration into genomic loci *attP40* and *attP2* (BestGene).

Antibodies

Mouse anti-pebbled (1G9, Developmental Studies Hybridoma Bank)(IHC 1:25, WB 1:50), mouse anti-ElaV (9F8A9, Developmental Studies Hybridoma Bank) (1:100), rat anti-ElaV (7E8A10, Developmental Studies Hybridoma Bank) (IHC 1:100, WB 1:50), mouse anti-tubulin (DM1A, Sigma) (WB 1:5000), goat anti-mouse IgG H&L Alexa Fluor 488 (ab150117, Abcam) (IHC 1:100), donkey anti-rat IgG H&L Alexa Fluor 568 (ab175475, Abcam) (IHC 1:100),, donkey anti-mouse IgG H&L Alexa Fluor 647 (Jackson) (IHC 1:100), sheep HRP anti-mouse (ab6080, Abcam), goat HRP anti-rabbit (ab6721, Abcam) (WB 1:5000), goat polyclonal to Myc ChIP-grade (Abcam, ab9132), and goat polyclonal IgG (Abcam, ab37373).

Mutagenesis screen and wing injury

Mutagenesis was performed as described previously (Neukomm et al., 2017). In brief, males were starved for 12 hours before consuming mutagen (25 mM ethyl

methane sulphonate (EMS) in 1% sucrose). Males recovered in fresh vials for 12 hours prior to breeding. Wing injury was performed as described previously (Neukomm et al., 2014). Wings were cut with MicroPoint Scissors (EMS, VANNAS Scissors; angled on side, delicate, 5-mm cutting edge, #72933–04) and mounted in Halocarbon Oil 27 (Sigma, H8773) on a microscopy slide and covered with a coverslip, and immediately used for microscopy.

Immunohistochemistry

Embryo fixation and staining – Embryos were collected on grape-juice agar plates overnight at 25°C and dechorionated for 3 min in 50% sodium hypochlorite solution. Dechorionated embryos were washed in PBT buffer (1X phosphate buffered saline, 1% bovine serum albumin, 0.1% Triton X-100) and fixed for 25 minutes in equal parts Heptane and PEMFA buffer (100 mM PIPES (pH 6.9), 2 mM EGTA, 1mM $MgSO_4$, 4% paraformaldehyde). Lower aqueous phase was removed and methanol was added. Sample was vortexed for 30 seconds to remove the vitelline membrane, followed by 3X methanol washing. Fixed embryos were washed 5X and blocked in PBT for 30 minutes then incubated with primary antibody at 4°C overnight. Embryos were washed 5X in PBT and incubated with secondary antibody for 2 hours at room temperature. Embryos were washed 5X in PBT and mounted in Vectashield anti-fade reagent for imaging.

Larval imaginal wing discs – Wandering third instar larvae were collected and imaginal wing discs were dissected as previously described (Spratford and Kumar, 2014). Immunohistochemsitry on imaginal wing discs was performed as described above.

Pupal wings –Pupae were staged and collected at 36 hours after puparium formation. Animals were dissected as previously described (Classen et al., 2008). Immunohistochemsitry on pupal wings was performed as described above.

GM2 cell culture

Drosophila GM2 cells (*Drosophila* Genomics Resource Center) were maintained at 25°C in Hyclone SFX-Insect cell culture medium (GE Healthcare Life Sciences) supplemented with 10% Fetal Bovine Serum (Hyclone, GE Healthcare Life Sciences) and 1x Penicillin-Streptomycin (Pen Strep) (ThermoFisher Scientific).

Western blot

GM2 cells – cells were collected and lysed in RIPA buffer (10 mM Tris-Cl (pH 8.0), 1 mM EDTA, 1% Triton X-100, 0.1% sodium deoxycholate, 0.1% SDS, 140 mM NaCl) supplemented with protease inhibitor tablet (cOmplete Mini EDTA-free, Roche). Laemmli buffer (0.1% β-Mercaptoethanol, 0.0005% Bromophenol blue, 10% glycerol, 2% sodium dodecyl sulfate, 63 mM Tris-HCl (pH 6.8)) was

added to the lysate and incubated at 95°C for 10 minutes. 10 µl samples were loaded per lane onto a 4%–12% gradient SDS-PAGE.

Adult wings – approximately 600 w^{1118} adult wings were removed from the animals with MicroPoint scissors and immediately placed in an Eppendorf tube on dry ice. Tissue was mechanically homogenized using a BioMasher II tube and pestle (Kimble) in 1X Laemmli buffer. Homogenate was incubated at 95°C for 10 minutes. 10 µl samples were loaded per lane onto a 4%–12% gradient SDS-PAGE.

ChIP-seq

Transfection. 1.2 x 10^7 GM2 cells were plated out in 10 cm plates 24h prior to transfection. Cells were transfected with *pAc-GAL4* (Addgene) with or without *UAS-Peb::Myc* constructs to a final concentration of 15 mg DNA using Mirus TransIT-Insect (Mirus Bio). Cells were harvested 48h after transfection and used for chromatin immunoprecipitation (ChIP) described below.

ChIP. Protocol was modified from Atianand *et al.,* 2016 (Atianand et al., 2016). Transfected GM2 cells were cross-linked in suspension with 1% formaldehyde (Thermo Fisher Scientific) for 10 min at room temperature, and the cross-linking was quenched twice with 125 mM Glycine/PBS for 5 min each. Cells were pelleted and washed twice with ice-cold PBS. Nuclear pellets were isolated by swelling cross-linked cells in hypotonic lysis buffer (25 mM Hepes pH

7.4, 1.5 mM MgCl2, 10 mM KCl, 0.5% NP-40 and 1 mM DTT) supplemented with 1x cOmplete Mini EDTA-free (Roche) at ice for 15 min, followed by Dounce homogenization. Nuclear pellets were suspended in sonication buffer (50 mM Hepes pH 7.4, 140 mM NaCl, 1 mM EDTA, 1% Triton-X 100, 0.1% Sodium deoxycholate, 0.5% SDS, 1 mM DTT and 1x protease inhibitor cocktail) and incubated at ice for 10 min. Nuclear extracts were sonicated using Bioruptor UCD-200 (Diagenode Inc., Sparta, NJ) for 12 cycles of "30 sec ON and 30 sec OFF" at the highest voltage setting to generate 200 - 500 bp chromatin fragments. In each experiment, chromatin was first processed to confirm DNA shearing to 200 - 500 bp fragments by agarose gel electrophoresis, and the DNA concentration was measured by fragment analysis. Equal quantities of sheared chromatin (20 µg per IP) was diluted 1:5 in sonication buffer (no SDS) to the final volume of 1.5 ml, and immunoprecipitated overnight with 2 µg of target-specific antibodies or isotype control IgG antibodies at 4° C, overnight. The antibodies used in ChIP were: anti-Myc ChIP-grade and rabbit polyclonal IgG. Chromatin complexes were captured using 20 µl ChIP-grade Protein A/G magnetic beads (Thermo Scientific) at 4° C for 1 hr. Beads were washed once with sonication buffer (containing 0.1% SDS), two times with high salt buffer (50 mM Hepes pH 7.4, 500 mM NaCl, 1 mM EDTA, 1% Triton-X 100, 0.1% Sodium deoxycholate, 0.1% SDS), two times with LiCl buffer (20 mM Tris pH 7.4, 250 mM LiCl, 1 mM EDTA, 0.5% NP-40, 0.1% Sodium deoxycholate, 0.05% Tween-20), and once with TE buffer (10 mM Tris pH 7.4, 1 mM EDTA). Each wash was performed at

room temperature for 5 min in 1 ml volume. Beads were captured using DynaMag spin magnet (Thermo Scientific). Elution was performed by suspending beads in 100 µl elution buffer (20 mM Tris pH 7.4, 1% SDS, 50 mM NaHCO3, 1 mM EDTA). ChIP eluates were reverse cross-linked at 650 C for 4 hr, digested with Proteinase K (10 mg/ml) at 550 C for 1 hr and 2 µl RNase A (Invitrogen) at 37° C for 30 min. ChIP purified DNA was cleaned using PCR purification columns (Qiagen) and subjected to fragment analysis for concentration and quality for library preparation.

ChIP-seq analysis. ChIP library was prepared using NEBNext Ultra II DNA Library Prep Kit for Illumina (New England Biolabs, E7645S) paired with NEBNext Multiplex Oligos for Illumina, Primer Set 1 (New England Biolabs, E7335S) and amplified 8 rounds in a thermocycler. Sequencing was performed using an Illumina HiSeq 2500 genome analyzer (50bp, single end) at the Bauer Core Facility at Harvard University. Data were analyzed according to the recommended best practices set out by the ENCODE and modENCODE projects (Landt et al., 2012). Briefly raw sequencing reads were aligned to build BDGP6 of the Drosophila reference genome using bwa (Li and Durbin, 2010). Duplicate reads were removed using picard (http://broadinstitute.github.io/picard). Peak calling was performed using the SPP caller (Kharchenko et al., 2008) as implemented in the phantompeakqualtools package (https://github.com/kundajelab/phantompeakqualtools). The significance of peak calls was assessed using the Irreproducible Discovery Rate (IDR) method (Li et

al., 2011; Landt et al., 2012) and code provided by the ENCODE consortium (https://sites.google.com/site/anshulkundaje/projects/idr). Annotation of peak calls was performed using PAVIS (Huang et al., 2013).

Figures & Tables

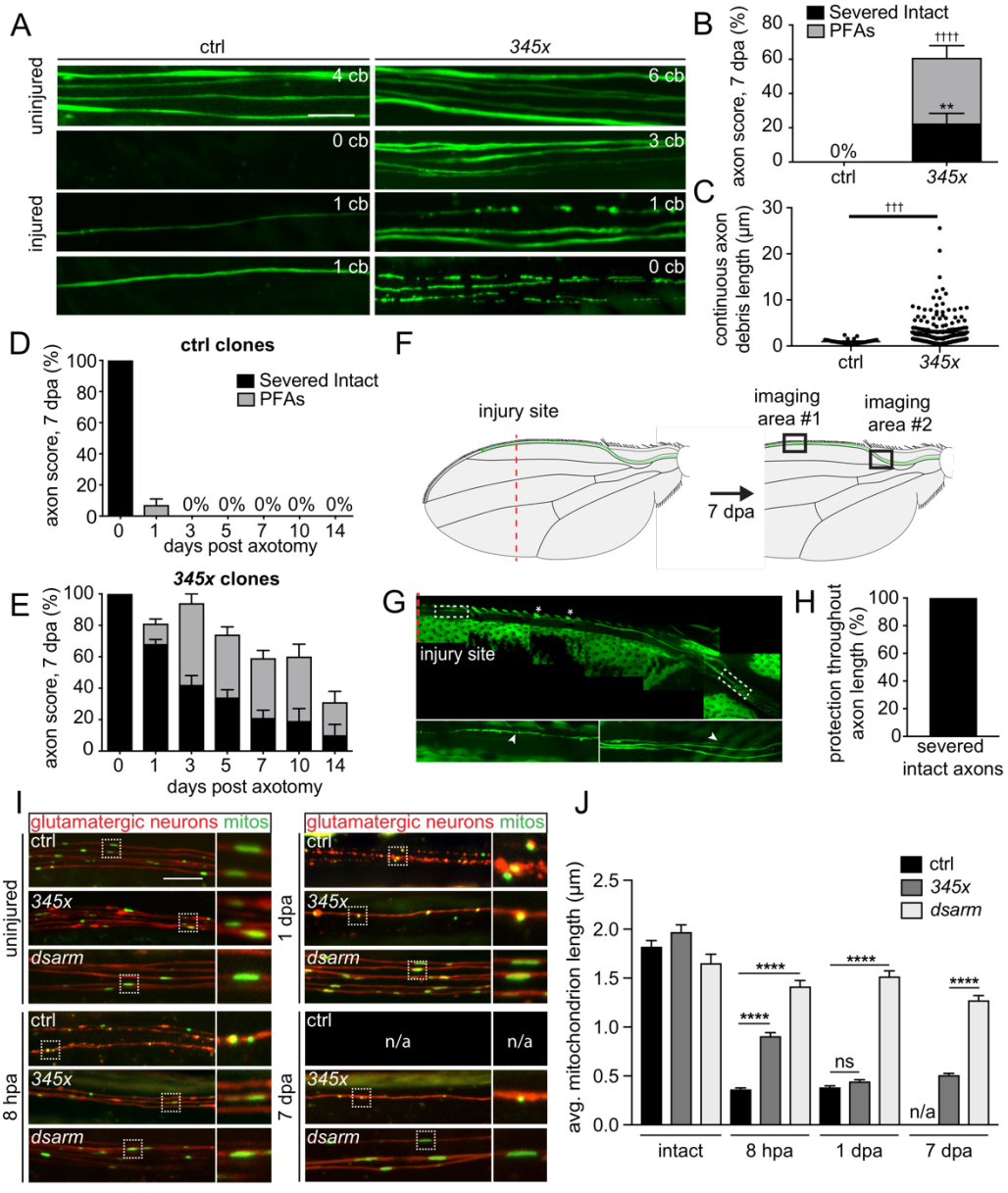

Figure 3.1. Mutation 345x Causes Defective Wallerian Degeneration *In Vivo*.

Figure 3.1. Mutation 345x Causes Defective Wallerian Degeneration *In Vivo*. (A) Glutamatergic clones within the L1 anterior margin vein of the adult wing were labeled with mCD8::GFP. Both uninjured and injured (7 days post axotomy, dpa) are shown (scale bar, 10 μM). Cell bodies (cb) of uninjured clones within each wing were counted and indicated in the upper right corner of each panel. Mutant 345x exhibited two axon death defective phenotypes: either severed intact or partially fragmented axons (PFAs). (B) Quantification of *peb* mutant phenotype. PFAs (gray) and severed intact axons (black). $n > 30$ wings. (C) Quantification of total continuous GFP^+ axon debris length, 7dpa. (D-E) Time course data for both controls and 345x mutants over 14 dpa ($n > 30$ wings). (F) schematic of the adult wing showing the distal and proximal imaging fields of view. (G-H) confocal image and quantification of severed intact axons were imaged and traced down the length of the wing. Asterisks indicate cell bodies of uninjured clones ($n = 14$ wings, 27 severed intact axons). (I) Mitochondria (green) and glutamatergic neurons (red) of control and *peb* mutant clones imaged and measured at various times after axotomy (scale bar, 10 μM). (J) Quantification of mitochondria length in control and *peb* mutant clones at 8 hpa (control: $n = 11$ wings, 185 measurements. *peb:* $n = 13$ wings, 241 measurements), 1 dpa (control: $n = 10$ wings, 211 measurements. *peb*: $n = 16$ wings 170 measurements), and 7 dpa (*peb*: $n = 15$ wings, 182 measurements). 2-way ANOVA, error = SEM (**,†† $p < 0.01$, ***,††† $p < 0.001$, ****,†††† $p < 0.0001$)). † and * represent PFA and severed intact significance, respectively.

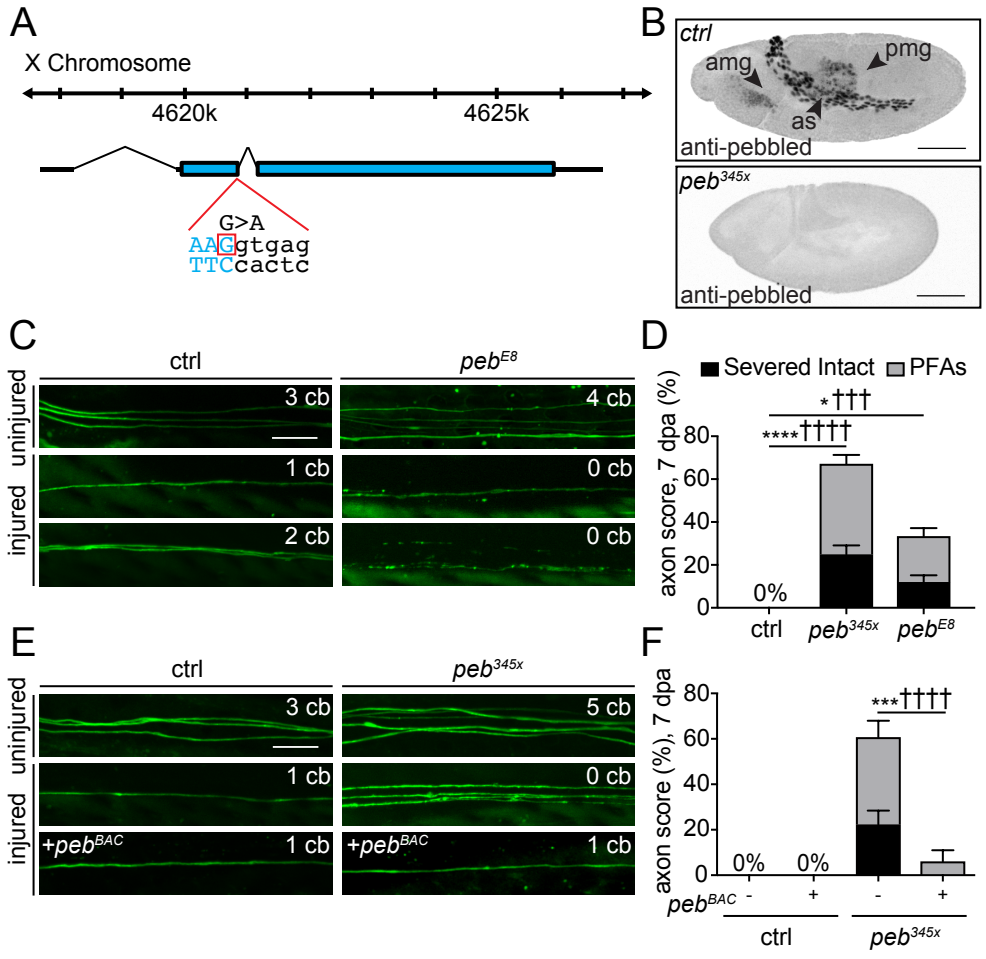

Figure 3.2. 345x Encodes the Transcription Factor Pebbled. (A) The 345x mutation lesion was identified as a splice donor variant (shown in blue) within exon two of the gene *pebbled* on the X chromosome. (B) Immunohistochemistry against Pebbled in w^{1118} control embryos showed localization to the amnioserosa (AS) and midgut (anterior AM, posterior PM). Homozygous peb^{345x} mutant embryos showed no immunoreactivity with the Peb antibody. Scale bar = 100 µm. (C) Peb^{E8} mutant allele phenocopies the axon death defect observed in peb^{345x} mutant clones (n>30 wings). (D) Genomic peb^{345x} is crossed into peb^{345x} mutant clones and completely rescued defective axon death back to control levels (n > 30 wings). Scale bar = 10 µm. 2-way ANOVA, error = SEM (*,† $p < 0.05$, ***,††† $p < 0.001$, ****,†††† $p < 0.0001$). † and * represent PFA and severed intact significance, respectively.

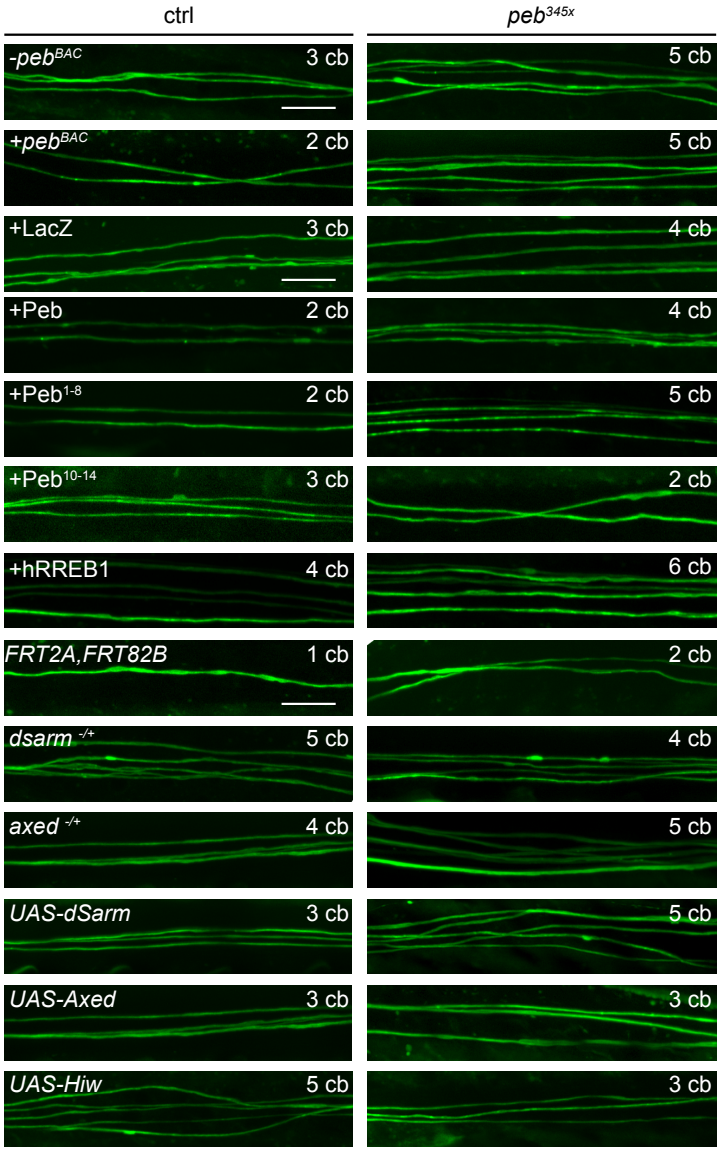

Figure 3.3. Uninjured Control and *peb*^{345x} Clones. Representative images of uninjured control and *peb*^{345x} mutant clones with various genetic manipulations. Manipulations did not alter axon morphology and did not induce spontaneous degeneration in either genotype.

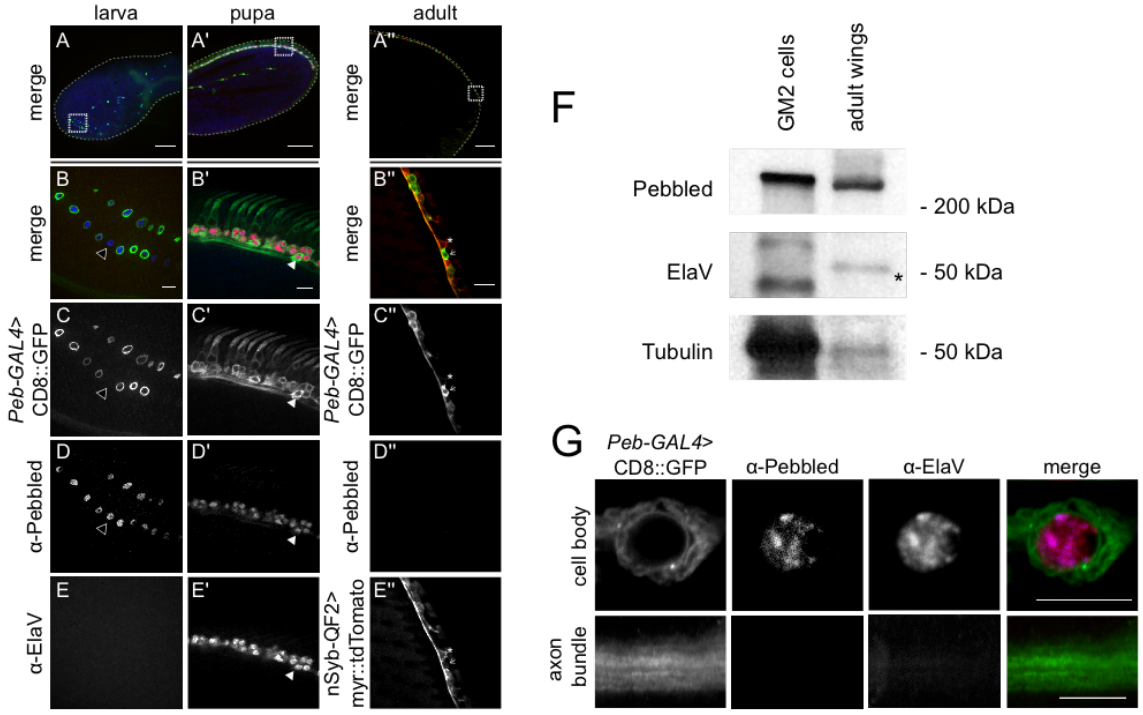

Figure 3.4. Pebbled is Expressed in Neuronal Nuclei Within the Developing Wing.

Figure 3.4. Pebbled is Expressed in Neurons Within the Developing Wing. (A-A") Immunohistochemistry of imaginal wing discs and wings at different stages of development (larva, pupa, and adult), scale bar = 100 μm. Dashed box indicates field of view of insets. (B-B") merged fluorescent image showing (C-C") *Peb-Gal4* driving expression of *UAS-mCD8::GFP* (green) was present in most sensory organ precursors (SOPs) within the larval wing disc, as well as the neurons in the pupal and adult wings. (D-D") Pebbled (blue) was expressed early and remains on during wing development. Hollow arrowhead indicates SOP that expresses Pebbled yet lacks GFP due to differential driver expression. (E-E') the neuronal protein ElaV (red) was expressed later during pupal wing development. Solid arrowhead in pupal wings indicates a neuron that expresses GFP from the *Peb-Gal4* driver, and endogenous Pebbled and ElaV. (E") The presence of the cuticle in adult wings prohibited IHC, therefore neurons were examined by the expression pattern of Q*UAS-myr::tdTomato* under the pan-neuronal driver, *nSyb-QF2* (red). While the *nSyb-QF2*$^{+}$ expression pattern colocalizes with the *Peb-Gal4* expression pattern in the adult wing, fluorescent intensity levels vary between neighboring neurons. Asterisk indicates a high intensity *nSyb-QF2*$^{+}$ neuron next to a high intensity *Peb-Gal4*$^{+}$ neuron, indicated by an arrow. Scale bar = 10 μm. (F) Western blot from GM2 cells and adult wings. Homogenate from adult wings showed Peb expression continued to remain on at high levels after development. ElaV immunoreactive band (asterisk).

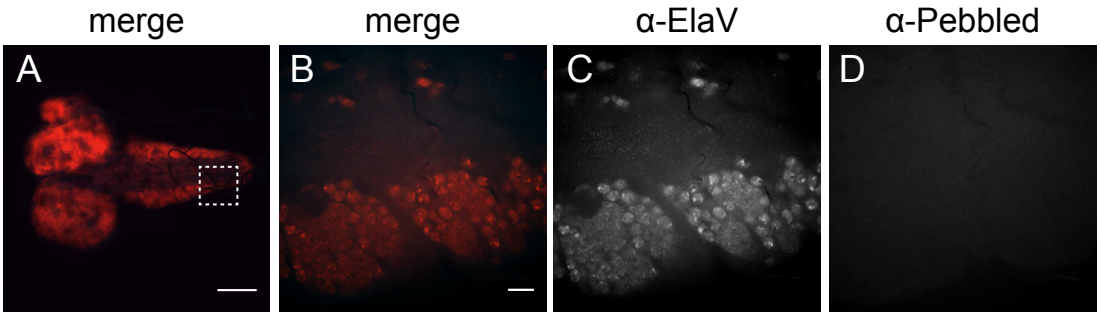

Figure 3.5. **Peb is not detectable in the CNS.** Immunohistochemistry against Pebbled (blue) and neuronal nuclear ElaV (red) in third instar larval brains. (**A**) Single slice low magnification fluorescent image showing Peb is not detectable in the CNS. Scale bar = 100 μm. Dashed box indicates field of view of inset. (**B**) Enlarged view of ventral nerve cord shows Peb is not detectable in ElaV^{+} neurons within the cortex. Scale bar = 10 μm.

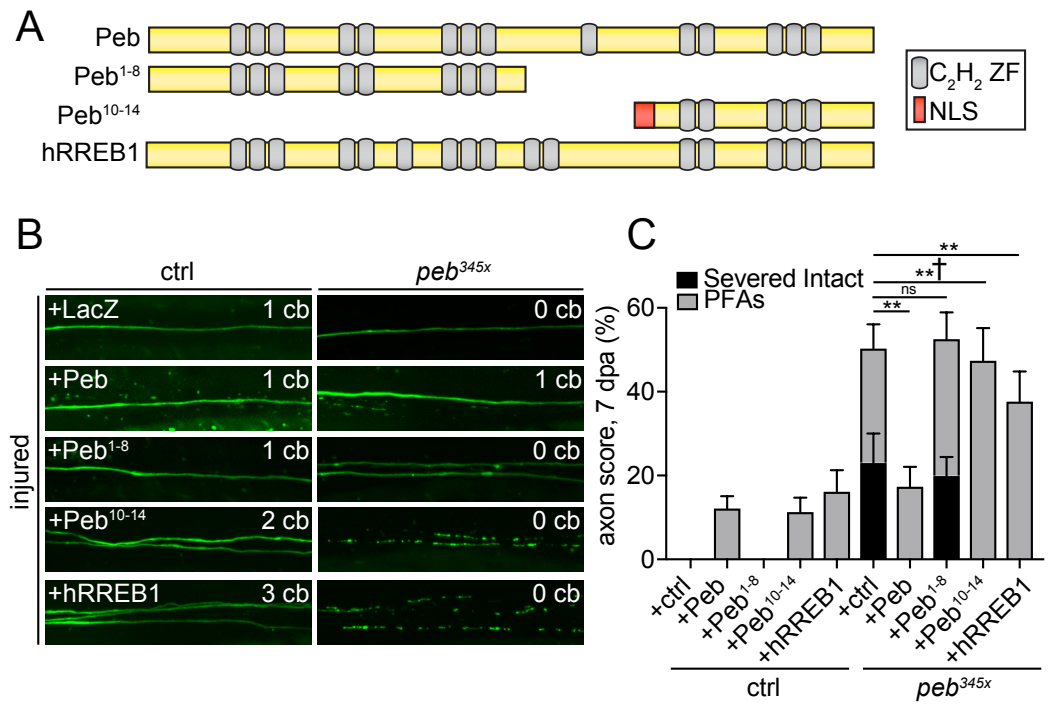

Figure 3.6. Human RREB1 Functionally Rescues Axon Death Defect in *peb* Mutants. (A) Schematic of Pebbled protein structure. Full length pebbled contains 14 C_2H_2 zinc finger domains (yellow ovals) clustered along the length of the protein. The human homolog of *peb,* Ras-responsive element binding protein 1 (hRREB1) is shown. (B-C) Representative images and quantification of Peb and hRREB1 functional rescue in control or *peb* clones, 7 dpa. Scale bar = 10 μm. (c) Quantification of axon score, 7 dpa (*n* > 30 wings). 2-way ANOVA, error = SEM (*,† p < 0.05, **,†† p < 0.01, ****,†††† p < 0.0001). † and * represent PFA and severed intact significance, respectively.

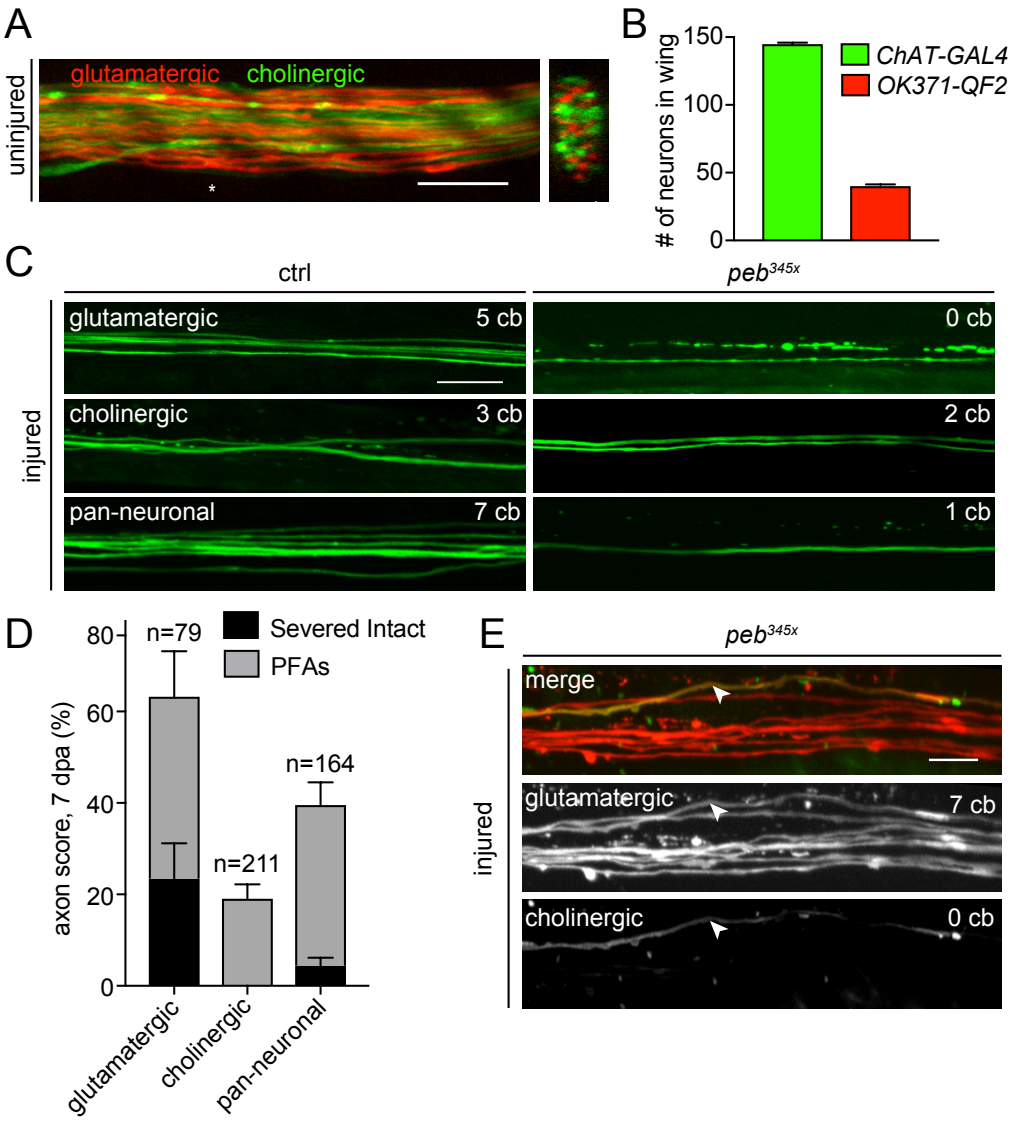

Figure 3.7. Pebbled Axon-Protective Phenotype Observed Only in Glutamatergic Neurons.

Figure 3.7. Pebbled Axon-Protective Phenotype Observed Only in Glutamatergic Neurons. (A) fluorescent projection image of two neuronal subsets within the L1 vein of the adult wing, cholinergic neurons (green) and glutamatergic neurons (red). Orthogonal view indicated at asterisk. Scale bar = 10 μm. (B) Quantifications of the number of cholinergic and glutamatergic neurons in the adult L1 wing vein using *ChAT-Gal4* and *vGlut-QF2.* (C) Representative images of axon death in three different neuronal populations (glutamatergic, cholinergic, and pan-neuronal). (D) Quantification of axon score at 7 dpa (n > 30 wings for each genotype. Glutamatergic = 79 injured neurons, cholinergic = 211 injured neurons, pan-neuronal = 164 injured neurons). (E) Severed intact *peb* clone was double labeled with *vGlut-QF2* (red) and *ChAT-Gal4* (green). Scale bar = 10 μm.

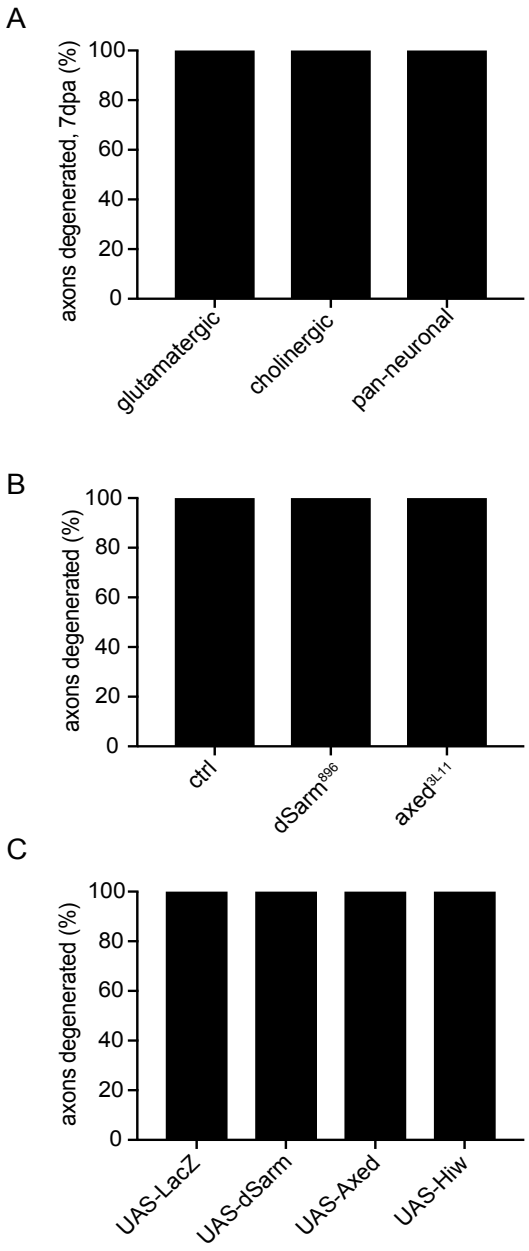

Figure 3.8. Quantifications of Injured Control Clones 7dpa. (A) Axon degeneration quantification of glutamatergic (*OK371-Gal4)*, cholinergic (*ChAT-Gal4*), and pan-neuronal (*nSyb-Gal4)* control clones showed normal axon death 7dpa (*n* > 30 wings per genotype). (B) Axon degeneration quantification of control clones lacking one allele of either *dsarm* or *axed* showed normal axon death 7dpa (*n* > 30 wings per genotype). (C) Axon degeneration quantification of control clones overexpressing axon death regulators *UAS-dSarm*, *UAS-Axed,* and *UAS-Hiw* showed normal axon death 7dpa (*n* > 30 wings per genotype).

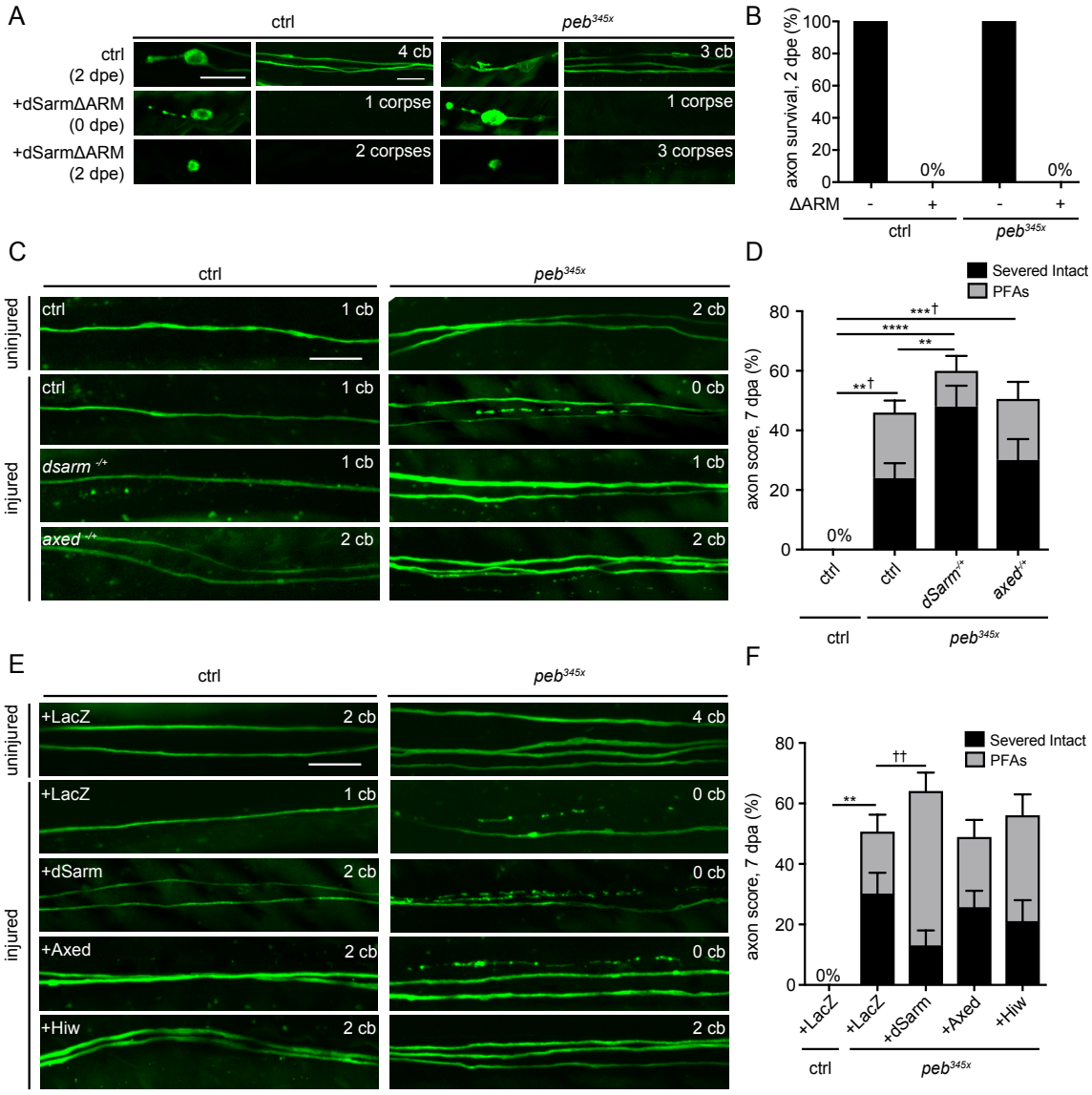

Figure 3.9. Pebbled Protective Phenotype is Enhanced When Removing One Copy of *dSarm*.

Figure 3.9. Pebbled Protective Phenotype is Enhanced When Removing One Copy of *dSarm*. (A-B) Overexpression dSarmΔARM, induced Wallerian-like death in 100% of both uninjured control and peb^{345x} clones, quantified at 2 days post eclosion (dpe) (*n* > 15 wings). (C) Images showing axon death 7dpa in control and peb^{345x} clones when one copy of either *dsarm* or *axed* was removed. Scale bar = 10 μm. (D) Quantifications of axon score at 7 dpa revealed a significant enhancement of severed intact axons in peb^{345x}, *dsarm* heterozygous (*n* > 30 wings). (E) Images showing axon death at 7dpa in control and peb^{345x} clones while over expressing the pro-axon death genes, dSarm, Axed, or Hiw. Scale bar = 10 μm. (F) Quantifications of axon score at 7 dpa, (*n* > 30 wings). 2-way ANOVA, error = SEM (*,† $p < 0.05$, **,†† $p < 0.01$, ***,††† $p < 0.001$, ****,†††† $p < 0.0001$). † and * represent PFA and severed intact significance, respectively.

Table 3.1. X-chromosome Coverage of Deficiency Lines Tested for Axon Death Defects.

Deficiency Name	BSC Stock #	Sequence Location	Axon Degeneration Phenotype
Df(1)Exel6221	7699	X:470743..523667	Wild Type
Df(1)ED6396	9052	X:493529..523630	Wild Type
Df(1)G1	34050	X:644873..654238	Wild Type
Df(1)ED6443	9053	X:656023..1026707	Wild Type
Df(1)Exel6223	7700	X:769982..909250	Wild Type
Df(1)ED404	8030	X:934942..1135445	Wild Type
Df(1)Exel6225	7702	X:986063..1134927	Wild Type
Df(1)Exel6226	7703	X:1134227..1322377	Wild Type
Df(1)ED6521	9281	X:1135273..1353976	Wild Type
Df(1)Exel6227	7704	X:1322377..1478819	Wild Type
Df(1)Exel8196	7769	X:1478819..1669248	Wild Type
Df(1)ED6565	9299	X:1894112..2317631	Wild Type
Df(1)ED409	8950	X:2042227..2317631	Wild Type
Df(1)ED6574	9054	X:2184630..2387766	Wild Type
Df(1)ED11354	9345	X:2325942..2517801	Wild Type
Df(1)Exel6230	7705	X:2387572..2545663	Wild Type
Df(1)Exel6231	7706	X:2387754..2469301	Wild Type
Df(1)ED411	8031	X:2469859..2642686	Wild Type
Df(1)ED6579	9518	X:2589210..2642686	Wild Type
Df(1)ED6584	9348	X:2636213..2685435	Wild Type
Df(1)ED6630	8948	X:2685540..3036910	Wild Type
Df(1)Exel6233	7707	X:3372961..3485687	Wild Type
Df(1)ED6712	9169	X:3432535..3789615	Wild Type
Df(1)ED6716	24145	X:3799196..4204584	Wild Type
Df(1)ED6720	9055	X:4204351..4544753	Wild Type
Df(1)ED6727 (*)	8956	X:4325174..4911061	Some Protection
Df(1)Exel6290	7753	X:5364532..5428543	Wild Type
Df(1)Exel6235	7709	X:5516611..5593966	Wild Type
Df(1)ED6802	8949	X:5679980..5965880	Wild Type
Df(1)Exel6236	7710	X:5679987..5770561	Wild Type

Deficiency Name	BSC Stock #	Sequence Location	Axon Degeneration Phenotype
Df(1)Exel6237	7711	X:5770561..5892790	Wild Type
Df(1)ED418	8032	X:5901689..6279401	Wild Type
Df(1)ED6829	8947	X:5901976..6353095	Wild Type
Df(1)Exel6238	7712	X:6068994..6268593	Wild Type
Df(1)Exel6239	7713	X:6344333..6516952	Wild Type
Df(1)Exel6240	7714	X:6543963..6669857	Wild Type
Df(1)ED6878	9625	X:6759293..6862948	Wild Type
Df(1)ED6906	8955	X:7195084..7405806	Wild Type
Df(1)Exel6241	7715	X:8709821..8806576	Wild Type
Df(1)Exel9049	7770	X:9247113..9252165	Wild Type
Df(1)ED6989	9056	X:9686653..10070473	Wild Type
Df(1)ED6991	9216	X:9686653..10211524	Wild Type
Df(1)ED7005	9153	X:10071922..10585431	Excess Fragments
Df(1)ED7010	9057	X:10546870..10629307	Wild Type
Df(1)ED7067	9154	X:11390038..11600997	Wild Type
Df(1)Exel6242	7716	X:11622385..11715783	Wild Type
Df(1)ED7170	8898	X:12752602..13277326	Wild Type
Df(1)ED7165	9058	X:12752602..13138948	Wild Type
Df(1)ED7217	8952	X:13642083..13822321	Excess Fragments
Df(1)ED7225	24146	X:13784406..14322206	Wild Type
Df(1)ED7229	9352	X:14222234..14653944	Excess Fragments
Df(1)ED7261	9218	X:14653809..14839412	Wild Type
Df(1)Exel6248	7719	X:14825993..14923667	Wild Type
Df(1)ED7265	9414	X:14826069..15007907	Wild Type
Df(1)ED7289 (**)	29732	X:15024777..15125750	Strong Protection
Df(1)ED7344	9220	X:15626447..15868141	Excess Fragments
Df(1)ED7355	8899	X:16091487..16278417	Wild Type
Df(1)ED7374	8954	X:16695187..17107632	Wild Type
Df(1)ED13478	29733	X:18085406..18102011	Wild Type

* Uncovers pebbled ; **Uncovers highwire

Table 3.1. X-chromosome Coverage of Deficiency Lines Tested for Axon Death Defects. Deficiency lines uncovering 38.7% of the X-chromosome were screened for defective axon death phenotypes. Chromosomal deletions with wild type axon degeneration are shown in blue, while two deletions, Df(1)ED6727 and Df(1)ED7289 with protective phenotypes, are shown in orange. Df(1)ED6727 uncovers *peb,* while Df(1)ED7289 uncovers the known axon death regulator, *hiw.*

Table 3.2. Top Candidate Genes from ChIP-seq

X Chromosome		Chromosome 2		Chromosome 3	
Gene ID	Gene Name	Gene ID	Gene Name	Gene ID	Gene Name
FBtr0071213	Trf4-1-RE	FBtr0071610	cv-2-RA	FBtr0072610	ebd1-RA
FBtr0074008	HDAC6-RA	FBtr0071775	dve-RA	FBtr0075941	CG10960-RC
FBtr0077250	CG15445-RA	FBtr0079747	Hnf4-RA	FBtr0078245	CG13252-RA
FBtr0100375	sdt-RF	FBtr0079869	IP3K1-RA	FBtr0078329	skd-RC
FBtr0112753	CG34449-RA	FBtr0080260	crol-RD	FBtr0078549	CG33169-RA
FBtr0300577	Trf2-RF	FBtr0081006	dl-RB	FBtr0078722	Madm-RA
FBtr0333768	Smr-RG	FBtr0081111	tup-RA	FBtr0081808	grn-RA
FBtr0340137	mys-RD	FBtr0081159	brat-RB	FBtr0082092	Unc-115a-RA
FBtr0340159	Smox-RB	FBtr0081193	ssp3-RA	FBtr0082139	CG8500-RA
FBtr0346134	IP3K2-RH	FBtr0086112	Adf1-RB	FBtr0083228	Akt1-RC
		FBtr0087493	Asx-RA	FBtr0083257	tara-RA
		FBtr0088099	shn-RB	FBtr0083812	CG31459-RA
		FBtr0088128	CG13204-RA	FBtr0084169	Eip93F-RA
		FBtr0091802	CG33798-RA	FBtr0089331	Mob2-RD
		FBtr0100298	Dyb-RD	FBtr0089717	pnt-RB
		FBtr0113043	CG10492-RB	FBtr0091929	snRNA
		FBtr0301538	Rtnl1-RH	FBtr0099989	kay-RA
		FBtr0302439	EcR-RG	FBtr0113246	Xrp1-RE
		FBtr0302439	EcR-RG	FBtr0290232	InR-RD
		FBtr0308815	tun-RC	FBtr0300747	CG11984-RH
		FBtr0330611	nvy-RC	FBtr0304468	ban-RM
		FBtr0330611	nvy-RC	FBtr0305351	CG43143-RD
		FBtr0330611	nvy-RC	FBtr0305351	CG43143-RD
		FBtr0330612	nvy-RD	FBtr0305912	nudC-RB
		FBtr0332593	CG10543-RE	FBtr0306814	Eip75B-RF
		FBtr0337091	CG5953-RD	FBtr0307368	CG43373-RC
		FBtr0342655	CG4496-RC	FBtr0307976	scny-RH
		FBtr0342796	otp-RG	FBtr0309032	CR42839-RB
		FBtr0343282	Sox14-RC	FBtr0309838	eIF5B-RE
		FBtr0343483	ITP-RG	FBtr0321266	CG5823-RB
		FBtr0344437	Kr-h1-RA	FBtr0321285	CG3764-RB
		FBtr0345487	HmgD-RD	FBtr0330090	MESR6-RB
		FBtr0345761	CR45355-RA	FBtr0332650	nkd-RC
		FBtr0345762	CR45354-RA	FBtr0332703	Lmpt-RN
				FBtr0332735	fz2-RG
				FBtr0333220	Mkp3-RD
				FBtr0335423	srp-RF
				FBtr0336474	Irk1-RE
				FBtr0339925	app-RT
				FBtr0342875	CR44720-RA
				FBtr0345217	E2f1-RE
				FBtr0345835	CR45393-RA
				FBtr0345835	CR45393-RA
				FBtr0347047	CR45939-RA
				FBtr0347047	CR45939-RA

* known Peb binding target, *nvy*, highlighted in red

Table 3.3. List of Animal Genotypes Used in Figures

Figure 3.1
FRT19A/tubGal80,hs-FLP,FRT19A ; OK371-Gal4,UAS-mCD8::GFP,ase-FLP^{2a}/+ ; UAS-mCD8::GFP,ase-FLP^{3b}/+
mut,FRT19A/tubGal80,hs-FLP,FRT19A ; OK371-Gal4,UAS-mCD8::GFP,ase-FLP^{2a}/+ ; UAS-mCD8::GFP,ase-FLP^{3b}/+*
FRT19A/tubGal80,hs-FLP,FRT19A ; OK371-Gal4,UAS-IVS-myr::tdTomato, UAS-mito-HA-GFP,ase-FLP^{2a}/+ ; UAS-IVS-myr::tdTomato,ase-FLP^{3b}/+
mut,FRT19A/tubGal80,hs-FLP,FRT19A ; OK371-Gal4,UAS-IVS-myr::tdTomato, UAS-mito-HA-GFP,ase-FLP^{2a}/+ ; UAS-IVS-myr::tdTomato,ase-FLP^{3b}/+*

Figure 3.2
y, w^{1118}
peb^{345x}, FRT19A
FRT19A/tubGal80,hs-FLP,FRT19A ; OK371-Gal4,UAS-mCD8::GFP,ase-FLP^{2a}/+ ; UAS-mCD8::GFP,ase-FLP^{3b}/+
peb^{E8},FRT19A/tubGal80,hs-FLP,FRT19A ; OK371-Gal4, UAS-mCD8::GFP,ase-FLP^{2a}/+ ; UAS-mCD8::GFP,ase-FLP^{3b}/+
FRT19A/tubGal80,hs-FLP,FRT19A ; OK371-Gal4, UAS-mCD8::GFP,ase-FLP^{2a}/+ ; UAS-mCD8::GFP,ase-FLP^{3b}/peb^{BAC}
peb^{345x},FRT19A/tubGal80,hs-FLP,FRT19A ; OK371-Gal4, UAS-mCD8::GFP,ase-FLP^{2a}/+ ; UAS-mCD8::GFP,ase-FLP^{3b}/peb^{BAC}

Figure 3.3
FRT19A/tubGal80,hs-FLP,FRT19A ; OK371-Gal4,UAS-mCD8::GFP,ase-FLP^{2a}/+ ; UAS-mCD8::GFP,ase-FLP^{3b}/+
peb^{345x},FRT19A/tubGal80,hs-FLP,FRT19A ; OK371-Gal4, UAS-mCD8::GFP,ase-FLP^{2a}/+ ; UAS-mCD8::GFP,ase-FLP^{3b}/+
FRT19A/tubGal80,hs-FLP,FRT19A ; OK371-Gal4, UAS-mCD8::GFP,ase-FLP^{2a}/+ ; UAS-mCD8::GFP,ase-FLP^{3b}/peb^{BAC}
peb^{345x},FRT19A/tubGal80,hs-FLP,FRT19A ; OK371-Gal4, UAS-mCD8::GFP,ase-FLP^{2a}/+ ; UAS-mCD8::GFP,ase-FLP^{3b}/peb^{BAC}
FRT19A/tubGal80,hs-FLP,FRT19A ; OK371-Gal4,UAS-mCD8::GFP,ase-FLP^{2a}/+ ; UAS-nls-LacZ/UAS-mCD8::GFP,ase-FLP^{3b}
peb^{345x},FRT19A/tubGal80,hs-FLP,FRT19A ; OK371-Gal4,UAS-mCD8::GFP,ase-FLP^{2a}/+ ; UAS-nls-LacZ/UAS-mCD8::GFP,ase-FLP^{3b}
FRT19A/tubGal80,hs-FLP,FRT19A ; OK371-Gal4,UAS-mCD8::GFP,ase-FLP^{2a}/+ ; FRT2A,FRT82B/UAS-mCD8::GFP,ase-FLP^{3b}
peb^{345x},FRT19A/tubGal80,hs-FLP,FRT19A ; OK371-Gal4,UAS-mCD8::GFP,ase-FLP^{2a}/+ ; FRT2A,FRT82B/UAS-mCD8::GFP,ase-FLP^{3b}
FRT19A/tubGal80,hs-FLP,FRT19A ; OK371-Gal4,UAS-mCD8::GFP,ase-FLP^{2a}/+ ; dsarm896,FRT2A,FRT82B/UAS-mCD8::GFP,ase-FLP^{3b}
peb^{345x},FRT19A/tubGal80,hs-FLP,FRT19A ; OK371-Gal4,UAS-mCD8::GFP,ase-FLP^{2a}/+ ; dsarm896,FRT2A,FRT82B/UAS-mCD8::GFP,ase-FLP^{3b}
FRT19A/tubGal80,hs-FLP,FRT19A ; OK371-Gal4,UAS-mCD8::GFP,ase-FLP^{2a}/+ ; axed0011,FRT2A,FRT82B/UAS-mCD8::GFP,ase-FLP^{3b}
peb^{345x},FRT19A/tubGal80,hs-FLP,FRT19A ; OK371-Gal4,UAS-mCD8::GFP,ase-FLP^{2a}/+ ; axed0011,FRT2A,FRT82B/UAS-mCD8::GFP,ase-FLP^{3b}
FRT19A/tubGal80,hs-FLP,FRT19A ; OK371-Gal4,UAS-mCD8::GFP,ase-FLP^{2a}/+ ; UAS-dSarm/UAS-mCD8::GFP,ase-FLP^{3b}
peb^{345x},FRT19A/tubGal80,hs-FLP,FRT19A ; OK371-Gal4,UAS-mCD8::GFP,ase-FLP^{2a}/+ ; UAS-dSarm/UAS-mCD8::GFP,ase-FLP^{3b}
FRT19A/tubGal80,hs-FLP,FRT19A ; OK371-Gal4,UAS-mCD8::GFP,ase-FLP^{2a}/+ ; UAS-Axed/UAS-mCD8::GFP,ase-FLP^{3b}
peb^{345x},FRT19A/tubGal80,hs-FLP,FRT19A ; OK371-Gal4,UAS-mCD8::GFP,ase-FLP^{2a}/+ ; UAS-Axed/UAS-mCD8::GFP,ase-FLP^{3b}
FRT19A/tubGal80,hs-FLP,FRT19A ; OK371-Gal4,UAS-mCD8::GFP,ase-FLP^{2a}/+ ; UAS-Hiw/UAS-mCD8::GFP,ase-FLP^{3b}
peb^{345x},FRT19A/tubGal80,hs-FLP,FRT19A ; OK371-Gal4,UAS-mCD8::GFP,ase-FLP^{2a}/+ ; UAS-Hiw/UAS-mCD8::GFP,ase-FLP^{3b}

Figure 3.4
y, w1118
peb-Gal4/+ ; UAS-mCD8::GFP/QUAS-mtdTomato-3xHA ; nSyb-QF2/+

Figure 3.5
y, w1118

Figure 3.6
FRT19A/tubGal80,hs-FLP,FRT19A ; OK371-Gal4,UAS-mCD8::GFP,ase-FLP^{2a}/+ ; UAS-nls-LacZ/UAS-mCD8::GFP,ase-FLP^{3b}
peb^{345x},FRT19A/tubGal80,hs-FLP,FRT19A ; OK371-Gal4,UAS-mCD8::GFP,ase-FLP^{2a}/+ ; UAS-nls-LacZ/UAS-mCD8::GFP,ase-FLP^{3b}
FRT19A/tubGal80,hs-FLP,FRT19A ; OK371-Gal4,UAS-mCD8::GFP,ase-FLP^{2a}/+ ; UAS-Peb/UAS-mCD8::GFP,ase-FLP^{3b}
peb^{345x},FRT19A/tubGal80,hs-FLP,FRT19A ; OK371-Gal4,UAS-mCD8::GFP,ase-FLP^{2a}/+ ; UAS-Peb/UAS-mCD8::GFP,ase-FLP^{3b}
FRT19A/tubGal80,hs-FLP,FRT19A ; OK371-Gal4,UAS-mCD8::GFP,ase-FLP^{2a}/+ ; UAS-Peb$^{1-8}$/UAS-mCD8::GFP,ase-FLP^{3b}
peb^{345x},FRT19A/tubGal80,hs-FLP,FRT19A ; OK371-Gal4,UAS-mCD8::GFP,ase-FLP^{2a}/+ ; UAS-Peb$^{1-8}$/UAS-mCD8::GFP,ase-FLP^{3b}
FRT19A/tubGal80,hs-FLP,FRT19A ; OK371-Gal4,UAS-mCD8::GFP,ase-FLP^{2a}/+ ; UAS-Peb$^{10-14}$/UAS-mCD8::GFP,ase-FLP^{3b}
peb^{345x},FRT19A/tubGal80,hs-FLP,FRT19A ; OK371-Gal4,UAS-mCD8::GFP,ase-FLP^{2a}/+ ; UAS-Peb$^{10-14}$/UAS-mCD8::GFP,ase-FLP^{3b}
FRT19A/tubGal80,hs-FLP,FRT19A ; OK371-Gal4,UAS-mCD8::GFP,ase-FLP^{2a}/+ ; UAS-hRREB1/UAS-mCD8::GFP,ase-FLP^{3b}
peb^{345x},FRT19A/tubGal80,hs-FLP,FRT19A ; OK371-Gal4,UAS-mCD8::GFP,ase-FLP^{2a}/+ ; UAS-hRREB1/UAS-mCD8::GFP,ase-FLP^{3b}

Figure 3.7
w ; vGlut-QF2,QUAS-mtdTomato-3xHA,ChAT-Gal4,UAS-mCD8::GFP; +/+
FRT19A/tubGal80,hs-FLP,FRT19A ; OK371-Gal4,UAS-mCD8::GFP,ase-FLP^{2a}/+ ; UAS-mCD8::GFP,ase-FLP^{3b}/+
peb^{345x},FRT19A/tubGal80,hs-FLP,FRT19A ; OK371-Gal4,UAS-mCD8::GFP,ase-FLP^{2a}/+ ; UAS-mCD8::GFP,ase-FLP^{3b}/+
FRT19A/tubGal80,hs-FLP,FRT19A ; ChAT-Gal4,UAS-mCD8::GFP/ase-FLP^{2a} ; UAS-mCD8::GFP,ase-FLP^{3b}/+
peb^{345x},FRT19A/tubGal80,hs-FLP,FRT19A ; ChAT-Gal4,UAS-mCD8::GFP/ase-FLP^{2a} ; UAS-mCD8::GFP,ase-FLP^{3b}/+
FRT19A/tubGal80,hs-FLP,FRT19A ; UAS-mCD8::GFP,ase-FLP^{2a}/+ ; nSyb-Gal4,UAS-mCD8::GFP,ase-FLP^{3b}/+
peb^{345x},FRT19A/tubGal80,hs-FLP,FRT19A ; UAS-mCD8::GFP,ase-FLP^{2a}/+ ; nSyb-Gal4,UAS-mCD8::GFP,ase-FLP^{3b}/+
peb^{345x},FRT19A/tubGal80,hs-FLP,FRT19A; vGlut-QF2,QUAS-mtdTomato-3xHA,ChAT-Gal4,UAS-mCD8::GFP/ase-FLP^{2a}; UAS-mCD8::GFP,ase-FLP^{3b}/+

Figure 3.8
FRT19A/tubGal80,hs-FLP,FRT19A ; OK371-Gal4,UAS-mCD8::GFP,ase-FLP^{2a}/+ ; UAS-mCD8::GFP,ase-FLP^{3b}/+
FRT19A/tubGal80,hs-FLP,FRT19A ; ChAT-Gal4,UAS-mCD8::GFP/ase-FLP^{2a} ; UAS-mCD8::GFP,ase-FLP^{3b}/+
FRT19A/tubGal80,hs-FLP,FRT19A ; UAS-mCD8::GFP,ase-FLP^{2a}/+ ; nSyb-Gal4,UAS-mCD8::GFP,ase-FLP^{3b}/+
FRT19A/tubGal80,hs-FLP,FRT19A ; OK371-Gal4,UAS-mCD8::GFP,ase-FLP^{2a}/+ ; FRT2A,FRT82B/UAS-mCD8::GFP,ase-FLP^{3b}
FRT19A/tubGal80,hs-FLP,FRT19A ; OK371-Gal4,UAS-mCD8::GFP,ase-FLP^{2a}/+ ; dsarm896,FRT2A,FRT82B/UAS-mCD8::GFP,ase-FLP^{3b}
FRT19A/tubGal80,hs-FLP,FRT19A ; OK371-Gal4,UAS-mCD8::GFP,ase-FLP^{2a}/+ ; axed0011,FRT2A,FRT82B/UAS-mCD8::GFP,ase-FLP^{3b}
FRT19A/tubGal80,hs-FLP,FRT19A ; OK371-Gal4,UAS-mCD8::GFP,ase-FLP^{2a}/+ ; UAS-nls-LacZ/UAS-mCD8::GFP,ase-FLP^{3b}
FRT19A/tubGal80,hs-FLP,FRT19A ; OK371-Gal4,UAS-mCD8::GFP,ase-FLP^{2a}/+ ; UAS-dSarm/UAS-mCD8::GFP,ase-FLP^{3b}
FRT19A/tubGal80,hs-FLP,FRT19A ; OK371-Gal4,UAS-mCD8::GFP,ase-FLP^{2a}/+ ; UAS-Axed/UAS-mCD8::GFP,ase-FLP^{3b}
FRT19A/tubGal80,hs-FLP,FRT19A ; OK371-Gal4,UAS-mCD8::GFP,ase-FLP^{2a}/+ ; UAS-Hiw/UAS-mCD8::GFP,ase-FLP^{3b}

Figure 3.9
FRT19A/tubGal80,hs-FLP,FRT19A ; OK371-Gal4,UAS-mCD8::GFP,ase-FLP^{2a}/UAS-dSarmΔARM ; UAS-mCD8::GFP,ase-FLP^{3b}/+
peb^{345x},FRT19A/tubGal80,hs-FLP,FRT19A ; OK371-Gal4,UAS-mCD8::GFP,ase-FLP^{2a}/UAS-dSarmΔARM ; UAS-mCD8::GFP,ase-FLP^{3b}/+
FRT19A/tubGal80,hs-FLP,FRT19A ; OK371-Gal4,UAS-mCD8::GFP,ase-FLP^{2a}/+ ; FRT2A,FRT82B/UAS-mCD8::GFP,ase-FLP^{3b}
peb^{345x},FRT19A/tubGal80,hs-FLP,FRT19A ; OK371-Gal4,UAS-mCD8::GFP,ase-FLP^{2a}/+ ; FRT2A,FRT82B/UAS-mCD8::GFP,ase-FLP^{3b}
FRT19A/tubGal80,hs-FLP,FRT19A ; OK371-Gal4,UAS-mCD8::GFP,ase-FLP^{2a}/+ ; dsarm896,FRT2A,FRT82B/UAS-mCD8::GFP,ase-FLP^{3b}
peb^{345x},FRT19A/tubGal80,hs-FLP,FRT19A ; OK371-Gal4,UAS-mCD8::GFP,ase-FLP^{2a}/+ ; dsarm896,FRT2A,FRT82B/UAS-mCD8::GFP,ase-FLP^{3b}
FRT19A/tubGal80,hs-FLP,FRT19A ; OK371-Gal4,UAS-mCD8::GFP,ase-FLP^{2a}/+ ; axed0011,FRT2A,FRT82B/UAS-mCD8::GFP,ase-FLP^{3b}
peb^{345x},FRT19A/tubGal80,hs-FLP,FRT19A ; OK371-Gal4,UAS-mCD8::GFP,ase-FLP^{2a}/+ ; axed0011,FRT2A,FRT82B/UAS-mCD8::GFP,ase-FLP^{3b}
FRT19A/tubGal80,hs-FLP,FRT19A ; OK371-Gal4,UAS-mCD8::GFP,ase-FLP^{2a}/+ ; UAS-nls-LacZ/UAS-mCD8::GFP,ase-FLP^{3b}
peb^{345x},FRT19A/tubGal80,hs-FLP,FRT19A ; OK371-Gal4,UAS-mCD8::GFP,ase-FLP^{2a}/+ ; UAS-nls-LacZ/UAS-mCD8::GFP,ase-FLP^{3b}
FRT19A/tubGal80,hs-FLP,FRT19A ; OK371-Gal4,UAS-mCD8::GFP,ase-FLP^{2a}/+ ; UAS-dSarm/UAS-mCD8::GFP,ase-FLP^{3b}
peb^{345x},FRT19A/tubGal80,hs-FLP,FRT19A ; OK371-Gal4,UAS-mCD8::GFP,ase-FLP^{2a}/+ ; UAS-dSarm/UAS-mCD8::GFP,ase-FLP^{3b}
FRT19A/tubGal80,hs-FLP,FRT19A ; OK371-Gal4,UAS-mCD8::GFP,ase-FLP^{2a}/+ ; UAS-Axed/UAS-mCD8::GFP,ase-FLP^{3b}
peb^{345x},FRT19A/tubGal80,hs-FLP,FRT19A ; OK371-Gal4,UAS-mCD8::GFP,ase-FLP^{2a}/+ ; UAS-Axed/UAS-mCD8::GFP,ase-FLP^{3b}
FRT19A/tubGal80,hs-FLP,FRT19A ; OK371-Gal4,UAS-mCD8::GFP,ase-FLP^{2a}/+ ; UAS-Hiw/UAS-mCD8::GFP,ase-FLP^{3b}
peb^{345x},FRT19A/tubGal80,hs-FLP,FRT19A ; OK371-Gal4,UAS-mCD8::GFP,ase-FLP^{2a}/+ ; UAS-Hiw/UAS-mCD8::GFP,ase-FLP^{3b}

Table 3.1
Deficiency,FRT19A/tubGal80,hs-FLP,FRT19A ; OK371-Gal4,UAS-mCD8::GFP,ase-FLP^{2a}/+ ; UAS-mCD8::GFP,ase-FLP^{3b}/+

CHAPTER IV: Discussion

Summary of Findings

This thesis investigates the underlying mechanism of Wallerian degeneration and identifies key molecules required to execute this axon death signal cascade. Using sensory neurons in the *Drosophila* adult wing to model WD *in vivo*, I have identified and characterized a novel role for a transcription factor known to be predominantly required in early embryonic development in regulating axon death after injury. This discovery expands on the current model widely accepted in the field of local signaling within the distal axon upon axotomy.

In CHAPTER II, I described the approach taken by myself, along with a number of colleagues in the lab, to identify novel genes required to execute the death of a distal axon after it has been separated from its respective neuronal cell body. Harnessing the power of an unbiased forward genetic mutagenesis screen paired with the sophisticated genetic manipulations capable in *Drosophila,* our hard work yielded a number of mutant alleles displaying defective axon degeneration. Together, at the end of three years, we screened through more than 40,000 independently mutated chromosomes and identified fifteen alleles showing axons with variable degrees of protection from degeneration: eleven were identified as mutations in the E3 ubiquitin ligase, *hiw*, two were independent loss of function alleles in the previously uncharacterized gene, *axed*, one was an allele of *dsarm,* and the final isolated *345x* mutation was an allele of the gene, *peb*.

While this screen did in fact result in the discovery of two new components of the WD signaling cascade, it was not as fruitful as we had anticipated. We had hopes of identifying a great number of genes allowing us to tease apart a complete genetic pathway, however as with any system, there are limitations and complications. Looking at the forward genetic F_1 screen, one complication that arose was the rate of recovery of the isolated mutants. Theoretically, one should have a 50% chance of recovering the mutation; either it reached the germline or the mutation was somatic. There are other factors that contribute to a decreased recovery rate, such as mosaicism or the mutation leading to lethality or sterility of the isolated male. Both Thomas Burdett and myself identified axon degeneration defective mutants on chromosome 2L but failed to recover them for validation and characterization. Another limiting factor of the screen is that, while the wing is significantly faster than previous models of WD, it is still time consuming and labor intensive. Therefore, we have not fully saturated the *Drosophila* genome while looking for suppressors of axon death. Finally, axonal transection is a severe injury and wanting complete axon survival after injury may be too demanding. Therefore, we must consider new approaches to identify remaining axon death regulators, which I will discuss in a later section.

The work described in CHAPTER III focused on the identification and further characterization of the mutant peb^{345x} allele, emphasizing its role as the first transcription factor involved in the regulation of WD. Preliminary data

showed a partial protection and delay of degeneration in *peb* mutant glutamatergic axons after transection, which can be observed up to two weeks after injury, albeit at decreased levels. Not only do loss of *peb* neurons display defective WD, they also exhibit a striking novel degenerative phenotype which I classify as partially fragmented axons (PFAs). Under normal conditions, severed distal axons undergo a catastrophic fragmentation, resulting in small pieces of axon debris. *Peb* mutant axons, on the other hand, frequently fragment into larger, intact pieces, measuring an average three-fold longer than control debris.

To confirm that both the axon death defect and PFA phenomenon were caused by the loss of function peb^{345x} allele, I performed a series of rescue experiments which re-expressed *peb* at endogenous levels as well as overexpressed via the GAL4-UAS binary system. Peb canonically functions as a zinc finger transcription factor essential in regulating a multiple cellular processes in the developing embryo (Yip et al., 1997; Reed et al., 2001; Sun and Deng, 2007), and most recently has been shown to be evolutionarily conserved, as its human homolog, Ras-responsive element binding protein 1 (RREB1), can functionally substitute for Peb in attenuating the transcription of the gene *nervy* (Ming et al., 2013). Consistent with these data, ectopic expression of RREB1 in peb^{345x} mutants completely rescues the observed axon death defective phenotype. Immunohistochemistry analyses show Peb expression is detectable only within the nuclei of sensory neurons of the PNS, and functionally requires the carboxy-terminal zinc finger domains 10-14 to implement axon degeneration.

These data strongly suggest that Peb is modulating WD at the transcriptional level. Which axon death genes are specifically regulated by Peb remains unclear and further research on this topic is required.

All of the axon death analyses thus far have be performed in *OK371-GAL4*$^{+}$ glutamatergic neurons. These cells represent only about 1/6 the total population of neurons within the L1 vein of the wing (as quantified by GAL4 expression) (Fang et al., 2012), while the majority of the remainder appear to be cholinergic. Therefore, I tested whether mutant *peb's* axon protective characteristic extended to other neuronal subsets present in the wing, similar to that of the other WD signaling molecules *dsarm, hiw,* and *axed* (Osterloh, 2013; Neukomm and Freeman, 2014; Neukomm et al., 2017). To address this question, I injured *peb* mutants labeled with a GAL4 driver specific for cholinergic neurons, *choline acetyltransferase-GAL4* (*ChAT-GAL4)*, along with the pan-neuronal driver *synaptobrevin-GAL4 (nSyb-GAL4)*. Only loss of function *peb* mutant glutamatergic neurons were protected from axotomy. This result was surprising, as the previously identified WD signaling molecules all regulate axon degeneration equally across neuronal subtypes. *peb* mutant cholinergic neurons either degenerated as normal or presented the PFA phenotype. Severed *nSyb-GAL4* clones showed a level of complete protection 1/6th that of glutamatergic neurons, further supporting the idea that *peb* regulates WD specifically in glutamatergic sensory neurons.

Finally, I wanted to see where *peb* may be operating in the WD signaling pathway. The first tool used was the gain of function molecule, dSarmΔARM, which constitutively signals for axon death in the absence of injury. ΔARM mimics active dSarm/Sarm1 signaling and can be partially suppressed by overexpression of Wld^S or completely blocked by loss of downstream *axed* (Gerdts et al., 2013; Neukomm et al., 2017). Loss of *peb*, however, is not sufficient to suppress ΔARM induced degeneration, suggesting that *peb* is functioning either upstream or in a parallel genetic pathway in WD signaling (Figure 4.1). To further examine where *peb* may be functioning, I performed a number of experiments to see a potential enhancement or suppression of the axon death defective phenotype by modulating the levels of either *dsarm* or *axed*. Traditionally, epistatic analyses assay the interaction of different genes by observing the strength or suppression of a given phenotype for each mutant allele, however this was not possible with *peb* and the other axon death genes. The *dsarm*, hiw, and *axed* mutant clones show complete inhibition of injury-induced degeneration, therefore any additive protection that *peb* may confer would be masked by their inherently strong protective natures. Complete protection from degeneration increased two-fold in *peb* mutants only when *dsarm,* and not *axed*, levels were reduced ($peb^{-/-}$, $dsarm^{-/+}$). Similarly, there was a trend toward suppression of protection with increased dSarm levels ($peb^{-/-}$, *UAS-dSarm),* but not overexpression of Axed or Hiw. These data indicate *peb* protection may be dependent on *dSarm* levels, however, I cannot conclude that

they interact genetically, as *peb/dsarm trans*-heterozygous analysis did not show a protective effect.

How is *peb* Regulating Axon Degeneration?

As mentioned above, the results from CHAPTER III lead me to believe that *peb* is indeed regulating axon death after injury at the transcriptional level. Current literature shows a number of cellular processes are transcriptionally regulated by *peb* during *Drosophila* embryogenesis. For instance, successful dorsal closure of the embryo requires the establishment of a high/low JNK signaling boundary between the epidermis and the amnioserosa (AS). This JNK boundary is *peb*-dependent, and is formed by the down regulation of JNK signaling within the AS through increased transcription of the JNK phosphatase, *puc* (Reed et al., 2001). Mammalian JNK signaling has recently been implicated in WD, as knocking down both MKK4 and MKK7 or all three JNK molecules (JNK1/JNK2/JNK3) in the MAPK signaling cascade modestly suppress axon death *in vitro* (Yang et al., 2015; Walker et al., 2017). These findings, paired with the fact that *peb* can modulate JNK signaling, suggests a potentially ideal WD mechanism. The AS expression data suggests loss of *peb* in neurons would, in theory, downregulate *puc* expression, increasing active phosphorylated JNK signaling after injury. In our hands, however, loss of function alleles of the *Drosophila* homologs of *MKK4/MKK7 (dMkk4/hemipterous, hep)* or JNK (*basket, bsk)* were insufficient to block WD *in vivo* (Osterloh et al., 2012; Neukomm et al., 2017). In contrast,

overexpression of Peb should upregulate *puc,* but has no axon protective effect after injury, further discrediting the involvement of JNK in axotomy in *Drosophila.*

Considering its primary role is gene regulation, it is most likely that *peb*'s protective nature is due to altered transcript levels of WD signaling molecules. I have demonstrated that the *peb* phenotype can be enhanced by modulating levels of *dsarm,* consequently, I hypothesized that loss of *peb* in the neurons could reduce levels of *dSarm* or potentially *hiw* and *axed.* Through ChIP analysis and qPCR validation, Peb has previously been shown to transcriptionally attenuate *nervy* expression through direct binding of Peb to the *nvy* locus (Ming et al., 2013). Therefore, I performed ChIP-seq in a homologous *in vitro* system in an attempt to find novel Peb binding sites in the genome, cross reference these sites to genes known to be involved in WD regulation, and further validate candidate genes. While my ChIP-seq dataset positively identified a known gene *nvy* as a Peb binding site, my analysis did not identify any other known WD genes. There are a few possible interpretations of these data: *peb* indirectly modulates the known axon death genes, or *peb* directly/indirectly modulates axon death genes that have yet to be identified. Due to limitations in starting material and antibody concentration, I opted to perform the ChIP *in vitro* using GM2 cells. A better execution of the experiment would involve performing the ChIP *in vivo,* in peripheral sensory neurons against endogenous Peb, perhaps yielding more physiologically relevant results.

While ChIP-seq would identify where Peb is directly binding and potentially regulating, looking at differential gene expression profiles will provide greater detail of the transcripts affected by loss of *peb.* Described in detail in Appendix 1, I performed RNA-seq in GM2 cells in which I decrease *peb* expression via clustered regularly interspaced short palindromic repeats/CRISPR-associated (CRISPR/Cas9). When *peb* expression was reduced, there was no significant changes in the transcript levels of identified WD regulators *dsarm, hiw, nmnat,* and *bsk.* Unexpectedly, *axed* levels in GM2 cells were significantly upregulated as compared to controls. This is surprising, since modulating levels of *axed* in *peb* mutants showed no enhancement or suppression of the *peb* degeneration defect. Perhaps removing one copy of *axed* is not enough to enhance protection in *peb* mutants after axotomy, as these neurons already show an increased basal level of Axed protein expression. Similar to the limitations mentioned with ChIP-seq, a more accurate list of differential gene expression would be derived from *peb* null sensory neurons rather than reduced *peb* expression in GM2 cells.

A large body of published literature, functional domain analysis, and IHC analysis strongly suggests *peb* is acting as a transcription factor in regulating WD. While these data support this most logical hypothesis, I cannot exclude the possibility of a non-canonical role for Peb in axon death. When looking at peripheral sensory neurons in the pupal wing, Peb was detectable only within the nucleus by IHC. Our attempts to visualize untagged endogenous dSarm or Axed

were also unsuccessful, implying that these molecules exist within the cytoplasm of distal axons at extremely low levels. Even the axon protective molecule Wld^S was detectable within the nucleus by IHC analysis, however it is known that Wld^S protein is present in the cytoplasm as well as the mitochondria (Beirowski et al., 2009; Avery et al., 2012). I hypothesize an undetectable level of Peb is present in the axoplasm and is required for the execution of axon degeneration. Further experiments would be required to investigate this possibility. In *peb* mutant clones, one could re-express a version of Peb containing a nuclear export signal, directing it to the cytoplasm of the axon, and whether axoplasmic Peb regulates axon degeneration after injury. Alternatively, sequential mutational analysis can prevent individual zinc finger domains from binding zinc ions, thus abolishing their DNA binding capacity and eliminating the transcriptional regulatory function of Peb. Re-expression of these mutated constructs in *peb* clones will isolate the zinc finger domains found to be both necessary and sufficient for execution of WD.

An interesting question that remains is when during the life of the neuron is *peb* required to initiate degeneration after injury? Does *peb* establish a cellular competence for axon death early during development once the neuron is differentiated, or is it continuously controlling WD gene transcription in mature, adult neurons? Using a combined approach of IHC and GAL4 expression, I show that Peb is present in all differentiated sensory neurons ($ElaV^+$ or *nSyb-GAL4*$^+$) within the mid-pupal and adult stage wings, suggesting *peb* may regulate

axon death gene expression early during development. Use of fluorescently labeled neurons by GAL4 expression is informative, but the relative stability of the membrane bound GFP protein can be misleading when looking to quantify expression levels over time. It would be ideal to examine levels of Peb in neurons at different developmental stages of the wing by IHC, however, I was restricted to a specific developmental window, as the formation of the waxy cuticle prohibits antibody penetration in late pupal and adult wings.

Overexpression of full-length Peb, the human homolog RREB1, and the C-terminal zinc fingers 10-14 (Peb^{10-14}) are sufficient to rescue the axon protective defect in *peb* mutant glutamatergic (*OK371-GAL4*$^{+}$) neurons. This GAL4 driver turns on expression during late embryogenesis and remains on for the duration of the life of the animal (Mahr and Aberle, 2006), therefore to address when *peb* may regulate WD, it would be ideal to temporally restrict expression of Peb rescue constructs to the adult. I attempted to re-express full length Peb after development by using a temperature sensitive (TS) version of the GAL4 repressor, $GAL80^{TS}$, but encountered a number of difficulties. The animals containing $GAL80^{TS}$ were raised at a restrictive temperature (18°C) until adulthood, then switched to a permissive temperature (29°C) to allow for GAL4 expression. This shift to a permissive temperature did not allow for sufficient accumulation of GFP in the *peb* mutant neurons while simultaneously increasing background autofluorescence of the wing cuticle itself. Together these made visualization of wing axons near impossible. Perhaps using the analogous

antennal ablation WD model would avoid these complications, however in my hands, all *peb* mutant *OR22a-GAL4* clones spontaneously degenerated and may suggest that *peb* expression is essential for the survival of these olfactory receptor neurons.

The Partially Fragmenting Axon Phenotype

One of the more unexpected findings from the mutagenesis screen was the novel degeneration phenotype observed in peb^{345x} mutants after injury. Normally, transected axons undergo a stereotypical and complete degenerative process in which the distal axon loses morphological integrity and fragments into small, membranous pieces (Sievers et al., 2003). In the case of *peb* mutants, I found the axonal fragments displaying this phenotype are present 7 dpa, and measure an average 3 times larger than any residual debris observed in control neurons. In some instances, I recorded axon fragments exceeding 30 μm in length. This discovery is exciting, as it may have revealed axon degeneration can be separated into two phases: initiation and execution. The transected axons which are completely preserved may have an inhibited initiation of degeneration, whereas the PFAs could possibly represent a defect in the execution of degeneration – these axons begin to fall apart, but do not go through that terminal, explosive fragmentation in WD. Two underlying questions remain unanswered: what specifically is causing these PFAs to appear, and what

intrinsic mechanism decides whether a *peb* mutant will degenerate, be protected, or present PFAs after axotomy.

One possibility could be a potential defect in calpains, the calcium dependent cysteine proteases ultimately responsible for the cytoskeletal breakdown during WD. During the tail-end of the latent phase, intra-axonal Ca^{2+} concentrations rise, causing the cleavage of axonal microtubules and spectrin by newly activated calpains (Billger et al., 1988; Johnson et al., 1991). Suppressing calpain function by overexpression of the endogenous calpain inhibitor has been shown to modestly protect axons from degenerating after injury *in vitro* (Yang et al., 2013), however, when suppression inevitably fails, these axons degenerate as normal, that is, all at once along the length of the distal severed axon. *Drosophila* have four endogenous calpains (Calpain A, B, C, and D) (Friedrich et al., 2004), therefore, if *peb* positively regulates one or more of these calpains, then perhaps loss of *peb* in neurons could lead to defective or inefficient cytoskeletal degradation and the PFA phenotype.

It would be interesting to understand exactly how the *peb* mutants degenerate after axotomy. Classically, degenerating axons take on a dystrophic, blebbed morphology resembling beads on a string, then, as if all at once, the axons fragment. In *peb* mutants presenting PFAs, it appears that there are sporadic sites of breakage forming these long axonal pieces, potentially representing focal defects in cytoskeletal integrity. A similar phenotype is seen in *C. elegans* harboring mutations in *β-spectrin*. Animals with defects in axonal

cytoskeletal integrity spontaneously fragment into long, continuous pieces resembling PFAs found in injured *peb* clones (Hammarlund et al., 2007). Live imaging could shed light on the nature of PFAs, how they are formed, their overall dynamics, and how they are eventually cleared from the animal. Do *peb* mutants break simultaneously or sequentially along the length of the axon? Once broken, do these PFAs further fracture or are they chewed back from their respective ends? Additional in depth research paired with differential gene analysis may answer some of these questions.

Cell Type Specific Protection in *peb* Mutants

Specific vulnerability of regions and neuronal subsets within the brain is a well-established feature in some neurodegenerative diseases. Selective loss of dopaminergic neurons within the *substantia nigra pars compacta* is a hallmark of Parkinson's disease (Barzilai and Melamed, 2003), while amyotrophic lateral sclerosis progressively affects both upper and lower motor neurons in the CNS (Blizzard et al., 2015). Not just limited to the CNS, neurons in the PNS are prone to degenerate in peripheral neuropathies, as seen in diabetes and in some cases, after chronic exposure to chemotherapeutic drugs (Coleman and Perry, 2002; Saxena and Caroni, 2011; Geisler et al., 2016). In WD, however, there is no known report of cell specific vulnerability after axonal transection; all wild-type neurons will degenerate after axotomy.

Up until now, we believed that WD signaling molecules were created equal, functioning the same in all axons. Removal of either *dsarm*, *hiw,* or *axed* in glutamatergic neurons will protect axons from injury-induced degeneration just as robustly as if they were removed from cholinergic neurons (Osterloh et al., 2012; Neukomm et al., 2014; 2017). As this was an accepted truth, it was most surprising when I observed loss of *peb* in cholinergic sensory neurons failed to confer protection after injury. While complete suppression of degeneration failed in these neurons, they still exhibited PFAs, suggesting the two phenotypes are potentially genetically separable.

How exactly *peb* regulates axon death in neurons is still unknown. As mentioned previously, I believe that the abundant amount of literature, in conjunction with my results in CHAPTER III, support the notion that *peb* is modulating axon death signaling at the transcriptional level. Perhaps increased expression of Peb during neuronal development could establish a cellular competence for axons to degenerate after injury. This notion of "competence" is not unheard of, as it has been observed that some axons in certain lower invertebrate species (rock lobster, crickets, sea slugs, and *C. elegans*) are not always genetically programed to die after physical injury and fail to undergo WD (Atwood et al., 1989; Parnas et al., 1991; Benbassat and Spira, 1994; Stengl, 1995; Neumann et al., 2011). Therefore, *peb* could be programming both glutamatergic and cholinergic neurons to degenerate. A second redundant

pathway specific to cholinergic neurons could compensate for the loss of *peb* function.

It would be of great interest and importance to tease apart this complex discovery. While the GM2 cell RNA-seq in appendix 1 could contain a substantial amount of information regarding the *peb* protective phenotype in general, a more specific approach would be required to understand the cell type specific protection of *peb* mutants. If it would be possible to independently isolate glutamatergic and cholinergic *peb* null clones from the adult wing, we could perform RNA-seq on each cell population. A four-way comparison of changes in gene expression between cholinergic and glutamatergic neurons, wild type and mutant, might highlight novel genes of importance.

How Do Transected Axons Survive?

The discovery of these intrinsic axon pro-degenerative molecules not only shifted seminal views in the axon degeneration field, but also has opened many avenues for new research and discoveries in neuron-glial biology. A puzzling idea still requiring further investigation is the notion that these mutant axons persist for weeks, or in the case of flies, the lifetime of the animal, without support from their respective cell bodies. In terms of energy production, degenerating axons experience massive energy depletions after axotomy (Sasaki et al., 2016; Essuman et al., 2017) and mitochondria appear to significantly shrink or fragment just prior to loss of axonal membrane integrity. In the case of severed intact *peb*

mutant axons, mitochondria are significantly smaller, resembling the compact, swollen mitochondria in control axons just prior to fragmentation, at 7dpa (Park et al., 2013). Presumably, these mitochondria have diminished capacity for energy production, however this is purely speculative. Interestingly, there is no change in mitochondria length in *dsarm* mutants at 7dpa, potentially explaining why these mutants completely avoid degeneration while *peb* mutants simply offer a delay in WD. Further research is required to fully understand the differences of mitochondria length between *peb* and *dsarm* mutants, and it would be worth investigating if this phenotype was caused by *peb* itself or genes that regulate mitochondrial fission or fusion.

Not only are axon death defective mutants surviving without nascent protein synthesis and support from the cell soma, but they have the capacity to release neurotransmitters either spontaneously or by artificial stimulation (Xiong et al., 2012; Neukomm et al., 2017). Most likely these surviving axons receive local metabolic support from surrounding glial cells. Mammalian data shows axons can take up lactate, pyruvate and other metabolites secreted from oligodendroglia, and genetic ablation of the monocarboxylate transporter 1, the means by which lactate is transported into the periaxonal space from myelin, causes degeneration of adjacent axons (Griffiths et al., 1998; Fünfschilling et al., 2012; Lee et al., 2012). Looking forward, we can harness the power of *Drosophila* genetics to identify glial specific genes required for axon support and maintenance. Exploiting the protective nature of the Wld^S protein, we can

prevent axons from degenerating while simultaneously modifying genes specifically in glia with RNAi. Resulting candidate genes can be potentially validated with loss of function alleles and maintenance of *dsarm, axed,* or *hiw* mutants can be evaluated.

Identifying Remaining Axon Death Signaling Molecules

Looking to the future of the axon death field, there are many questions remaining to be answered. In particular, what are the remaining genes and molecules required for axon degeneration signaling? Recent research has made many advancements in filling in the gaps of knowledge, but the picture remains incomplete. We know injury to an axon leads to an activation of dSarm/Sarm1 while simultaneously blocking the anterograde transport of the pro-survival molecule dNmnat/Nmant2 (Gilley and Coleman, 2010; Osterloh et al., 2012; Gerdts et al., 2013). Recent research showed the massive energy depletion in distal axons is primarily due to a novel NADase function for the TIR domain in active Sarm1 signaling (Essuman et al., 2017), but what specifically functions upstream and causes Sarm activation remains to be discovered. Similarly, the discovery of *axundead* shows multiple pathways of axon degeneration (axotomy, NAD+ depletion, gain of function dSarm) converge on Axed to execute degeneration, but downstream effectors are still unknown.

In moving forward, we have to ask ourselves, what is the best method for identifying these unknown WD signaling molecules? Unbiased mutagenesis

screening with axotomy has been fruitful multiple times over in isolating novel components of this pathway, however, the abundance of genes has proven to be less than we predicted. When the axotomy screen was first started, we believed we would find a plethora of genes and piece by piece, we could assemble a complete mechanism for axon death. It appears that after screening over 40,000 individual mutant chromosomes, there may be fewer genes required to execute degeneration, or perhaps there are redundant pathways, and only few key molecules such as *dsarm, hiw,* and *axed* can suppress WD completely. Continuing this screen until saturation of the genome is reached may further pull out WD regulators.

Axotomy is an extreme injury, and expecting an axon to survive after being cut in half may be asking too much from a neuron. Therefore, we should turn to other ways in which to find WD molecules *in vivo*, specifically, performing suppressor screens of axon death. We can do this two ways: first, we can continue the dSarmΔARM suppressor screen which I initiated and describe in Appendix 2, and secondly, we can look for suppressors of NAD+ depletion induced cell death. Overexpression of either gain of function dSarmΔARM or d*Nmnat*^{RNAi} causes spontaneous degeneration of both axons and their cell bodies and can be suppressed in *axed* loss of function mutants, serving as a proof of concept (Neukomm et al., 2017). Using EMS mutagenesis methods established in CHAPTER II, we can quickly screen for candidates in which

neurons do not degenerate when ΔARM is expressed or dNmnat levels are knocked down.

Axon Death Molecules and Neurodegeneration Therapeutics

Understanding the underlying molecules governing injury-induced axon degeneration goes beyond furthering scientific knowledge in basic axon biology, but can ultimately serve a greater purpose in the treatment and prevention of devastating neurodegenerative diseases. Premature axon loss preceding neuronal cell death is a prevalent feature observed in a number of nervous system diseases and disorders (Stoll and Müller, 1999; Adalbert and Coleman, 2013; Geisler et al., 2016) as well as chronic injury (Kelley et al., 2006; Henninger et al., 2016). The loss of synaptic terminals and retrograde axonal die-back is observed in mammalian models of Alzheimer's disease, Parkinson's disease, and Huntington's disease (Li et al., 2001; Scheff et al., 2006; Tagliaferro and Burke, 2016). As it is known that Wld^S or Sarm1 mutant mice can prevent axon death from injury, it is no wonder it they are appealing therapeutic candidates for these neurodegenerative diseases. If it is possible to prevent the early loss of the axon, then perhaps it can prevent or delay the future loss of the neuron itself, leading to a better quality of life for the affected individuals.

Wld^S mutant mice demonstrate moderate to robust protection from diseases such as peripheral neuropathy, progressive motor neuronopathy, and glaucoma (Ferri et al., 2003; Coleman, 2005; Beirowski et al., 2008), however it

is not an endogenous protein, therefore not a viable therapeutic target. Overall, current research evaluating the efficacy of Sarm1 mutant mice in preventing various models of neurodegenerative disease draws one conclusion: Sarm1 robustly protects axons from degenerating in context of acute disease or injury, such as physical injury, diabetes, and chemotherapeutic induced peripheral neuropathies (Geisler et al., 2016; Henninger et al., 2016; Turkiew et al., 2017), however Sarm1 offers little protection from chronic, progressive diseases such as Alzheimer's disease, Parkinson's Disease, and Huntington's Disease (personal communication of preliminary data, Dr. Owen Peters).

With the new discovery of *peb* in regulating axon degeneration, I've increased the pool of possible therapeutic candidate genes, however, *peb* already has two strikes against it. Firstly, considering *peb*'s only reported function is regulating gene transcription, any small molecule agonist or antagonist specific for Peb could have massive adverse effects on unknown downstream genes and subsequent biological processes. Any forward advancements in therapeutic targeting would require the identification of all genes modified by *peb* and their respective functional outcomes. Secondly, Peb only partially suppresses and delays axon degeneration after injury, *in vivo,* in *Drosophila*. In collaboration with members of the Tessier-Lavigne lab, knockdown of RREB1 in murine DRG did not suppress axon degeneration after axotomy (personal communication), however the efficacy of the knockdown was not tested, therefore we cannot completely exclude the role of RREB1 in WD.

Thus, it is not logical to target a gene which doesn't completely suppress axon degeneration and whose function may not be evolutionarily conserved.

A better molecule to target therapeutically would be Axed, as it is currently placed furthest downstream in the injury response signaling cascade, and is capable of completely inhibiting multiple pathways of axon death. While current research is exploring the functional conservation of *axed* from flies to mammals, preliminary *in vitro* data shows promising potential. Further research is critical to understand how *axed* is functioning as well as to determine whether *axed* mutants succeed in preventing the progressive axon loss in various neurodegenerative disease models, where Sarm1 mutants have failed. Overall, targeting WD signaling molecules can lead to breakthrough treatments and increasing the quality of life in patients experiencing these devastating diseases.

Conclusion

The work presented in this thesis described the discovery and characterization of a novel role for the C_2H_2 zinc finger transcription factor, Pebbled, in regulating axon degeneration after injury in *Drosophila.* I have demonstrated that the peb^{345x} loss of function allele isolated from an unbiased forward genetic screen significantly suppresses and delays WD, and presents a novel degenerative phenotype of partially fragmenting axons. The nuclear localization and functional analyses of the various zinc finger domains suggest Peb is functioning canonically as a transcriptional regulator, potentially modulating expression of

other molecules involved in the WD signaling cascade. *peb* mutants also show a specificity for blocking axon degeneration only within glutamatergic neurons, as cholinergic neurons degenerate as normal. Finally, genetically modulating the expression levels of known pro-degenerative molecules indicate that the axon protective phenotype in *peb* mutants is sensitive to levels of *dsarm*. Together, these data expand the current model of axotomy-induced degeneration, drawing our attention away from local mechanisms within the distal severed axon and towards the cell body, to include transcriptional regulation of genes in the nucleus.

Figures

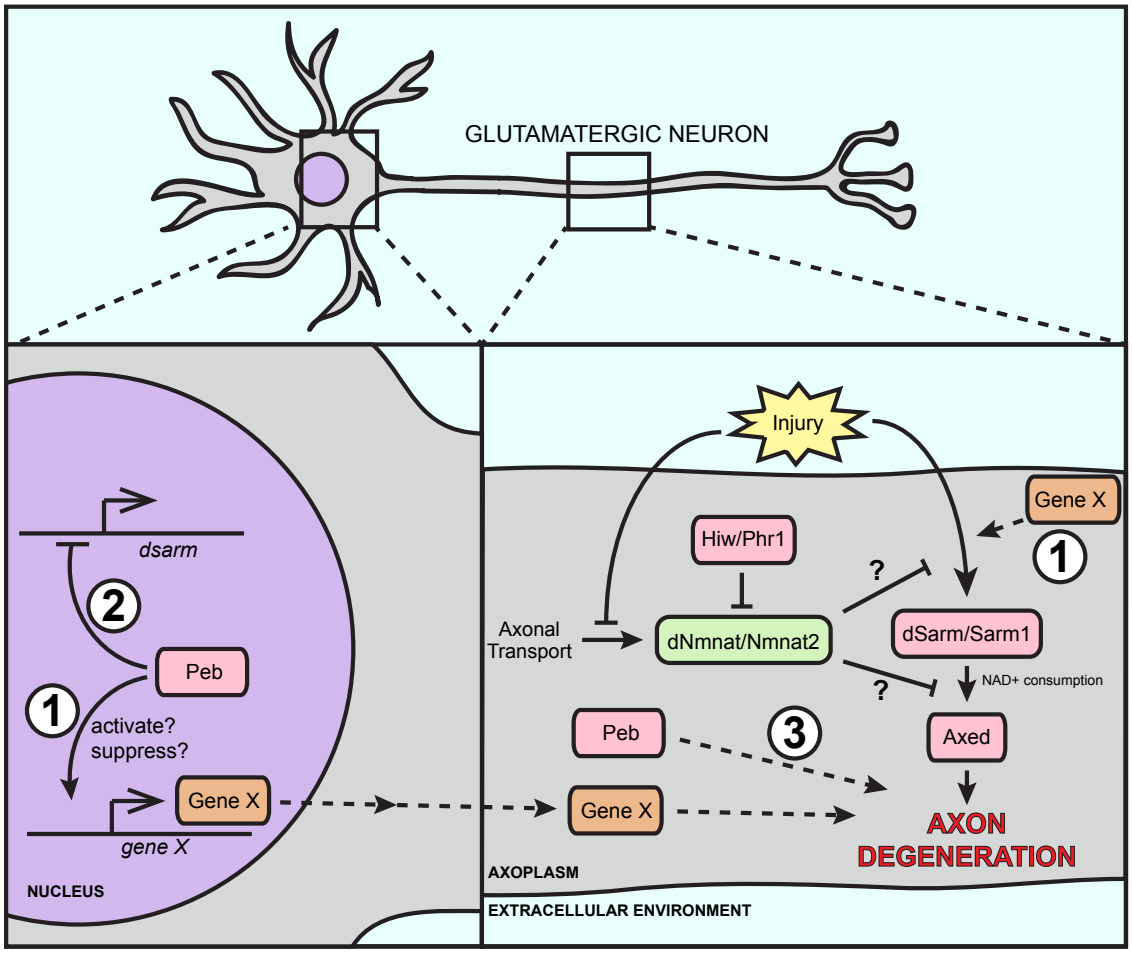

Figure 4.1. Expanded Model of Wallerian Degeneration Signaling. Schematic describing a proposed, modified model of intra-axonal signaling after injury to include Peb with pro-degenerative molecules (red) and protective molecules (green). (1) Within glutamatergic neurons, the nuclear localized transcription factor Peb can either positively or negatively regulate an unknown gene (Gene X, orange) required for axon degeneration which will function upstream of *dsarm* in a parallel genetic pathway. (2) Peb can negatively regulate levels of the pro-degenerative molecule dSarm, effectively decreasing levels in the axon. (3) Peb can have a non-canonical role in regulating axon degeneration by acting locally in the axoplasm of the distal axon.

Appendices

This work was conducted in the laboratory of Marc Freeman at the University of Massachusetts Medical School.

Appendix I: I performed all work with assistance in RNA isolation and library preparation from Pei-Hsuan (Xuan) Wu in the lab of Phil Zamore. Next generation sequencing analysis of the RNA-seq dataset was done by Kevin Kenna in the laboratory of John Landers.

Appendix II: I performed the forward genetic suppressor screen with assistance from Elizabeth Allen.

Appendix I: Differential Gene Expression in CRISPR Knockout of *pebbled in vitro*

Pebbled encodes a zinc finger transcription factor and has been shown to negatively regulate genes *in vivo* (Ming et al., 2013; Oliva et al., 2015). I have shown that loss of function *peb* mutants have defects in injury-induced axon death. To identify how *peb* is regulating WD, I wanted to check the differential gene expression profiles in cells lacking *peb* as compared to controls. In order to approach this question, I needed to find a system in which I could isolate a substantial number of cells with decreased levels of Peb protein. *Peb* is an essential gene, and homozygous animals do not survive past early embryo development, therefore analyzing homozygous loss of function mutant animals was not a possibility. The entirety of my analyses has been done by generating mosaic clones in heterozygous animals, so using these animals may not show a significant change in *peb* expression levels. To avoid these complications, I used a homologous *in vitro* system of embryonic *Drosophila* cells that endogenously express Peb, GM2 cells. While Schneider 2 (S2) cells are the most common *Drosophila* cells used in culture, Peb is not detectable by western blot analysis.

I used the CRISPR/Cas9 gene editing technology to significantly decrease expression of *peb in vitro* (Figure A1.1). From these cells, along with controls, I isolated RNA transcripts and generated triplicate libraries for Illumina deep sequencing analysis. Similar to the ChIP-seq data, *nervy* is present in the

dataset acting as a positive control, as its levels are upregulated when *peb* is decreased, implying the data from this analysis is promising. An analysis of this list shows no significant expression changes in most genes involved in the known axon death pathway (*dsarm, hiw, nmnat)* however *axed* does appear to be significantly upregulated (2.67-fold increase) when *peb* expression is decreased in GM2 cells. These data are interesting since there was no enhancement or suppression of degeneration when *axed* levels were altered, however, it must be noted that these data are not from *peb* mutant neurons, but embryonically derived cells with 80% reduction in Peb levels. This dataset may contribute to future investigations of *peb's* role in injury-induced axon degeneration, however, due to time constraints, I am unable to follow up on validation of potential genes. The differential gene expression dataset is too large to be placed in this dissertation, but the entire Excel spreadsheet can be viewed through LabArchives.com under the DOI:10.6070/H4X928S9 (https://doi.org/10.6070/H4X928S9).

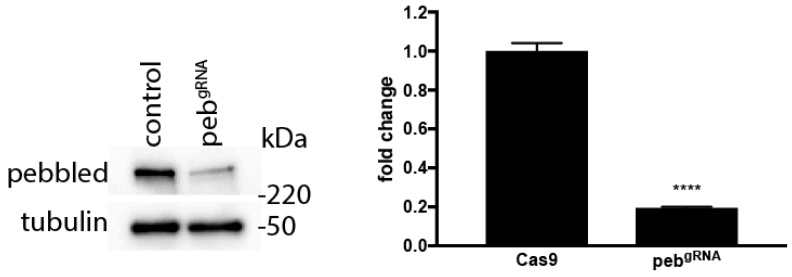

Figure A1.1. CRISPR Knockout of *peb* in GM2 Cells. Immunoblot from GM2 cells using CRISPR/Cas9 to knockout endogenous *peb* (*peb*^{gRNA} lane) after 2 weeks of puromycin selection. Cell line did not undergo clonal selection, therefore does not show complete loss of Peb protein. Quantifications show an 80% reduction in overall Peb protein as compared to controls after 2 weeks of puromycin selection. error = SEM, **** = p<.0001, unpaired two-tailed t-test.

Materials & Methods

Plasmids

gRNA sequence targeting the 5' end of the *peb* open reading frame (5'-GTTGTTGTGCTGTTGCTGTGCGG, determined by flyCRISPR Optimal Target Finder) (Gratz et al., 2014) was subcloned into the *pAc-sgRNA-Cas9*, a gift from Ji-Long Liu (Addgene plasmid # 49330), for use with transfections.

Transfection and Cell Selection

1.2 x 10^7 GM2 cells were plated out in 10 cm plates 24h prior to transfection. Cells were transfected with either *pAc-peb*^{gRNA}*-Cas9* or empty *pAc-sgRNA-Cas9* constructs to a final concentration of 15 mg DNA using Mirus TransIT-Insect (Mirus Bio). Transfected cells underwent puromycin selection (Sigma) diluted to a

final concentration of 5 µg/mL in Hyclone SFX-Insect cell culture medium (GE Healthcare Life Sciences) supplemented with 10% Fetal Bovine Serum (Hyclone, GE Healthcare Life Sciences) and 1x Penicillin-Streptomycin (Pen Strep) (ThermoFisher Scientific) for 14 days. Cells were collected 14 days after selection for western blot and RNA-seq analysis.

Western blot

Cells were collected and lysed in RIPA buffer (10 mM Tris-Cl (pH 8.0), 1 mM EDTA, 1% Triton X-100, 0.1% sodium deoxycholate, 0.1% SDS, 140 mM NaCl) supplemented with protease inhibitor tablet (cOmplete Mini EDTA-free, Roche). Laemmli buffer (0.1% β-Mercaptoethanol, 0.0005% Bromophenol blue, 10% glycerol, 2% sodium dodecyl sulfate, 63 mM Tris-HCl (pH 6.8)) was added to the lysate and incubated at 95°C for 10 minutes. 10 µl samples were loaded per lane onto a 4%–12% gradient SDS-PAGE. Membrane was probed with mouse anti-pebbled (1G9, Developmental Studies Hybridoma Bank) (1:50), mouse anti-tubulin (DM1A, Sigma) (1:5000), sheep HRP anti-mouse (ab6080, Abcam), goat HRP anti-rabbit (ab6721, Abcam) (WB 1:5000). Desitometric analysis performed using ImageJ.

RNA-seq

RNA was extracted from 3.0 x 10^6 cells and 2 µg RNA was used in cDNA library preparation as described in (Zhang et al., 2012). Sequencing was performed

using an Illumina HiSeq 2500 genome analyzer (125bp, paired end) at the Bauer Core Facility at Harvard University. Raw sequencing reads were aligned to build BDGP6 of the Drosophila reference genome using hisat2 (Kim et al., 2015), with known splice sites defined as per Ensembl release 89 (Yates et al., 2016). Read counts per transcript were generated using HTSeq (Anders et al., 2015). All downstream analyses of HTSeq read counts were performed using DESeq2 as per recommended guidelines (Love et al., 2014). Differential expression analyses included modelling of read counts with respect to both sample batch (replicate number) and sample phenotype. Transcripts were only considered where the observed read count exceeded a minimum threshold of 3.

Appendix II: Gain of Function dSarmΔARM Suppressor Screen

Similar to the forward genetic axotomy screen described in CHAPTER II, I also performed a large-scale EMS mutagenesis suppressor screen during the first three and a half years of my graduate career. In this screen, I utilized the gain of function dSarmΔARM (ΔARM) to induce Wallerian-like degeneration (degeneration that is suppressible by the protective molecule, Wld^S) in glutamatergic sensory neurons within the adult wing. Recent literature from mammalian data suggests endogenous dSarm/Sarm1 is believed to signal for axon destruction upon injury in the following manner: Axon injury induces a conformational change in Sarm through an unknown mechanism, relieving the auto-inhibitory N-terminal ARM domain. This disinhibition allows the TIR domains of homodimerized Sarm molecules to signal for axon degeneration (Gerdts et al., 2013; 2015). By removing the ARM domain, we have generated constitutively active ΔARM molecule, signaling for degeneration in the absence of injury (Figure A2.1A) (Neukomm et al., 2017). As proof of concept, expression of ΔARM in wildtype glutamatergic clones within the wing induces neuron degeneration in the absence of injury. Co-expression of Wld^S in a ΔARM background confers axon protection, but does not spare the cell body from degeneration, suggesting ΔARM does in fact signal Wallerian-like degeneration (Figure A2.1B).

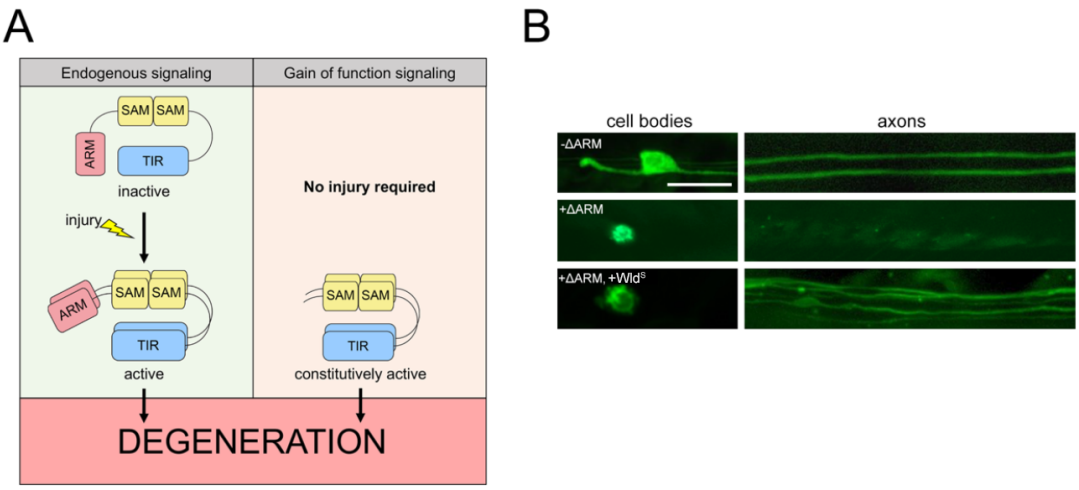

Figure A2.1. Gain of function dSarmΔARM induces Wallerian-like degeneration in the absence of injury. (A) Signaling mechanism of both endogenous dSarm/Sarm1 and dSarmΔARM (ΔARM) in degeneration. (B) Representative images of glutamatergic clones in the wing undergo cellular degeneration when ΔARM is expressed. Co-expression of the protective Wld^S prevents axon but not cell body degeneration. Scale bar = 10 μm.

Execution of the ΔARM F_1 suppressor screen is similar to that of the axotomy screen, where chromosome specific *FRT* males are fed the chemical mutagen EMS and crossed to tester virgins containing the correct genetic elements for expressing ΔARM in glutamatergic neuron clones in the wing. In the ΔARM screen however, wings from F_1 males to be screened are not injured, just aged to allow for accumulation of membrane tethered GFP expression. Wings are removed from the animals and mounted 5-7 days post eclosion. Positive hits identified from the screen would have axons and or cell bodies present in wing, suggesting suppression of ΔARM induced axon degeneration, would be re-crossed to balancer virgins for mutation isolation and phenotype

validation. From this screen, I initially identified 5 potential suppressors of gain of function ΔARM: four on the left arm of chromosome 2 (2L) and one on the right arm of chromosome 3 (3R) (Figure A2.2). The primary phenotypes of the mutants ranged from protection of both cell bodies and axons (2L.1, 2L.2, 3R.1) to just cell body protection (2L.3, 2L.4). After isolation of each hit, re-validation of all five mutants failed to suppress ΔARM activity.

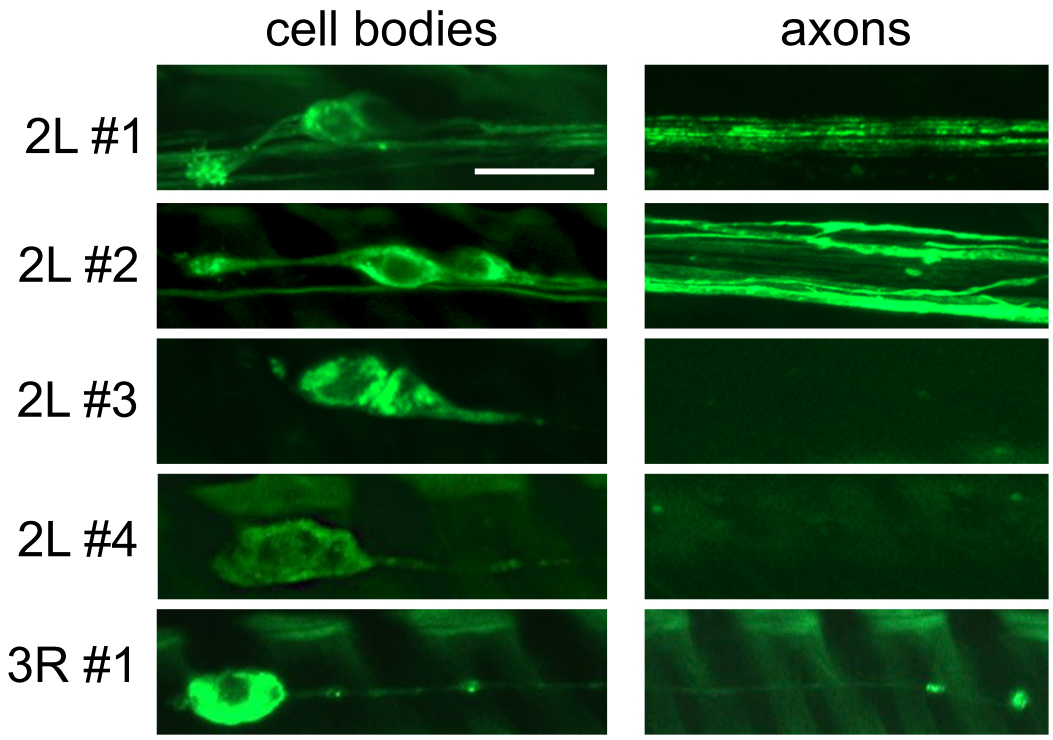

Figure A2.2. Primary hits identified from suppressor screen. Five hits identified as potential suppressors of ΔARM induced degeneration demonstrate protection of the axon, cell body, or both. Four mutations were on chromosome 2L and one mutation on chromosome 3R. Scale bar = 10 μm.

There are a few possible explanations for the failure of the re-isolated mutants to suppress ΔARM signaling. First, since this was a mosaic screen, the mutation may be somatic and not in the germline, resulting in a failure to be transmitted to subsequent generations. Secondly, primary hits could have been false positives due to transgenic mutations. Since expression of ΔARM under the *OK371-GAL4* driver results in lethality of the animal, the ΔARM transgene had to be incorporated into the background of the EMS mutagenized males. This could introduce random mutations within the either UAS sequence or the ΔARM open reading frame, both of which could result in insufficient ΔARM transgenic expression.

Over three years, I screened through a total of 20,798 independent mutagenized chromosome arms, the majority focused on chromosome 2L (Table A2). While gain of function suppressor screens are powerful genetic tools that can identify downstream genes in genetic pathways, this particular screen was not fruitful. Further screening on the remaining chromosome arms would be required to reach saturation of the genome, however, time constraints forced me to abandon this project.

Chromosome	X	2L	2R	3L	Total
Chromosome Arms Screened	210	12,874	493	7221	20,798

Table A.2. Total number of chromosome arms screened in gain of function dSarmΔARM suppressor screen.

Materials & Methods

Fly Strains

Flies (*D. melanogaster*) were kept on standard cornmeal agar supplemented with dry yeast at 25°C unless stated otherwise. The following lines were obtained from Bloomington Drosophila Stock Center unless otherwise stated:

X Chromosome: *y, w^{1118}, Nrg/FM7c, ElaV-Gal4, hs-FLP, UAS-mCD8::GFP, tub-GAL80,* and *FRT19A.*

2nd Chromosome: *OK371-Gal4, UAS-mCD8::GFP, FRT40A, FRTG13, tub-GAL80. ase-FLP^{2a} and ase-FLP^{2e}* (Neukomm et al., 2014), *UAS-dSarmΔARM::Myc* (Neukomm et al., 2017)

3rd Chromosome: *UAS-mCD8::GFP, FRT2A, FRT42B, tub-GAL80. ase-FLP^{3a} and ase-FLP^{3b}* (Neukomm et al., 2014), *UAS-dSarmΔARM::GFP* (Neukomm et al., 2017).

Mutagenesis screen and wing injury

Mutagenesis was performed as described previously (Neukomm et al., 2017). In brief, males were starved for 12 hours before consuming mutagen (25 mM ethyl methane sulphonate (EMS) in 1% sucrose). Males recovered in fresh vials for 12 hours prior to breeding. Wings were dissected with MicroPoint Scissors (EMS, VANNAS Scissors; angled on side, delicate, 5-mm cutting edge, #72933–04) and mounted in Halocarbon Oil 27 (Sigma, H8773) on a microscopy slide and covered with a coverslip, and immediately used for microscopy.

Appendix III: *Pebbled* Mutant Neurons Within the Wing Display Abnormal Dendrite Morphology

When characterizing the loss of function *peb* phenotype in axon degeneration, I noticed the dendrites of mutant neurons within the wing showed an abnormal morphology. Typically, sensory neurons in the wing vein have a relatively short, single dendrite that projects into the socket of a bristle allowing for mechanosensation (Neukomm et al., 2014; Singhania and Grueber, 2014). *peb* mutants, on the other hand, displayed a range of abnormal dendrite morphologies which I categorized into four qualitative phenotypes: normal (resembles control neurons), mild (short dendrite stump or loss of sensilla at dendrite tip), moderate (one single dendrite showing membrane blebbing or ectopic growths off of dendrite and/or cell body), and severe morphology abnormalities (extremely long dendrite, excessive branching) (Figure A3.1A-B). I measured the length of GFP^+ dendrite membrane of *peb* mutants and found a significant increase in average dendrite length, with the largest measuring around 100 μm in length (Figure A3.1C).

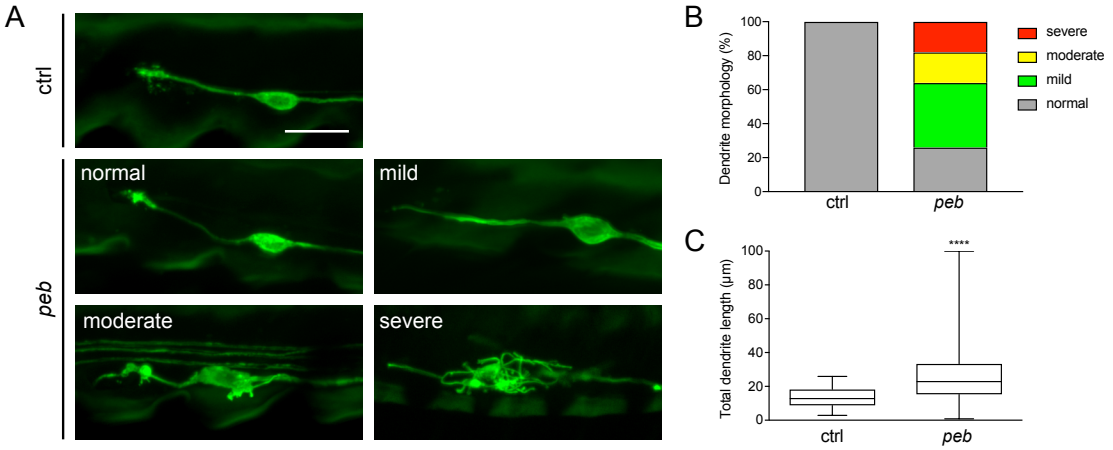

Figure A3.1. Pebbled Mutant Neurons Show Abnormal Dendrite Morphology.
(A) GFP^{+} sensory neurons in the wing. Control neuron morphology showing normal dendrite morphology. *peb* mutant neurons display abnormal outgrowth dendritic outgrowth and morphology, categorized into 4 severities: normal, mild, moderate, severe. Scale bar = 10 µm. (B) Quantification of observed abnormal dendrite morphologies (normal = gray, mild = green, moderate = yellow, severe = red) in *peb* mutants, *n* = 50. (C) Quantifications of total dendrite length, *n* = 50. **** = p<.0001, unpaired two-tailed t-test.

To confirm the abnormal morphology phenotype was due to the loss of function *peb* mutation, I performed a series of rescue experiments. First, I crossed in a copy of the genomic *peb* by using the *peb*^{BAC} described in CHAPTER III. Re-expression of endogenous levels of Peb protein completely rescued both dendrite morphology as well as the increase in dendrite length, as compared to controls (Figure 3.2A-C). Secondly, I overexpressed the zinc finger domain deletion constructs Peb$^{1-8}$ and Peb$^{10-14}$ as well as the human homolog of *peb,* hRREB1 (Figure 3.3A-C). Similar to the results of axotomy, the *peb* dendrite defect was rescued by both the C-terminal zinc finger domains 10-14 and hRREB1, but not by the N-terminal zinc fingers 1-8. Together, these data

show the dendrite abnormality is in fact an effect of loss of *peb* in the neuron, and suggests these changes are due to Peb's role in regulating gene transcription.

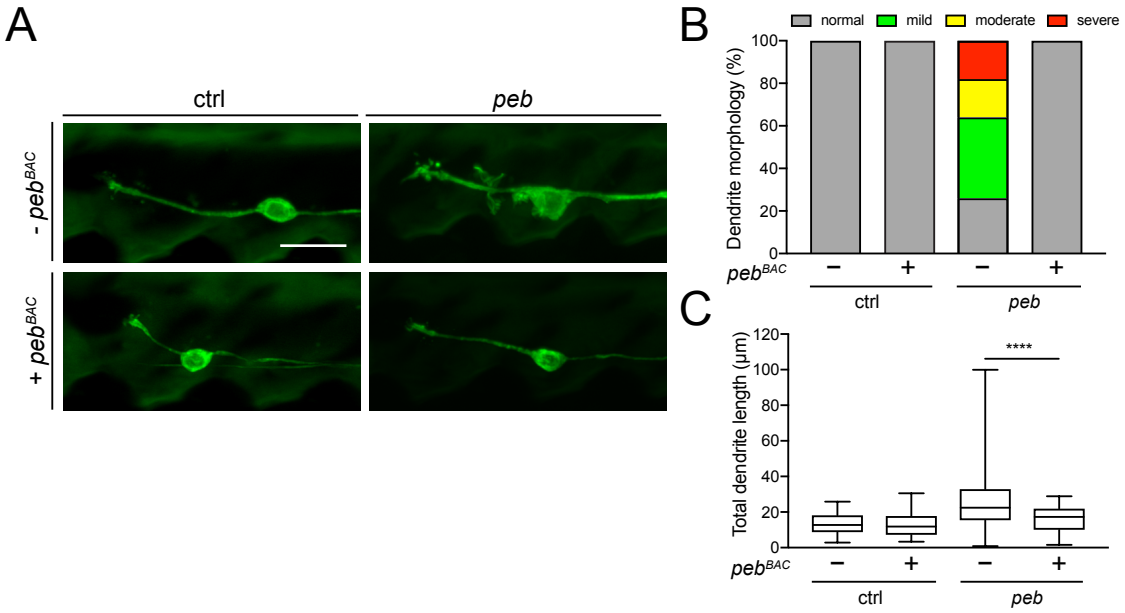

Figure A3.2. Abnormal Dendrite Morphology is Rescued by Genomic *peb*^{BAC}

(A) Representative images showing *peb* mutant dendrite phenotype is rescued with re-expression of genomic *peb*^{BAC}. No observed change in control dendrite morphology with *peb*^{BAC}. Scale bar = 10 µm. (B) Quantification of observed abnormal dendrite morphologies (normal = gray, mild = green, moderate = yellow, severe = red) in *peb*^{BAC} rescue, *n* = 50. (C) Quantifications of total dendrite length, *n* = 50. **** = p<.0001, One-way ANOVA, Dunnett's multiple comparisons test.

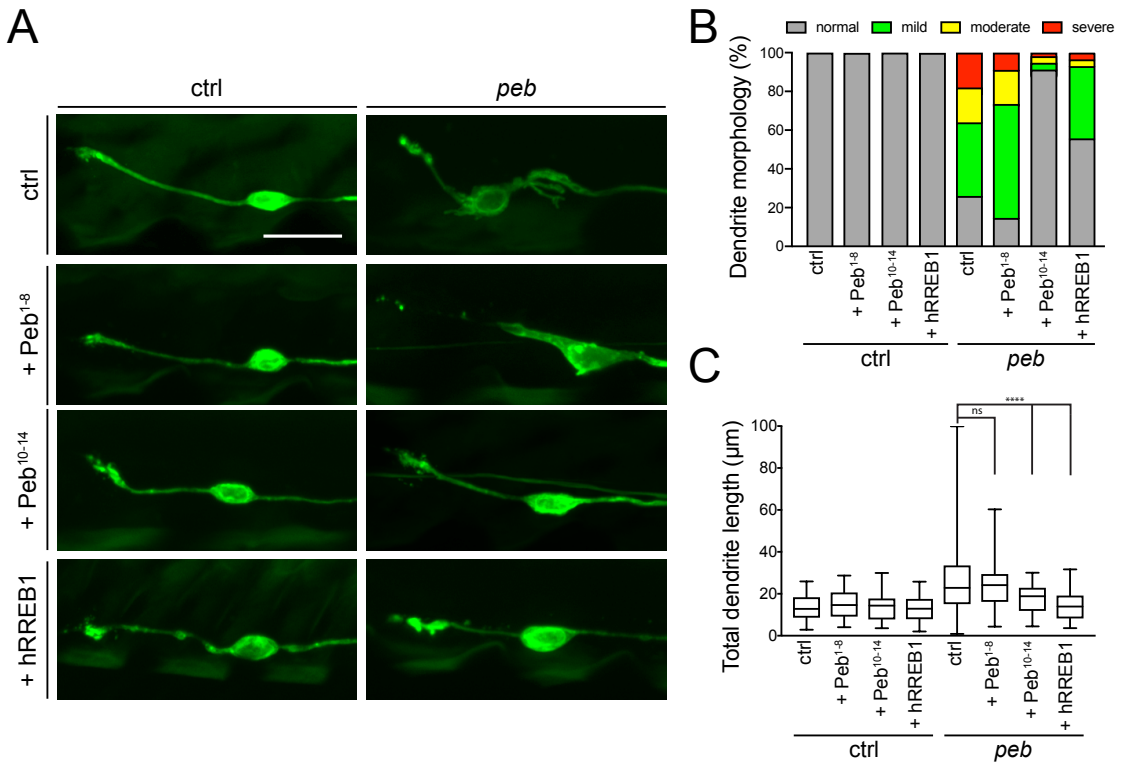

Figure A3.3. The C-Terminal Zinc Fingers and hRREB1 Can Rescue the Dendrite Phenotype.
(A) Representative images showing *peb* mutant dendrite phenotype is rescued with overexpression of known DNA binding C-terminal zinc finger domains 10-14, but not N-terminal domains 1-8. Similarly, overexpression of hRREB1 can functionally rescue *peb* mutant dendrite morphology defect. No observed change in control dendrite morphology. Scale bar = 10 µm. (B) Quantification of observed abnormal dendrite morphologies (normal = gray, mild = green, moderate = yellow, severe = red), *n* = 50. (C) Quantifications of total dendrite length, *n* = 50. **** = p<.0001, One-way ANOVA, Dunnett's multiple comparisons test.

Materials & Methods

Fly strains

Flies (*D. melanogaster*) were kept on standard cornmeal agar supplemented with dry yeast at 25°C unless stated otherwise. The following lines were obtained from Bloomington Drosophila Stock Center: y, w^{1118}, $FM7c^{Kr\text{-}Gal4,\ GFP}$, *FRT 19A, hs-FLP,tub-Gal80,FRT19A, 5xUAS-mCD8::GFP. OK371-Gal4* (Mahr and Aberle, 2006), $ase\text{-}FLP^{2a}$ and $ase\text{-}FLP^{3e}$ (Neukomm et al., 2014), *UAS-hRREB1, UAS-*$Peb^{1\text{-}8}$, and $UAS\text{-}Peb^{10\text{-}14}$ (gifts from H. Lipshitz, U of Toronto, Toronto, Canada), peb^{BAC} was generated by injection of the bacterial artificial chromosome CH321-46J02 (BAC PAC Resources, Children's Hospital Oakland Research Institute) with Phi31-mediated integration into the genomic locus *attP2* (BestGene).

Dendrite Length Analysis

Dendrites were traced and length was measured using the ImageJ plugin NeuronJ (Meijering et al., 2004).

References

Adalbert R, Coleman MP. Review: Axon pathology in age-related neurodegenerative disorders. Neuropathology and Applied Neurobiology. 2013 Jan 25;39(2):90–108.

Adalbert R, Gillingwater TH, Haley JE, Bridge K, Beirowski B, Berek L, et al. A rat model of slow Wallerian degeneration (WldS) with improved preservation of neuromuscular synapses. Eur J Neurosci. Blackwell Science Ltd; 2005 Jan;21(1):271–7.

Anders S, Pyl PT, Huber W. HTSeq--a Python framework to work with high-throughput sequencing data. Bioinformatics. 2015 Jan 15;31(2):166–9. PMCID: PMC4287950

Araki T. Increased Nuclear NAD+Biosynthesis and SIRT1 Activation Prevent Axonal Degeneration. Science. 2004 Aug 13;305(5686):1010–3.

Atianand MK, Hu W, Satpathy AT, Shen Y, Ricci EP, Alvarez-Dominguez JR, et al. A Long Noncoding RNA lincRNA-EPS Acts as a Transcriptional Brake to Restrain Inflammation. Cell. 2016 Jun 16;165(7):1672–85. PMCID: PMC5289747

Atwood HL, Dudel J, Feinstein N, Parnas I. Long-term survival of decentralized axons and incorporation of satellite cells in motor neurons of rock lobsters. Neuroscience Letters. 1989 Jun 19;101(2):121–6.

Avery MA. Axon Death Prevented: Wld^s and Other Neuroprotective Molecules: A Dissertation. University of Massachusetts Medical School; 2010. p. 1–185.

Avery MA, Rooney TM, Pandya JD, Wishart TM, Gillingwater TH, Geddes JW, et al. WldS prevents axon degeneration through increased mitochondrial flux and enhanced mitochondrial Ca2+ buffering. Curr. Biol. 2012 Apr 10;22(7):596–600. PMCID: PMC4175988

Avery MA, Sheehan AE, Kerr KS, Wang J, Freeman MR. WldS requires Nmnat1 enzymatic activity and N16-VCP interactions to suppress Wallerian degeneration. J. Cell Biol. Rockefeller University Press; 2009 Feb 23;184(4):501–13. PMCID: PMC2654119

Babetto E, Beirowski B, Russler EV, Milbrandt J, DiAntonio A. The Phr1 ubiquitin ligase promotes injury-induced axon self-destruction. CellReports. 2013 May 30;3(5):1422–9. PMCID: PMC3671584

Bardwell VJ, Treisman R. The POZ domain: a conserved protein-protein

interaction motif. Genes & Development. 1994 Jul 15;8(14):1664–77.

Barzilai A, Melamed E. Molecular mechanisms of selective dopaminergic neuronal death in Parkinson's disease. Trends in Molecular Medicine. 2003 Mar;9(3):126–32.

Beirowski B, Babetto E, Coleman MP, Martin KR. The WldS gene delays axonal but not somatic degeneration in a rat glaucoma model. Eur J Neurosci. 2008 Sep;28(6):1166–79.

Beirowski B, Babetto E, Gilley J, Mazzola F, Conforti L, Janeckova L, et al. Non-Nuclear WldS Determines Its Neuroprotective Efficacy for Axons and Synapses In Vivo. J. Neurosci. 2009 Jan 21;29(3):653–68.

Benbassat D, Spira ME. The survival of transected axonal segments of cultured Aplysia neurons is prolonged by contact with intact nerve cells. Eur J Neurosci. 1994 Oct 1;6(10):1605–14.

Berger F. Subcellular Compartmentation and Differential Catalytic Properties of the Three Human Nicotinamide Mononucleotide Adenylyltransferase Isoforms. Journal of Biological Chemistry. 2005 Sep 6;280(43):36334–41.

Billger M, Wallin M, Karlsson JO. Proteolysis of tubulin and microtubule-associated proteins 1 and 2 by calpain I and II. Difference in sensitivity of assembled and disassembled microtubules. Cell Calcium. 1988 Feb;9(1):33–44.

Blizzard CA, Southam KA, Dawkins E, Lewis KE, King AE, Clark JA, et al. Identifying the primary site of pathogenesis in amyotrophic lateral sclerosis - vulnerability of lower motor neurons to proximal excitotoxicity. Dis Model Mech. 2015 Mar;8(3):215–24. PMCID: PMC4348560

Bökel C. EMS screens : from mutagenesis to screening and mapping. Methods Mol. Biol. 2008;420:119–38.

Campenot RB. Local control of neurite development by nerve growth factor. Proc Natl Acad Sci U S A. National Academy of Sciences; 1977 Oct;74(10):4516–9. PMCID: PMC431975

Carty M, Goodbody R, Schröder M, Stack J, Moynagh PN, Bowie AG. The human adaptor SARM negatively regulates adaptor protein TRIF-dependent Toll-like receptor signaling. Nat Immunol. 2006 Oct;7(10):1074–81.

Chaharbakhshi E, Jemc JC. Broad-complex, tramtrack, and bric-à-brac (BTB) proteins: Critical regulators of development. genesis. 2016 Oct;54(10):505–18.

Chevalier-Larsen E, Holzbaur ELF. Axonal transport and neurodegenerative disease. Biochim. Biophys. Acta. 2006 Nov;1762(11-12):1094–108.

Chuang C-F, Bargmann CI. A Toll-interleukin 1 repeat protein at the synapse specifies asymmetric odorant receptor expression via ASK1 MAPKKK signaling. Genes & Development. 2005 Jan 15;19(2):270–81. PMCID: PMC545892

Classen AK, Aigouy B, Giangrande A. Imaging Drosophila pupal wing morphogenesis. Drosophila: Methods and …. 2008.

Coleman M. Axon degeneration mechanisms: commonality amid diversity. Nat. Rev. Neurosci. 2005 Nov;6(11):889–98.

Coleman MP, Conforti L, Buckmaster EA, Tarlton A, Ewing RM, Brown MC, et al. An 85-kb tandem triplication in the slow Wallerian degeneration (Wlds) mouse. Proc Natl Acad Sci U S A. 1998 Aug 18;95(17):9985–90.

Coleman MP, Perry VH. Axon pathology in neurological disease: a neglected therapeutic target. Trends Neurosci. 2002 Oct;25(10):532–7.

Conforti L, Fang G, Beirowski B, Wang MS, Sorci L, Asress S, et al. NAD(+) and axon degeneration revisited: Nmnat1 cannot substitute for Wld(S) to delay Wallerian degeneration. Cell Death Differ. 2007 Jan;14(1):116–27.

Conforti L, Gilley J, Coleman MP. Wallerian degeneration: an emerging axon death pathway linking injury and disease. Nat. Rev. Neurosci. Nature Publishing Group; 2014 Jun 1;15(6):394–409.

Conforti L, Janeckova L, Wagner D, Mazzola F, Cialabrini L, Di Stefano M, et al. Reducing expression of NAD+ synthesizing enzyme NMNAT1 does not affect the rate of Wallerian degeneration. FEBS J. Blackwell Publishing Ltd; 2011 Aug;278(15):2666–79.

Dobritsa AA, van der Goes van Naters W, Warr CG, Steinbrecht RA, Carlson JR. Integrating the molecular and cellular basis of odor coding in the Drosophila antenna. Neuron. 2003 Mar 6;37(5):827–41.

Doherty J, Logan MA, Tasdemir OE, Freeman MR. Ensheathing Glia Function as Phagocytes in the Adult Drosophila Brain. J. Neurosci. 2009 Apr 15;29(15):4768–81.

Duffy JB. GAL4 system in *Drosophila*: A fly geneticist's swiss army knife. genesis. 2002 Sep 25;34(1-2):1–15.

Eddleman CS, Ballinger ML, Smyers ME, Fishman HM, Bittner GD. Endocytotic formation of vesicles and other membranous structures induced by Ca2+ and axolemmal injury. J. Neurosci. 1998 Jun 1;18(11):4029–41.

Essuman K, Summers DW, Sasaki Y, Mao X, DiAntonio A, Milbrandt J. The SARM1 Toll/Interleukin-1 Receptor Domain Possesses Intrinsic NAD. Neuron. Elsevier Inc; 2017 Mar 22;93(6):1334–5.

Fang Y, Bonini NM. Axon Degeneration and Regeneration: Insights from DrosophilaModels of Nerve Injury. Annu. Rev. Cell Dev. Biol. 2012 Nov 10;28(1):575–97.

Fang Y, Soares L, Teng X, Geary M, Bonini NM. A Novel Drosophila Model of Nerve Injury Reveals an Essential Role of Nmnat in Maintaining Axonal Integrity. Current Biology. Elsevier Ltd; 2012 Apr 10;22(7):590–5. PMCID: PMC3347919

Ferri A, Sanes JR, Coleman MP, Cunningham JM, Kato AC. Inhibiting axon degeneration and synapse loss attenuates apoptosis and disease progression in a mouse model of motoneuron disease. Curr. Biol. 2003 Apr 15;13(8):669–73.

Frank LH, Rushlow C. A group of genes required for maintenance of the amnioserosa tissue in Drosophila. Development. 1996 May;122(5):1343–52.

Freeman MR, Doherty J. Glial cell biology in Drosophila and vertebrates. Trends Neurosci. 2006 Feb;29(2):82–90.

Friedrich P, Tompa P, Farkas A. The calpain-system of Drosophila melanogaster: coming of age. Bioessays. 2004 Oct;26(10):1088–96.

Furman DP, Bukharina TA. How Drosophila melanogaster Forms its Mechanoreceptors. Curr. Genomics. 2008;9(5):312–23. PMCID: PMC2685642

Fünfschilling U, Supplie LM, Mahad D, Boretius S, Saab AS, Edgar J, et al. Glycolytic oligodendrocytes maintain myelin and long-term axonal integrity. Nature. 2012 Apr 29;485(7399):517–21. PMCID: PMC3613737

Geisler S, Doan RA, Strickland A, Huang X, Milbrandt J, DiAntonio A. Prevention of vincristine-induced peripheral neuropathy by genetic deletion of SARM1 in mice. Brain. 2016 Dec 2;139(12):3092–108.

George EB, Glass JD, Griffin JW. Axotomy-induced axonal degeneration is mediated by calcium influx through ion-specific channels. J. Neurosci. 1995 Oct;15(10):6445–52.

Gerdts J, Brace EJ, Sasaki Y, Milbrandt J. SARM1 activation triggers axon degeneration locally via NAD+ destruction. Science. 2015 Apr 23;348(6233):453–7.

Gerdts J, Sasaki Y, Vohra B, Marasa J, Milbrandt J. Image-based Screening Identifies Novel Roles for I B Kinase and Glycogen Synthase Kinase 3 in Axonal Degeneration. Journal of Biological Chemistry. 2011 Aug 5;286(32):28011–8.

Gerdts J, Summers DW, Sasaki Y, DiAntonio A, Milbrandt J. Sarm1-Mediated Axon Degeneration Requires Both SAM and TIR Interactions. J. Neurosci. 2013 Aug 14;33(33):13569–80.

Gilley J, Coleman MP. Endogenous Nmnat2 Is an Essential Survival Factor for Maintenance of Healthy Axons. Barres BA, editor. PLoS Biol. 2010 Jan 26;8(1):e1000300.

Gilley J, Orsomando G, Nascimento-Ferreira I, Coleman MP. Absence of SARM1 Rescues Development and Survival of NMNAT2-Deficient Axons. CellReports. The Authors; 2015 Mar 31;10(12):1974–81.

Gilley J, Ribchester RR, Coleman MP. Sarm1 Deletion, but Not Wld. CellReports. ElsevierCompany; 2017 Oct 3;21(1):10–6.

Glass JD, Brushart TM, George EB, Griffin JW. Prolonged survival of transected nerve fibres in C57BL/Ola mice is an intrinsic characteristic of the axon. J Neurocytol. Kluwer Academic Publishers; 1993;22(5):311–21.

Golic KG, Lindquist S. The FLP recombinase of yeast catalyzes site-specific recombination in the Drosophila genome. Cell. 1989 Nov 3;59(3):499–509.

Gratz SJ, Ukken FP, Rubinstein CD, Thiede G, Donohue LK, Cummings AM, et al. Highly Specific and Efficient CRISPR/Cas9-Catalyzed Homology-Directed Repair in Drosophila. Genetics. 2014 Jan 29.

Griffiths I, Klugmann M, Anderson T, Yool D, Thomson C, Schwab MH, et al. Axonal swellings and degeneration in mice lacking the major proteolipid of myelin. Science. 1998 Jun 5;280(5369):1610–3.

Grill B, Murphey RK, Borgen MA. The PHR proteins: intracellular signaling hubs in neuronal development and axon degeneration. Neural Dev. BioMed Central; 2016 Mar 23;11(1):8. PMCID: PMC4806438

Hagg T, Oudega M. Degenerative and spontaneous regenerative processes after spinal cord injury. Journal of Neurotrauma. 2006 Mar;23(3-4):264–80.

Hales KG, Korey CA, Larracuente AM, Roberts DM. Genetics on the Fly: A Primer on the Drosophila Model System. Genetics. Genetics; 2015 Nov;201(3):815–42. PMCID: PMC4649653

Hammarlund M, Jorgensen EM, Bastiani MJ. Axons break in animals lacking β-spectrin. J. Cell Biol. 2007 Jan 29;176(3):269–75.

Henninger N, Bouley J, Sikoglu EM, An J, Moore CM, King JA, et al. Attenuated traumatic axonal injury and improved functional outcome after traumatic brain injury in mice lacking Sarm1. Brain. 2016 Mar 24;139(4):1094–105.

Hoppe T. Multiubiquitylation by E4 enzymes: 'one size‘ doesn’t fit all. Trends Biochem. Sci. 2005 Apr;30(4):183–7.

Huang W, Loganantharaj R, Schroeder B, Fargo D, Li L. PAVIS: a tool for Peak Annotation and Visualization. Bioinformatics. 2013 Dec 1;29(23):3097–9. PMCID: PMC3834791

Itoh K, Nakamura K, Iijima M, Sesaki H. Mitochondrial dynamics in neurodegeneration. Trends in Cell Biology. Elsevier Ltd; 2013 Feb 1;23(2):64–71.

Johnson GV, Litersky JM, Jope RS. Degradation of microtubule-associated protein 2 and brain spectrin by calpain: a comparative study. J Neurochem. 1991 May;56(5):1630–8.

Johnson VE, Stewart W, Smith DH. Axonal pathology in traumatic brain injury. Experimental Neurology. 2013 Aug;246:35–43. PMCID: PMC3979341

Kelley BJ, Farkas O, Lifshitz J, Povlishock JT. Traumatic axonal injury in the perisomatic domain triggers ultrarapid secondary axotomy and Wallerian degeneration. Experimental Neurology. 2006 Apr;198(2):350–60.

Kerschensteiner M, Schwab ME, Lichtman JW, Misgeld T. In vivo imaging of axonal degeneration and regeneration in the injured spinal cord. Nat. Med. 2005 May;11(5):572–7.

Kharchenko PV, Tolstorukov MY, Park PJ. Design and analysis of ChIP-seq experiments for DNA-binding proteins. Nat Biotechnol. Nature Publishing Group; 2008 Dec;26(12):1351–9. PMCID: PMC2597701

Kim CA, Bowie JU. SAM domains: uniform structure, diversity of function. Trends Biochem. Sci. 2003 Dec;28(12):625–8.

Kim D, Langmead B, Salzberg SL. HISAT: a fast spliced aligner with low memory

requirements. Nat Meth. 2015 Apr;12(4):357–60. PMCID: PMC4655817

Kitay BM, McCormack R, Wang Y, Tsoulfas P, Zhai RG. Mislocalization of neuronal mitochondria reveals regulation of Wallerian degeneration and NMNAT/WLDS-mediated axon protection independent of axonal mitochondria. Human Molecular Genetics. 2013 Mar 22;22(8):1601–14.

Klug A. The Discovery of Zinc Fingers and Their Applications in Gene Regulation and Genome Manipulation. Annu. Rev. Biochem. 2010 Jun 7;79(1):213–31.

Knoferle J, Koch JC, Ostendorf T, Michel U, Planchamp V, Vutova P, et al. Mechanisms of acute axonal degeneration in the optic nerve in vivo. Proceedings of the National Academy of Sciences. 2010 Mar 30;107(13):6064–9.

Knott AB, Perkins G, Schwarzenbacher R, Bossy-Wetzel E. Mitochondrial fragmentation in neurodegeneration. Nat. Rev. Neurosci. 2008 Jul;9(7):505–18.

Koegl M, Hoppe T, Schlenker S, Ulrich HD, Mayer TU, Jentsch S. A novel ubiquitination factor, E4, is involved in multiubiquitin chain assembly. Cell. 1999 Mar 5;96(5):635–44.

Lamka ML, Lipshitz HD. Role of the amnioserosa in germ band retraction of the Drosophila melanogaster embryo. Developmental Biology. 1999 Oct 1;214(1):102–12.

Landt SG, Marinov GK, Kundaje A, Kheradpour P, Pauli F, Batzoglou S, et al. ChIP-seq guidelines and practices of the ENCODE and modENCODE consortia. Genome Res. Cold Spring Harbor Lab; 2012 Sep;22(9):1813–31. PMCID: PMC3431496

Laser H, Conforti L, Morreale G, Mack TG, Heyer M, Haley JE, et al. The slow Wallerian degeneration protein, WldS, binds directly to VCP/p97 and partially redistributes it within the nucleus. Mol. Biol. Cell. Am Soc Cell Biol; 2006;17(3):1075–84.

Lee T, Luo L. Mosaic analysis with a repressible cell marker (MARCM) for Drosophila neural development. Trends Neurosci. 2001 May;24(5):251–4.

Lee Y, Morrison BM, Li Y, Lengacher S, Farah MH, Hoffman PN, et al. Oligodendroglia metabolically support axons and contribute to neurodegeneration. Nature. 2012 Jul 11;487(7408):443–8.

Li H, Durbin R. Fast and accurate long-read alignment with Burrows-Wheeler

transform. Bioinformatics. 2010 Mar 1;26(5):589–95. PMCID: PMC2828108

Li H, Li SH, Yu ZX, Shelbourne P, Li XJ. Huntingtin aggregate-associated axonal degeneration is an early pathological event in Huntington's disease mice. Journal of Neuroscience. 2001 Nov 1;21(21):8473–81.

Li Q, Brown JB, Huang H, Bickel PJ. Measuring reproducibility of high-throughput experiments. Ann. Appl. Stat. Institute of Mathematical Statistics; 2011 Sep;5(3):1752–79.

Lin MT, Beal MF. Mitochondrial dysfunction and oxidative stress in neurodegenerative diseases. Nature. 2006 Oct 19;443(7113):787–95.

Llense F, Martín-Blanco E. JNK Signaling Controls Border Cell Cluster Integrity and Collective Cell Migration. Current Biology. 2008 Apr;18(7):538–44.

Love MI, Huber W, Anders S. Moderated estimation of fold change and dispersion for RNA-seq data with DESeq2. Genome biology. 2014;15(12):550. PMCID: PMC4302049

Lubińska L. Early course of Wallerian degeneration in myelinated fibres of the rat phrenic nerve. Brain Research. 1977 Jul 8;130(1):47–63.

Lum L, Beachy PA. The Hedgehog response network: sensors, switches, and routers. Science. American Association for the Advancement of Science; 2004 Jun 18;304(5678):1755–9.

Lunn ER, Perry VH, Brown MC, Rosen H, Gordon S. Absence of Wallerian Degeneration does not Hinder Regeneration in Peripheral Nerve. Eur J Neurosci. 1989 Jan 1;1(1):27–33.

Lynch HE, Crews SM, Rosenthal B, Kim E, Gish R, Echiverri K, et al. Cellular mechanics of germ band retraction in Drosophila. Developmental Biology. 2013 Dec 15;384(2):205–13. PMCID: PMC3856716

Lyon MF, Ogunkolade BW, Brown MC, Atherton DJ, Perry VH. A gene affecting Wallerian nerve degeneration maps distally on mouse chromosome 4. Proc Natl Acad Sci U S A. National Academy of Sciences; 1993 Oct 15;90(20):9717–20. PMCID: PMC47641

Ma M, Ferguson TA, Schoch KM, Li J, Qian Y, Shofer FS, et al. Calpains mediate axonal cytoskeleton disintegration during Wallerian degeneration. Neurobiology of Disease. 2013 Aug;56:34–46. PMCID: PMC3721029

MacDonald JM, Beach MG, Porpiglia E, Sheehan AE, Watts RJ, Freeman MR.

The Drosophila Cell Corpse Engulfment Receptor Draper Mediates Glial Clearance of Severed Axons. Neuron. 2006 Jun;50(6):869–81.

MacDonald JM, Doherty J, Hackett R, Freeman MR. The c-Jun kinase signaling cascade promotes glial engulfment activity through activation of draper and phagocytic function. Cell Death Differ. Nature Publishing Group; 2013 Apr 26;20(9):1140–8.

Mack TG, Reiner M, Beirowski B, Mi W, Emanuelli M, Wagner D, et al. Wallerian degeneration of injured axons and synapses is delayed by a Ube4b/Nmnat chimeric gene. Nat Neurosci. 2001 Nov 19;4(12):1199–206.

Mahr A, Aberle H. The expression pattern of the Drosophila vesicular glutamate transporter: A marker protein for motoneurons and glutamatergic centers in the brain. Gene Expression Patterns. 2006 Mar;6(3):299–309.

Martin SM, O'Brien GS, Portera-Cailliau C, Sagasti A. Wallerian degeneration of zebrafish trigeminal axons in the skin is required for regeneration and developmental pruning. Development. 2010 Dec;137(23):3985–94. PMCID: PMC2976282

Massaro CM, Pielage J, Davis GW. Molecular mechanisms that enhance synapse stability despite persistent disruption of the spectrin/ankyrin/microtubule cytoskeleton. J. Cell Biol. Rockefeller University Press; 2009 Oct 5;187(1):101–17. PMCID: PMC2762090

Mayer PR, Huang N, Dewey CM, Dries DR, Zhang H, Yu G. Expression, localization, and biochemical characterization of nicotinamide mononucleotide adenylyltransferase 2. Journal of Biological Chemistry. American Society for Biochemistry and Molecular Biology; 2010 Dec 17;285(51):40387–96. PMCID: PMC3001018

McCabe BD, Hom S, Aberle H, Fetter RD, Marques G, Haerry TE, et al. Highwire regulates presynaptic BMP signaling essential for synaptic growth. Neuron. 2004 Mar 25;41(6):891–905.

Meijering E, Jacob M, Sarria J-CF, Steiner P, Hirling H, Unser M. Design and validation of a tool for neurite tracing and analysis in fluorescence microscopy images. Cytometry A. Wiley Subscription Services, Inc., A Wiley Company; 2004 Apr;58(2):167–76.

Miller BR, Press C, Daniels RW, Sasaki Y, Milbrandt J, DiAntonio A. A dual leucine kinase–dependent axon self-destruction program promotes Wallerian degeneration. Nat Neurosci. 2009 Mar 15;12(4):387–9.

Ming L, Wilk R, Reed BH, Lipshitz HD. Drosophila Hindsight and mammalian RREB-1 are evolutionarily conserved DNA-binding transcriptional attenuators. Differentiation. 2013 Nov;86(4-5):159–70.

Mink M, Fogelgren B, Olszewski K, Maroy P, Csiszar K. A Novel Human Gene (SARM) at Chromosome 17q11 Encodes a Protein with a SAM Motif and Structural Similarity to Armadillo/β-Catenin That Is Conserved in Mouse, Drosophila, and Caenorhabditis elegans. Genomics. 2001 Jun 1;74(2):234–44.

Mosna G, Dolfini S. Morphological and chromosomal characterization of three new continuous cell lines of Drosophila melanogaster. Chromosoma. 1972;38(1):1–9.

Neukomm LJ, Burdett TC, Gonzalez MA, Zuchner S, Freeman MR. Rapid in vivo forward genetic approach for identifying axon death genes in Drosophila. Proceedings of the National Academy of Sciences. 2014 Jul 8;111(27):9965–70.

Neukomm LJ, Burdett TC, Seeds AM, Hampel S, Coutinho-Budd JC, Farley JE, et al. Axon Death Pathways Converge on Axundead to Promote Functional and Structural Axon Disassembly. Neuron. Elsevier Inc; 2017 Jul 5;95(1):78–91.e5.

Neukomm LJ, Freeman MR. Diverse cellular and molecular modesof axon degeneration. Trends in Cell Biology. Elsevier Ltd; 2014 Sep 1;24(9):515–23.

Neumann B, Nguyen KCQ, Hall DH, Ben-Yakar A, Hilliard MA. Axonal regeneration proceeds through specific axonal fusion in transected C. elegans neurons. Dev. Dyn. 2011 Jun;240(6):1365–72. PMCID: PMC3092806

O'Neill LAJ, Bowie AG. The family of five: TIR-domain-containing adaptors in Toll-like receptor signalling. Nat Rev Immunol. 2007 May;7(5):353–64.

Oliva C, Molina-Fernandez C, Maureira M, Candia N, López E, Hassan B, et al. Hindsight regulates photoreceptor axon targeting through transcriptional control of jitterbug/Filamin and multiple genes involved in axon guidance in Drosophila. Devel Neurobio. 2015 Sep;75(9):1018–32.

Oliva C, Sierralta J. Regulation of axonal development by the nuclear protein hindsight (pebbled) in the Drosophila visual system. Developmental Biology. 2010 Aug 15;344(2):911–21.

Osterloh J. dSARM/SARM1 Governs a Conserved Axon Death Program. University of Massachusetts Medical School; 2013. p. 1–203.

Osterloh JM, Yang J, rooney TM, Fox AN, Adalbert R, Powell EH, et al. dSarm/Sarm1 Is Required for Activation of an Injury-Induced Axon Death Pathway. Science. 2012 Jul 26;337(6093):481–4.

Park JY, Jang SY, Shin YK, Koh H, Suh DJ, Shinji T, et al. MITOCHONDRIAL SWELLING AND MICROTUBULE DEPOLYMERIZATION ARE ASSOCIATED WITH ENERGY DEPLETION IN AXON DEGENERATION. Neuroscience. IBRO; 2013 May 15;238(C):258–69.

Parnas I, Dudel J, Atwood HL. Synaptic transmission in decentralized axons of rock lobster. J. Neurosci. 1991 May;11(5):1309–15.

Pfeiffer BD, Ngo TTB, Hibbard KL, Murphy C, Jenett A, Truman JW, et al. Refinement of Tools for Targeted Gene Expression in Drosophila. Genetics. 2010 Oct 12;186(2):735–55.

Pickup AT, Lamka ML, Sun Q, Yip MLR, Lipshitz HD. Control of photoreceptor cell morphology, planar polarity and epithelial integrity during Drosophila eye development. Development. 2002 May;129(9):2247–58.

Pintard L, Willems A, Peter M. Cullin-based ubiquitin ligases: Cul3-BTB complexes join the family. The EMBO Journal. EMBO Press; 2004 Apr 21;23(8):1681–7. PMCID: PMC394240

Razin SV, Borunova VV, Maksimenko OG, Kantidze OL. Cys2His2 zinc finger protein family: Classification, functions, and major members. Biochemistry Moscow. 2012 Mar 16;77(3):217–26.

Reed BH, Wilk R, Lipshitz HD. Downregulation of Jun kinase signaling in the amnioserosa is essential for dorsal closure of the Drosophila embryo. Curr. Biol. 2001 Jul 24;11(14):1098–108.

Reed BH, Wilk R, Schöck F, Lipshitz HD. Integrin-dependent apposition of Drosophila extraembryonic membranes promotes morphogenesis and prevents anoikis. Curr. Biol. 2004 Mar 9;14(5):372–80.

Rooney TM, Freeman MR. Drosophila models of neuronal injury. ILAR J. 2014;54(3):291–5. PMCID: PMC3962260

Sasaki Y, Milbrandt J. Axonal Degeneration Is Blocked by Nicotinamide Mononucleotide Adenylyltransferase (Nmnat) Protein Transduction into Transected Axons. Journal of Biological Chemistry. 2010 Dec 24;285(53):41211–5.

Sasaki Y, Nakagawa T, Mao X, DiAntonio A. NMNAT1 inhibits axon

degeneration via blockade of SARM1-mediated NAD+ depletion. eLife. 2016.

Saxena S, Caroni P. Mechanisms of axon degeneration: From development to disease. Progress in Neurobiology. 2007 Oct;83(3):174–91.

Saxena S, Caroni P. Selective neuronal vulnerability in neurodegenerative diseases: from stressor thresholds to degeneration. Neuron. 2011 Jul 14;71(1):35–48.

Scheff SW, Price DA, Schmitt FA, Mufson EJ. Hippocampal synaptic loss in early Alzheimer's disease and mild cognitive impairment. Neurobiol. Aging. 2006 Oct;27(10):1372–84.

Schlaepfer WW. Calcium-induced degeneration of axoplasm in isolated segments of rat peripheral nerve. Brain Research. 1974 Apr 5;69(2):203–15.

Schlaepfer WW, Hasler MB. Characterization of the calcium-induced disruption of neurofilaments in rat peripheral nerve. Brain Research. 1979 May 25;168(2):299–309.

Schöck F, Perrimon N. Cellular processes associated with germ band retraction in Drosophila. Developmental Biology. 2002 Aug 1;248(1):29–39.

Scuderi A, Letsou A. Amnioserosa is required for dorsal closure in Drosophila. Dev. Dyn. 2005 Mar;232(3):791–800.

Shin JE, DiAntonio A. Highwire regulates guidance of sister axons in the Drosophila mushroom body. Journal of Neuroscience. 2011 Nov 30;31(48):17689–700. PMCID: PMC3457808

Sievers C, Platt N, Perry VH, Coleman MP, Conforti L. Neurites undergoing Wallerian degeneration show an apoptotic-like process with annexin V positive staining and loss of mitochondrial membrane potential. Neuroscience Research. 2003 Jun;46(2):161–9.

Singhania A, Grueber WB. Development of the embryonic and larval peripheral nervous system of Drosophila. WIREs Dev Biol. 2014 Apr 16;3(3):193–210.

Spratford CM, Kumar JP. Dissection and Immunostaining of Imaginal Discs from Drosophila melanogaster. JoVE. 2014;(91).

St Johnston D. The art and design of genetic screens: Drosophila melanogaster. Nat. Rev. Genet. 2002 Mar;3(3):176–88.

Stengl M. Pigment-dispersing hormone-immunoreactive fibers persist in crickets which remain rhythmic after bilateral transection of the optic stalks. Journal of

Comparative Physiology A: Neuroethology. 1995.

Stogios PJ, Privé GG. The BACK domain in BTB-kelch proteins. Trends Biochem. Sci. 2004 Dec;29(12):634–7.

Stoll GG, Müller HWH. Nerve injury, axonal degeneration and neural regeneration: basic insights. Brain Pathol. 1999 Apr 1;9(2):313–25.

Strecker TR, Yip ML. Zygotic genes that mediate torso receptor tyrosine kinase functions in the Drosophila melanogaster embryo. 1991.

Sun J, Deng W-M. Hindsight Mediates the Role of Notch in Suppressing Hedgehog Signaling and Cell Proliferation. Developmental Cell. 2007 Mar;12(3):431–42. PMCID: PMC1851662

Sweeney LB, Couto A, Chou Y-H, Berdnik D, Dickson BJ, Luo L, et al. Temporal Target Restriction of Olfactory Receptor Neurons by Semaphorin-1a/PlexinA-Mediated Axon-Axon Interactions. Neuron. 2007 Jan;53(2):185–200.

Tagliaferro P, Burke RE. Retrograde Axonal Degeneration in Parkinson Disease. J Parkinsons Dis. 2016;6(1):1–15. PMCID: PMC4927911

Terman JR, Kolodkin AL. Nervy links protein kinase a to plexin-mediated semaphorin repulsion. Science. 2004 Feb 20;303(5661):1204–7.

Turkiew E, Falconer D, Reed N, Höke A. Deletion of Sarm1 gene is neuroprotective in two models of peripheral neuropathy. J. Peripher. Nerv. Syst. 2017 Sep;22(3):162–71. PMCID: PMC5585053

Vargas ME, Yamagishi Y, Tessier-Lavigne M, Sagasti A. Live Imaging of Calcium Dynamics during Axon Degeneration Reveals Two Functionally Distinct Phases of Calcium Influx. Journal of Neuroscience. 2015 Nov 11;35(45):15026–38. PMCID: PMC4642236

W M Deng CAAHR-B. Notch-Delta signaling induces a transition from mitotic cell cycle to endocycle in Drosophila follicle cells. 2001 Nov 5;:1–10.

Walker LJ, Summers DW, Sasaki Y, Brace EJ. MAPK signaling promotes axonal degeneration by speeding the turnover of the axonal maintenance factor NMNAT2. eLife. 2017.

Waller A. Experiments on the Section of the Glossopharyngeal and Hypoglossal Nerves of the Frog, and Observations of the Alterations Produced Thereby in the Structure of Their Primitive Fibres. Philosophical Transactions of the Royal Society of London. 1850 Jan 1;140:423–9.

Wan HI, DiAntonio A, Fetter RD, Bergstrom K, Strauss R, Goodman CS. Highwire regulates synaptic growth in Drosophila. Neuron. 2000 May;26(2):313–29.

Wang J, Zhai Q, Chen Y, Lin E, Gu W, McBurney MW, et al. A local mechanism mediates NAD-dependent protection of axon degeneration. J. Cell Biol. 2005 Aug 1;170(3):349–55. PMCID: PMC2171458

Wang JT, Medress ZA, Barres BA. Axon degeneration: Molecular mechanisms of a self-destruction pathway. J. Cell Biol. 2012 Jan 9;196(1):7–18.

Wilbrey AL, Haley JE, Wishart TM, Conforti L, Morreale G, Beirowski B, et al. VCP binding influences intracellular distribution of the slow Wallerian degeneration protein, WldS. Molecular and Cellular Neuroscience. 2008 Jul;38(3):325–40.

Wildonger J, Mann RS. Evidence that nervy, the Drosophila homolog of ETO/MTG8, promotes mechanosensory organ development by enhancing Notch signaling. Developmental Biology. 2005 Oct;286(2):507–20.

Wilk R, Reed BH, Tepass U, Lipshitz HD. The hindsight Gene Is Required for Epithelial Maintenance and Differentiation of the Tracheal System in Drosophila. Developmental Biology. 2000 Mar;219(2):183–96.

Wolfe SA, Nekludova L, Pabo CO. DNA recognition by Cys2His2 zinc finger proteins. Annual review of biophysics …. 2000.

Wu C. Highwire Function at the Drosophila Neuromuscular Junction: Spatial, Structural, and Temporal Requirements. Journal of Neuroscience. 2005 Oct 19;25(42):9557–66.

Xiong X, Hao Y, Sun K, Li J, Li X, Mishra B, et al. The Highwire Ubiquitin Ligase Promotes Axonal Degeneration by Tuning Levels of Nmnat Protein. Barres BA, editor. PLoS Biol. 2012 Dec 4;10(12):e1001440.

Xiong X, Wang X, Ewanek R, Bhat P, DiAntonio A, Collins CA. Protein turnover of the Wallenda/DLK kinase regulates a retrograde response to axonal injury. J. Cell Biol. 2010 Oct 4;191(1):211–23.

Yahata N, Yuasa S, Araki T. Nicotinamide mononucleotide adenylyltransferase expression in mitochondrial matrix delays Wallerian degeneration. Journal of Neuroscience. Society for Neuroscience; 2009 May 13;29(19):6276–84.

Yamagishi Y, Tessier-Lavigne M. An Atypical SCF-like Ubiquitin Ligase Complex Promotes Wallerian Degeneration through Regulation of Axonal Nmnat2.

CellReports. 2016 Oct 11;17(3):774–82. PMCID: PMC5075525

Yang J, Weimer RM, Kallop D, Olsen O, Wu Z, Renier N, et al. Regulation of Axon Degeneration after Injury and in Development by the Endogenous Calpain Inhibitor Calpastatin. Neuron. Elsevier Inc; 2013 Nov 5;:1–15.

Yang J, Wu Z, Renier N, Simon DJ, Uryu K, Park DS, et al. Pathological Axonal Deaththrough a MAPK Cascade that Triggers a Local Energy Deficit. Cell. Elsevier Inc; 2015 Jan 15;160(1-2):161–76.

Yates A, Akanni W, Amode MR, Barrell D, Billis K, Carvalho-Silva D, et al. Ensembl 2016. Nucleic Acids Research. 2016 Jan 4;44(D1):D710–6. PMCID: PMC4702834

Yip ML, Lamka ML, Lipshitz HD. Control of germ-band retraction in Drosophila by the zinc-finger protein HINDSIGHT. Development. 1997 Jun;124(11):2129–41.

Zelená J, Lubińska L, Gutmann E. Accumulation of organelles at the ends of interrupted axons. Z Zellforsch Mikrosk Anat. 1968;91(2):200–19.

Zhai Q, Wang J, Kim A, Liu Q, Watts R, Hoopfer E, et al. Involvement of the ubiquitin-proteasome system in the early stages of Wallerian degeneration. Neuron. Elsevier; 2003;39(2):217–25.

Zhang J-N, Michel U, Lenz C, Friedel CC, Köster S, d'Hedouville Z, et al. Calpain-mediated cleavage of collapsin response mediator protein-2 drives acute axonal degeneration. Nature Publishing Group. Nature Publishing Group; 2016 Nov 15;6(1):37050. PMCID: PMC5109185

Zhang X, Kurnasov OV, Karthikeyan S, Grishin NV, Osterman AL, Zhang H. Structural characterization of a human cytosolic NMN/NaMN adenylyltransferase and implication in human NAD+biosynthesis. J. Biol. Chem. American Society for Biochemistry and Molecular Biology; 2003 Apr 11;278(15):13503–11.

Zhang Z, Theurkauf WE, Weng Z, Zamore PD. Strand-specific libraries for high throughput RNA sequencing (RNA-Seq) prepared without poly(A) selection. Silence. BioMed Central; 2012 Dec 28;3(1):9. PMCID: PMC3552703